INL/EXT-16-40799

Advanced 3D Characterization and Reconstruction of Reactor Materials

FY16 Final Report

Assel Aitkaliyeva
Bradley S. Fromm
Benjamin Hauch
Kumar Sridharan

December 2016

The INL is a U.S. Department of Energy National Laboratory
operated by Battelle Energy Alliance

INL/EXT-16-

Advanced 3D Characterization and Reconstruction of Reactor Materials
FY16 Final Report

Assel Aitkaliyeva
Bradley S. Fromm
Benjamin Hauch
Kumar Sridharan

December 2016

Idaho National Laboratory
Idaho Falls, Idaho 83415

http://www.inl.gov

Prepared for the
U.S. Department of Energy
Office of Nuclear Science
Under DOE Idaho Operations Office
Contract DE-AC07-05ID14517

Advanced 3D Characterization and Reconstruction of Reactor Materials

FY16 Final Report

INL/EXT-16-40799

December 2016

ABSTRACT

A coordinated effort to link advanced materials characterization methods and computational modeling approaches is critical to future success for understanding and predicting the behavior of reactor materials that operate at extreme conditions. The difficulty and expense of working with nuclear materials have inhibited the use of modern characterization techniques on this class of materials. Likewise, mesoscale simulation efforts have been impeded due to insufficient experimental data necessary for initialization and validation of the computer models. The objective of this research is to develop methods to integrate advanced materials characterization techniques developed for reactor materials with state-of-the-art mesoscale modeling and simulation tools.

Research to develop broad-ion beam sample preparation, high-resolution electron backscatter diffraction, and digital microstructure reconstruction techniques; and methods for integration of these techniques into mesoscale modeling tools are detailed. Results for both irradiated and un-irradiated reactor materials are presented for FY14 - FY16 and final remarks are provided.

CONTENTS

FIGURES

TABLES

1. Introduction

A coordinated effort to link advanced materials characterization methods and computational modeling approaches is critical to future success for understanding and predicting the behavior of reactor materials that operate at extreme conditions. The difficulty and expense of working with nuclear materials have inhibited the use of modern characterization techniques on this class of materials. Likewise, mesoscale simulation efforts have been impeded due to insufficient experimental data necessary for initialization and validation of the computer models. The objective of this research is to develop a critical line of inquiry that integrates advanced materials characterization techniques developed for reactor materials with state-of-the-art mesoscale modeling and simulation tools.

INL researchers have developed the capability to serial section unirradiated and irradiated nuclear materials with a focused ion beam (FIB) and then apply electron backscatter diffraction (EBSD) techniques coupled with energy-dispersive x-ray spectroscopy (EDS) to produce 2D slices of the material [1-2]. These 2D slices are then reconstructed into a 3D digital microstructure as illustrated in Figure 1(a). The 3D microstructure can be used to establish realistic initial conditions for simulations in MARMOT [3-4] (a finite element-based, multi-physics, phase-field modeling framework developed at INL). Figure 1(a) and Figure 1(b) show results of a Marmot simulation that predicts effective thermal conductivity of a mixed oxide fuel microstructure [5]. These types of simulations are important for validation of the computer models [6].

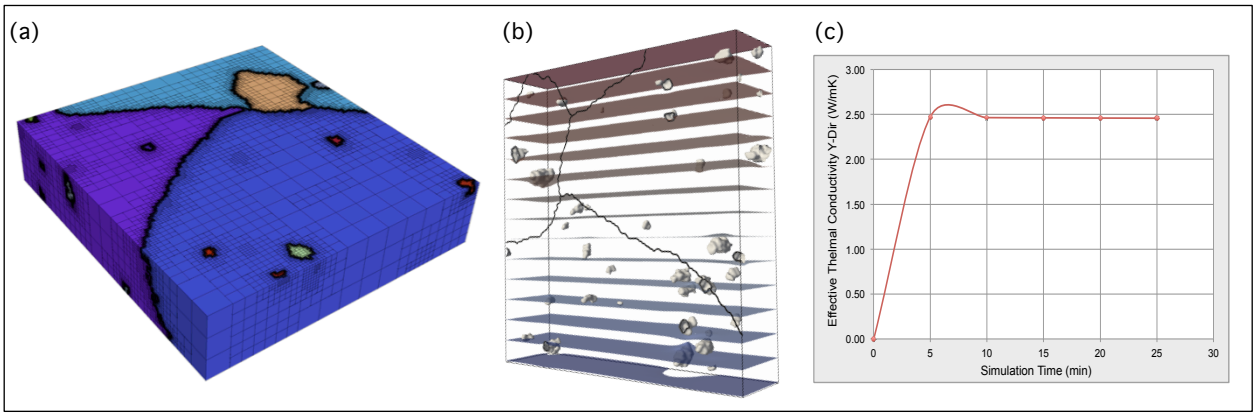

Figure 1: Example of high burn-up MOX microstructure characterized and reconstructed in MARMOT: (a) Initial microstructure reconstructed from EBSD data; (b) temperature plot from MARMOT simulation of the MOX microstructure with isotherms illustrating the effect of metallic precipitates (shown in gray) on the microstructure; (c) effective thermal conductivity plot of the MOX microstructure

Unfortunately, the new techniques have limitations that need to be addressed. First, the sample area that can be prepared is limited to ~150 μm x 150 μm regions. Second, the in-situ FIB sample preparation is a manual, time-consuming method that occupies a high-demand instrument (the FIB) for long periods of time. Third, traditional sample preparation methods are not sufficient to obtain high-quality electron backscatter patterns necessary for characterization of the material

because they must be carried out manually in a hot cell or glovebox with limited equipment and range of motion.

1.1 Project Objectives

For this project, we proposed realistic steps to address current characterization limitations and to enhance the advanced characterization and reconstruction capabilities recently developed at INL in order to allow for efficient characterization of reactor microstructures and their reconstruction within MARMOT. This 3-year project consisted of three key objectives that will push the limits of present technology, including:

1) Explore new sample preparation techniques for reactor materials using broad beam ion-etching methods to decrease sample preparation time, improve scan quality, increase scan size, and reduce radiation exposure/waste.

2) Implement an advanced characterization technique known as high-resolution EBSD (HR-EBSD) to enable estimation of critical material properties like dislocation density and residual strain from reactor materials.

3) Develop necessary post-processing tools and procedures to utilize the HR-EBSD data obtained in Objective 2 for microstructure reconstruction into MARMOT.

1.2 Project Milestones

A list of milestones for each year of the project is summarized below.

1.2.1 FY14 Milestones

- Develop broad ion beam technique
- Perform HR-EBSD on un-irradiated material
- First Annual Progress Report

1.2.2 FY15 Milestones

- Perform serial sectioning and reconstruct slices on nuclear material samples
- Perform HR-EBSD on neutron irradiated material
- Second Annual Progress Report

1.2.3 FY16 Milestones

- Integrate 3D reconstructed EBSD data set into MARMOT for Simulations
- Perform 3D EBSD on irradiated material sample
- Final Technical Report

2. FY14 Results

2.1 Material Selection

The first project task was to determine an appropriate material test matrix for the experiments. The requirements laid out for proposed materials were: 1) a current or proposed reactor material; 2) ability to obtain unirradiated and irradiated samples during 3 year project; 3) represent range of milling parameters. After assessing potential materials, the following materials were selected: Zircaloy-4 cladding, HT-9, and SiC/SiC composites. Westinghouse generously provided unirradiated Zircaloy-4 cladding, unirradiated HT-9 was available at INL, and EPRI provided unirradiated SiC/SiC composites for method development. INL has a high dose Zircaloy-4 cladding sample from the BR-3 reactor that was taken to 45 GWd/tHM, and an HT-9 sample irradiated in FFTF to ~100 DPA as part of ACO-3 fuel irradiation. EPRI has kindly agreed to supply MIT irradiated SiC/SiC composites for analysis in FY15.

Table 1: Material Selection Matrix

Material	Uses	Irradiated Material	Notes
Zircaloy-4	Cladding, channel boxes	Have high-dose Zircaloy-4-4 cladding from BR-3 Reactor	Most challenging material chosen, oxidation and high strain complicate sample preparation
HT-9	Cladding, structural, fast reactor primarily	Have high-dose HT-9 from FFTF ACO3 cladding	A stainless steel alloy, should give good parameters for preparation of other reactor steels
SiC/SiC	Potential cladding, potential channel boxes	SiC/SiC from MIT reactor testing	Will provide data on preparing ceramic materials, typically a difficult sample to prepare with mechanical methods

2.2 Broad-beam Ion Etching Facilities

Section 2.2 contains a description of the broad-ion etching facilities at Idaho National Laboratory and The University of Wisconsin-Madison.

2.2.1 Idaho National Laboratory Facilities

Broad-beam ion etching at INL is performed with one of two precision etching coating systems (PECS 682) from Gatan Corporation. One instrument is located in CAES and is capable of preparing non-radioactive samples, a second unit is located in the Electron Microscopy Laboratory (EML) at the Material Fuel Complex, and is capable of handling all classes of radiological materials from irradiated materials, to irradiated transuranic fuels. The PECS 682 is

capable of preparing samples up to 1.25” diameter and 0.75” tall. The accelerating voltage capability of the instrument is from 1-10 keV.

2.2.2 University of Wisconsin-Madison

Broad-beam ion etching at UW is performed with a Fischione Model 1050 TEM mill. This instrument offers simultaneous dual-gun operation, and each gun emits ~0.2 sccm UHP Argon ions having energy between 0.1 and 6.0 keV. The gun optics are such that the maximum beam current density is 10 mA/cm². The ion impingement angles are independently customizable to ±10° relative to the sample surface.

The Model 1050 provides different ion etching capabilities than what is present at the INL PIE preparation facility (“hot cell”). Most importantly, the Model 1050 does not support the standard 1” or 1.25” sample puck geometry, and instead requires a specially fabricated sample mount of maximum diameter 0.75”. As UW is tasked with demonstrating feasibility of the methodology using cold samples, and not with performing the procedure on active samples prepared in the INL hot cell (which would be 1.25” mounts), this difference between the two instruments is acceptable.

2.3 Parameter Development

HT-9 was selected as the first material for technique development due to our previous experiences with the materials; we determined it was our best chance for early success. Zircaloy-4 is extremely challenging due to oxidation and strain, and the SiC/SiC composites with multiple phases were felt to be likely challenges as well. All unirradiated materials were thoroughly characterized to ensure we knew the starting material state prior to commencing milling development.

2.3.1 HT-9 Parameter Development

The received HT-9 cladding was sectioned into samples 2-3mm in height. One standard 1.25” mount was developed for comparison purposes, while the remaining sectioned samples were entrained in using the same epoxy mounting system as is used at the INL hot cell. The as-received material was characterized in the scanning electron microscope (SEM) with energy-dispersive x-ray spectrometry (EDS), EBSD, and x-ray diffractometry (XRD). Following initial characterization, the effect of ion milling on surface quality and EBSD quality was investigated.

2.3.1.1 Initial Characterization

HT-9 is a commercial ferritic-martensitic steel with nominal composition 12 wt. % Cr, 1 wt. % Mo. A standard 1.25” phenolic mount was used to package the sample, and standard metallographic preparation techniques were used to prepare it for imaging. These techniques involve water-lubricated rough grinding with SiC abrasive sheets, rough polishing with polycrystalline diamond abrasives, and fine polishing with colloidal silica, followed by ultrasonic cleanings in acetone and ethanol to remove solvents and residues. Following the cleaning steps, the sample was imaged with a JEOL JSM-6610 scanning electron microscope.

2.3.1.2 EDS Results

A semi-quantitative verification of the received material’s composition was performed using a Thermo Scientific UltraDry EDS detector and the Noran System Six (NSS) software package.

The data was collected using both phase-selective x-ray mapping and point-shoot modes with an accelerating voltage of 15 kV and working distance of 14mm. The compositions yielded by each technique were in agreement despite each being in a different area.
The phase-selective x-ray mapping was performed at a magnification of 180X. The point-and-shoot measurement was performed on a different area at 500X, and was repeated in the same position 4 additional times.

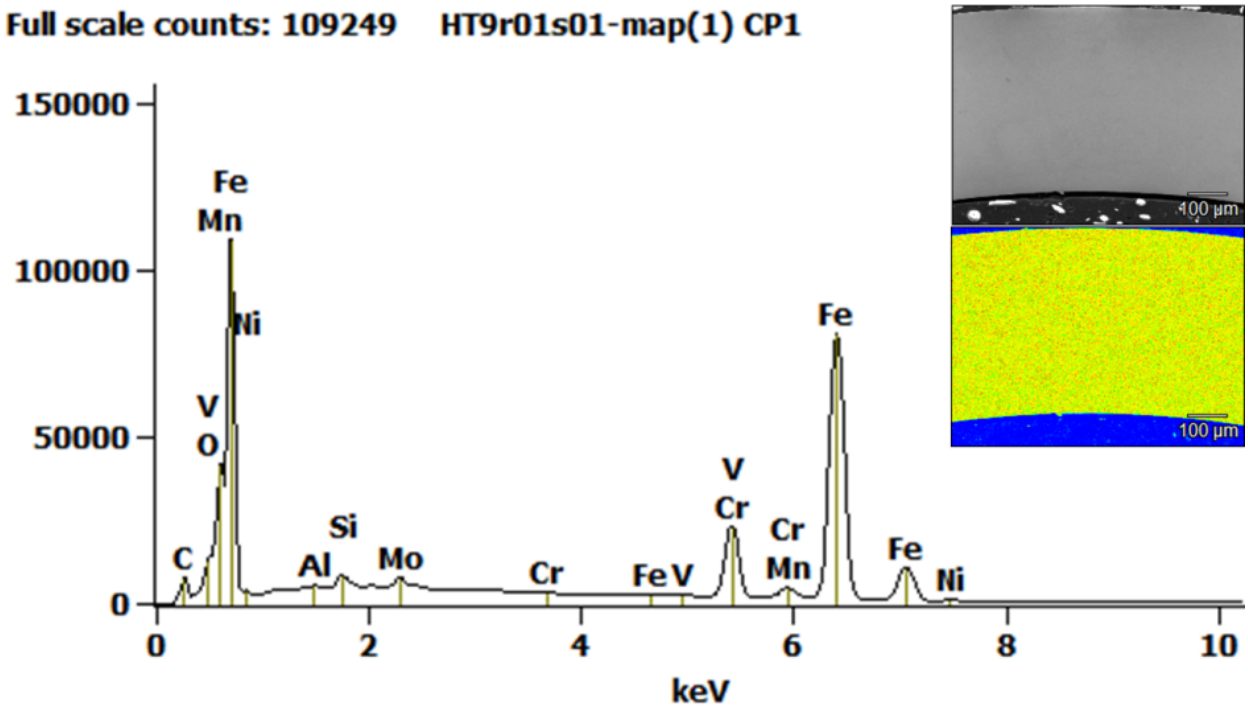

Figure 2: The collected and indexed EDS spectrum for all positions identified as the CP1 phase by the NSS software. Top inset: greyscale SEM image of the mapped area. Bottom inset: yellow and green points indicate the physical location of CP1 pixels.

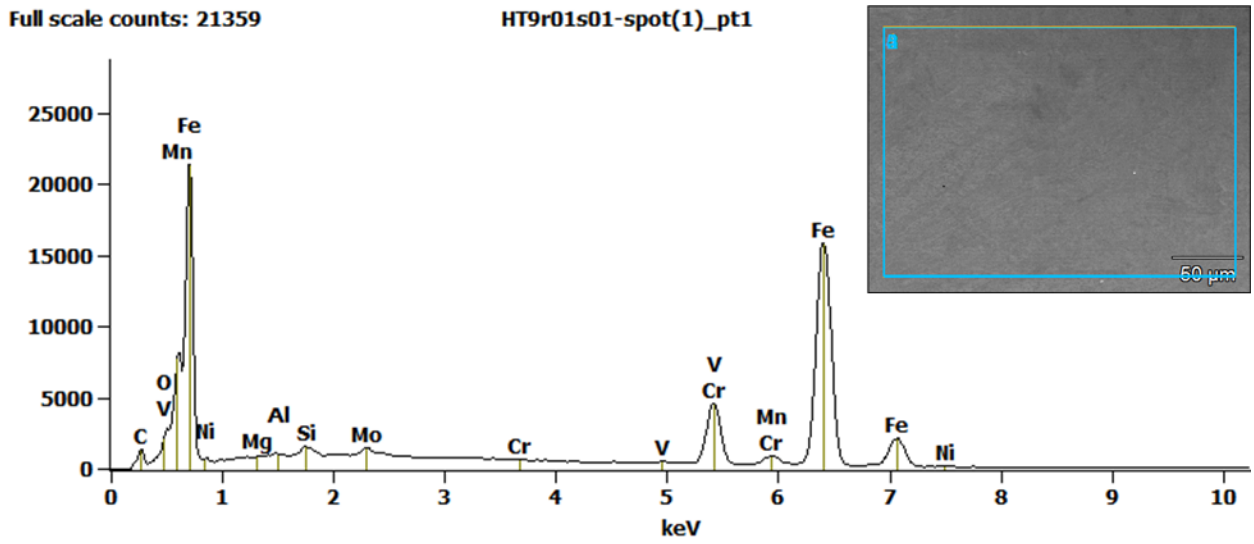

Figure 3: An HT-9 x-ray spectrum as collected and indexed by the NSS software in point-and-shoot mode. Inset: Greyscale SEM image of the analyzed area. Five rectangular collection areas were overlaid.

Table 2: Comparison of HT-9 composition as determined by two different measurement methods in two different areas. Only one of the five spectrums is reported for the Point-and-Shoot data; the rest are equivalent.

Element	Weight % (Mapping)	±Weight %	Weight % (P&S)	±Weight %
C	1.23	± 0.01	1.18	±0.02
O	0	± 0.00	0	±0.00
Mg	0	± 0.00	0.02	±0.02
Al	0.07	± 0.01	0.09	±0.01
Si	0.56	± 0.01	0.56	±0.02
V	0.35	± 0.01	0.37	±0.03
Cr	11.93	± 0.05	11.9	±0.10
Mn	0.78	± 0.06	1.02	±0.13
Fe	83.37	± 0.17	83.05	±0.31
Ni	0.62	± 0.08	0.72	±0.09
Mo	1.09	± 0.03	1.09	±0.04

2.3.1.3 EBSD Results

In order to classify if broad-beam ion milling offers acceptable EBSD quality, the observed EBSD quality should first be determined for standard preparation procedures. Initial EBSD characterization was performed with the same JEOL JSM-6610 SEM. Additional EBSD was collected using a Leo 1530 field emission SEM. Both data collections were performed on the same colloidal silica-polished surface, but significantly improved results were obtained using the Leo 1530 FESEM. It is likely significant improvements to the data collection process could be made to improve data quality when using the JEOL SEM, but it is more prudent to forgo the

extra optimization and continue using the already-optimized data collection process with the Leo 1530 FESEM. In-depth analysis of the collected EBSD patterns was not attempted, as the objective of data collection is to determine whether or not ion milling from a 1200 grit finish can achieve comparable or superior pattern quality.

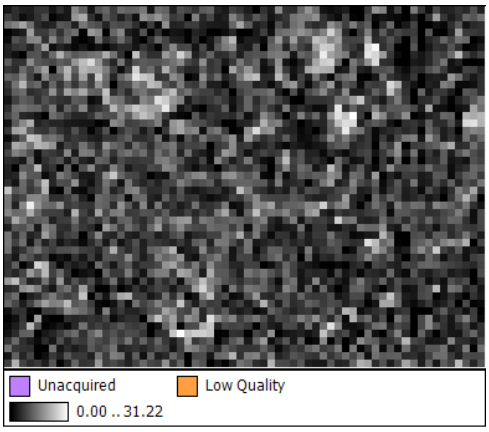

Figure 4: Pattern quality map for EBSD data collected using the NSS software on the JEOL JSM-6610 SEM. No additional effort to refine collection parameters was made.

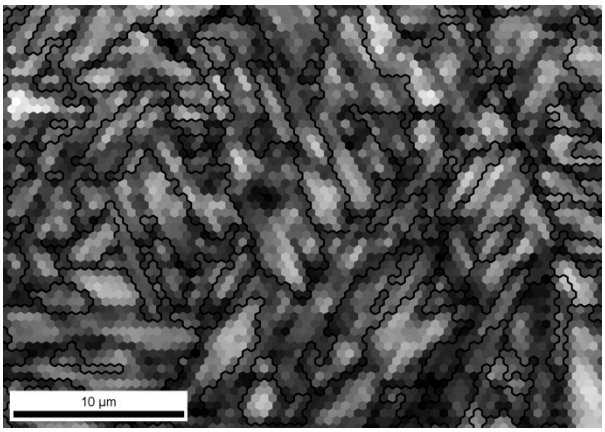

Figure 5: Post-processed pattern quality map for EBSD data collected using the NSS software on the Leo 1530 FESEM.

2.3.1.4 XRD Characterization

In parallel to the SEM-based characterization of the received HT-9 cladding, X-ray diffraction spectra were collected. Two different diffractometers were used: 1) STOE Bragg-Brentano Cu K-alpha with post-sample monochromator; 2) Bruker D8 Discovery Cu K-alpha with 2D detector. As only diffractometers with Cu x-ray sources were available, the older STOE diffractometer was initially selected, as the post-sample monochromator would eliminate excess background data resulting from fluorescence. Unfortunately, due to the geometry of the available sample and the lack of precision alignment optics, only minimal data (I_{max} < 50 counts) was collected. The data collected when using the Bruker D8 diffractometer agrees with the STOE data despite the significant observed fluorescence background.

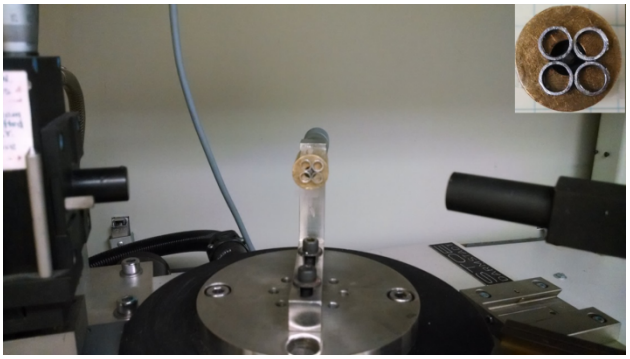

Figure 6: Four HT-9 cross-sections (inset) were positioned in the approximate Cu K_α x-ray beam of the STOE diffractometer due to the small

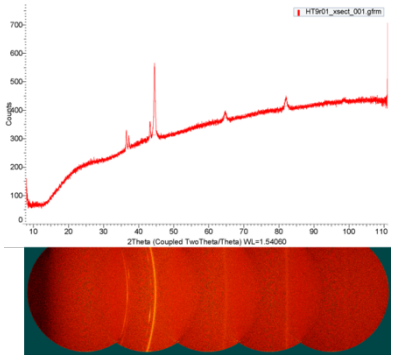

Figure 7: As-collected integrated (top) and raw (bottom) x-ray spectra for an HT-9 cross-section analyzed with the Bruker D8

cross section of each and the lack of positioning optics.

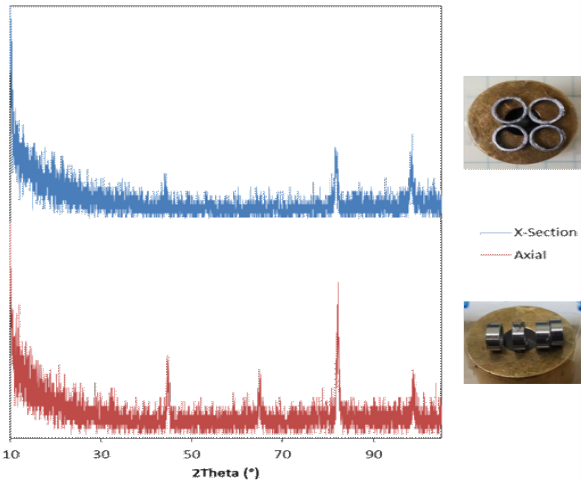

Figure 8: XRD spectra for as-received HT-9 collected in the cross section and axial orientations with the STOE diffractometer. The peak at ~64° here seen only in the axial orientation data was seen in the Bruker data for the cross-section.

diffractometer. The significant background is due to the pairing of a Cu K_α x-ray beam and the presence of iron in the sample.

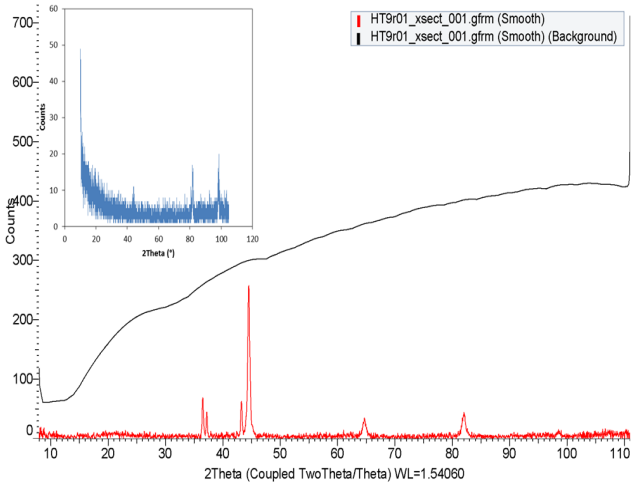

Figure 9: XRD spectra from both the STOE (inset) and Bruker D8 diffractometers. Despite the large background in the Bruker data due to Fe fluorescence, data quality is improved due to the D8's positioning optics.

2.3.1.5 Ion Milling & Characterization

Four ion milling programs were conducted with HT-9 samples. The primary parameters adjusted between each trial were the sample height and the ion beam energy (Table 3).

Table 3: Comparison of sample height and ion milling energy for HT-9 samples

Trial #	Sample Height (mm)	Beam Energy (keV)	Total Milling Time (hr.)
0	11.13	3 – 6 keV	1.5
1	10.85	6 keV	4
2	10.85	3	60
3	10.0	3	35
4	10.0	6kV-3kV cycles	25

For Trials #0 and #1, it was noticed that a fair amount of discoloration was occurring on the sides of the sample, and that the discoloration darkened as milling time increased. However, this discoloration only covered the bottom 7mm of the sample's side (Figure **10**). Milling also progressed very slowly but by the end of the trials scattered ellipsoidal depressions were noticed in the surface of the sample, with the elongated axis aligned in the radial direction. These depressions were also detected in Trial #2 (Figure **11**).

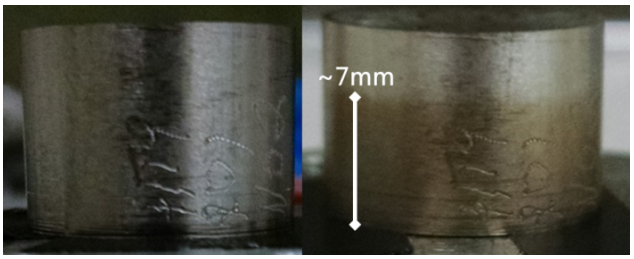

Figure 10: Optical photographs of the same sample before milling (left) and after 13 hours of 3kV milling (right) highlight the discoloration that occurs and strengthens with increasing milling time.

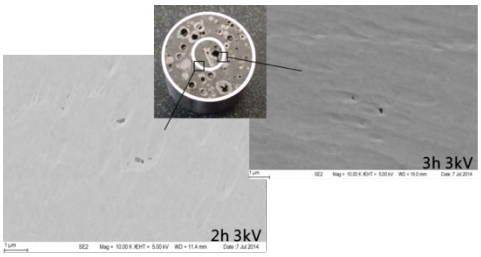

Figure 11: Radially aligned ellipsoidal depressions offer confirmation that some beam fraction is able to act upon the sample surface.

Trial #2 again used the same sample after a short refinishing step to remove effects from Trial #1 ion milling. Milling was performed only at 3kV, for varied amounts of time at first, and then in batches of 10 hours of continuous milling. In between milling sessions, surface features such as scribe marks or microhardness indentations were observed to verify that surface modification was occurring in each milling session (Figure **12**).

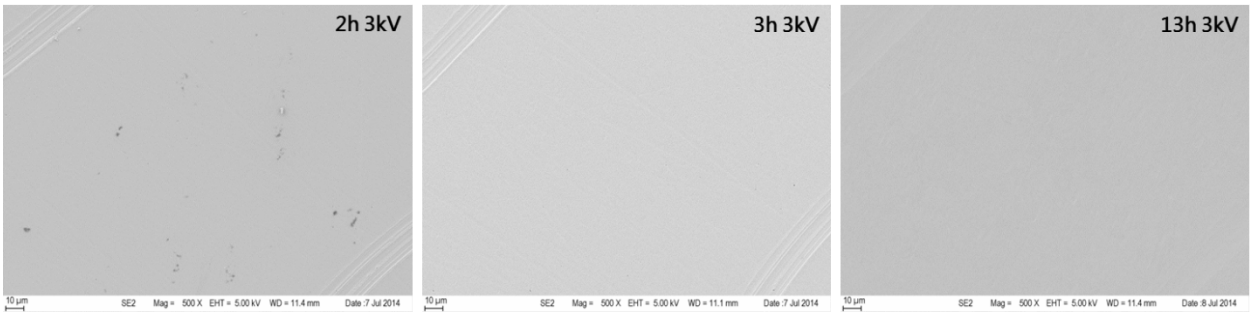

Figure 12: Diamond scribe markings on the surface of the sample are progressively less noticeable as the amount of ion milling increases. The pictured scribe marks are roughly aligned in the radial direction.

In addition to tracking the quality of EBSD patterns as a function of ion milling duration and energy, a second measurement of surface quality was desired. It was hypothesized that, due to the surface sensitivity of EBSD pattern collection – electrons captured by the detector originate in the extreme near-surface volume – monitoring the surface roughness could serve as an adequate predictor of the progress of the ion milling procedure. As the duration of ion milling increases, the exposed sample surface should homogenize and the measured surface roughness should decrease. At some critical surface roughness, deformation layers that resulted from the rough grinding steps will have been milled away, and the exposed surface will support high-quality EBSD analysis. To monitor the surface roughness as a function of milling time and energy, a white-light interferometer was used to analyze the same 8 areas, distributed evenly across the circumference of the HT-9 cladding cross-section. For each measurement, the surface roughness and peak-valley differential were recorded, in addition to a contour map.

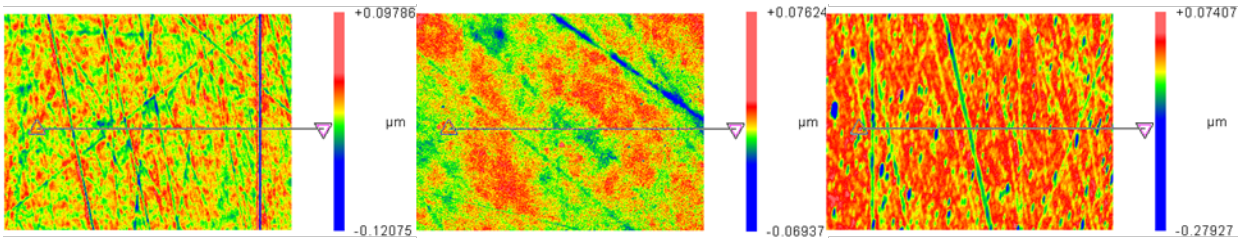

Figure 13: Optical profilometer contour maps of epoxy-mounted HT-9 steel at surface finishes from (l) 1200 grit SiC abrasive, (c) colloidal SiO2 polishing, and (r) 4 hours of 6kV argon ion milling. In the 4h6kV image, the ellipsoidal indentations appear in blue.

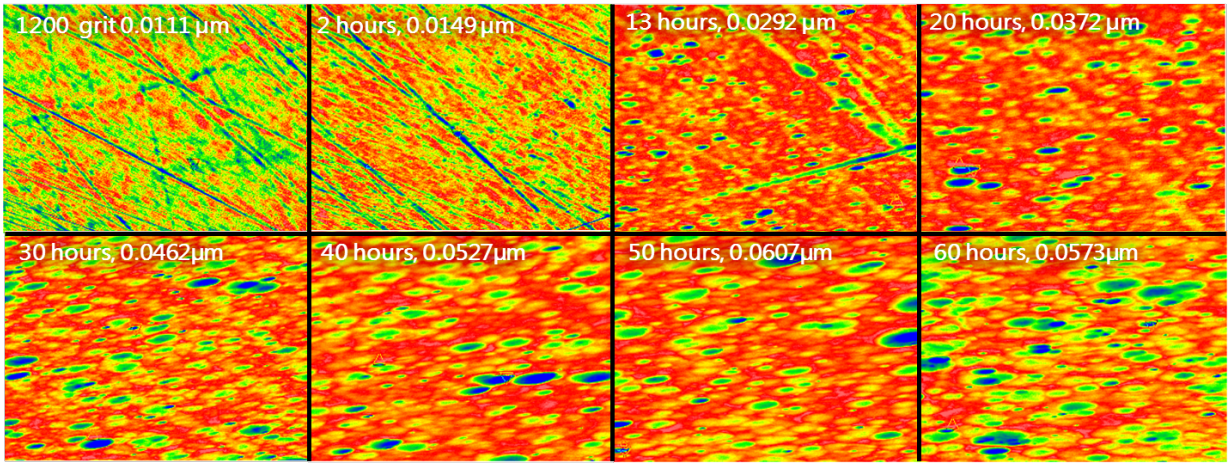

Figure 14: Surface contour plots as a function of total milling time with 3kV Argon ions from 0 to 60 hours (Trial #2). Surface roughness is reported as rms. All contours shown are from the same approximate location on the same sample.

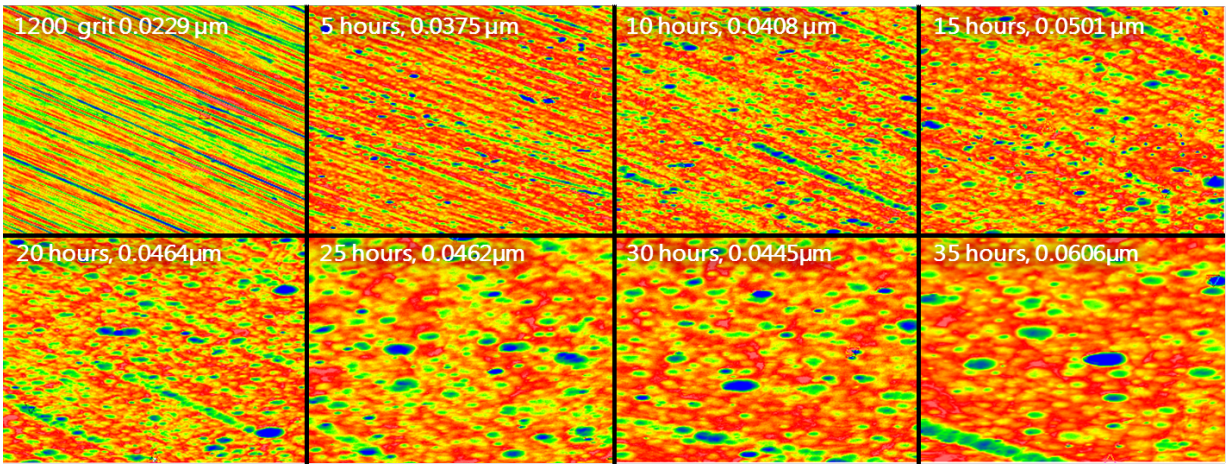

Figure 15: Surface contour plots as a function of total milling time with 3kV Argon ions from 0 to 35 hours (Trial #3). Surface roughness is reported as rms. All contours shown are from the same approximate location on the same sample. This sample is 0.85mm shorter than that in Trial #2 (Figure 14).

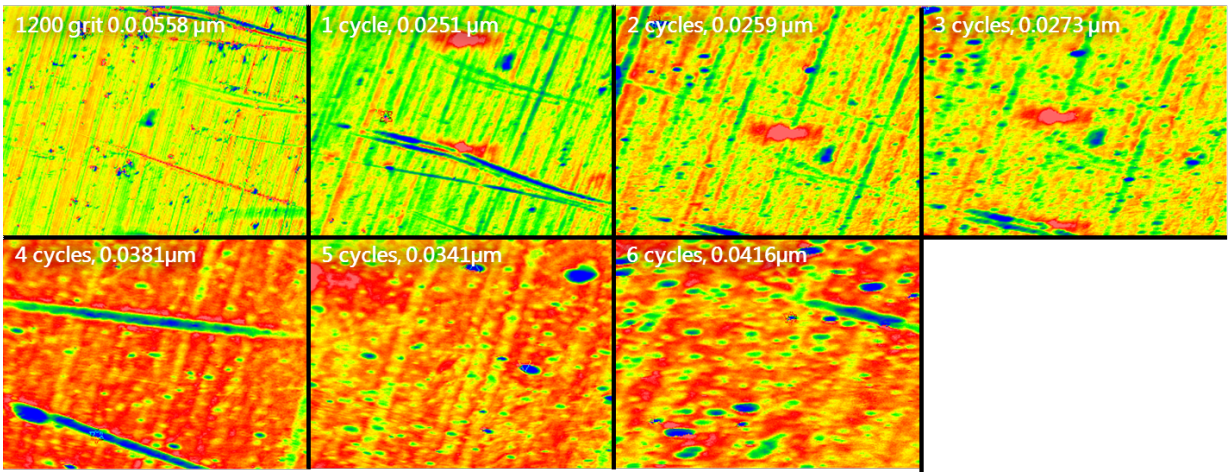

Figure 16: Surface contour plots as a function of milling cycles (Trial #4). Each cycle involved 3 hours of 6kV Argon ion milling followed by 1 hour of 3kV Argon ion milling. This sample is the same height as in Trial #3 (Figure 15).

Observation of surface roughness as a function of milling time did not trend in accordance with the initial hypothesis. As the exposure to ion milling increases, so does the surface roughness. As evidenced in Figure **14**-Figure **16**, increasing milling does reduce the prominence of surface features such as polishing scratches and indentations. Plotting the both the arithmetic average and the RMS average of the data yields monotonically increasing functions of surface roughness as measured by the optical profilometer with increasing ion milling time.

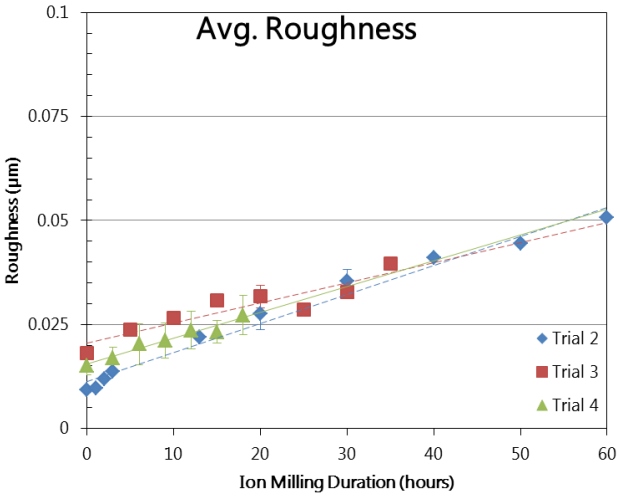

Figure 17: arithmetic average surface roughness as a function of milling time for each of the long trials

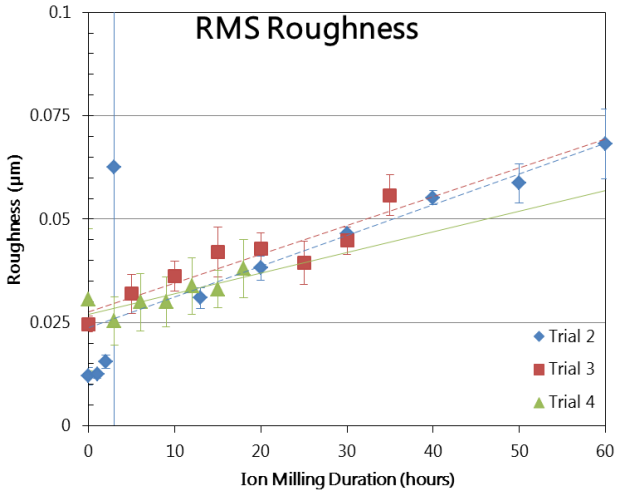

Figure 18: Root-mean-square surface roughness as a function of milling time for each of the long trials.

Despite the continuous increase in surface roughness, quality metrics for the EBSD patterns indicates monotonic increases in pattern quality. The quality of collected EBSD images does not start to become appreciably recognizable until about 75% indexed points. However, this is a subjective measure and as such, it was appropriate to track the more objective measures in Figure **19**.

To characterize the quality of any given EBSD pattern, several factors were tracked. This includes the fraction of indexable points, the number of points altered when performing a "grain dilation" post-processing step, and the number of indexed points altered when neighboring confidence indexes are correlated together. The indexable fraction desired is 100%, and similarly it is desired that no data points need to be adjusted in post-processing to obtain quality data. As Figure **19** shows, a reduction in height from 10.85mm to 10.0 mm is significant enough to reduce the required milling time from 50-60 hours to 35 hours. In Trial #4, the same sample height was used and the independent variable became the ion gun energy. Doubling the primary milling energy from 3kV to 6kV followed by a 1 hour cleaning session reduces the required milling time from 35 hours at 3kV to 18 hours of 6kV milling. These are promising reductions in required milling time, with additional gains likely following a second round of lowering the sample height relative to the TEM mill's stage floor.

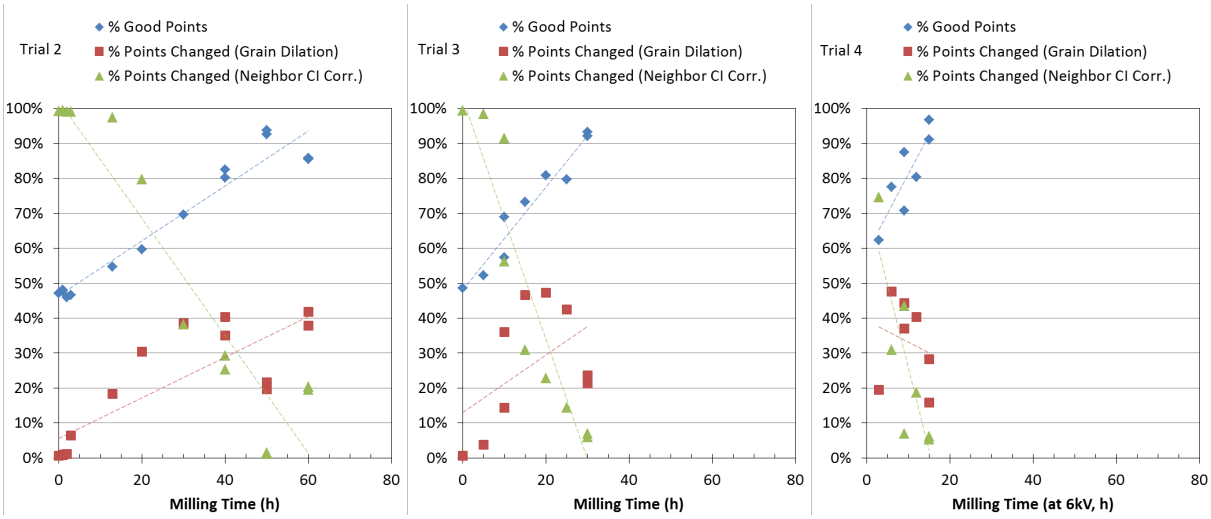

Figure 19: Comparison of EBSD quality metrics over time in each milling trial. Reducing the sample height and increasing the ion energy are shown to decrease the number of milling hours required to obtain a >90% indexable fraction. Horizontal axes are the same scale and size.

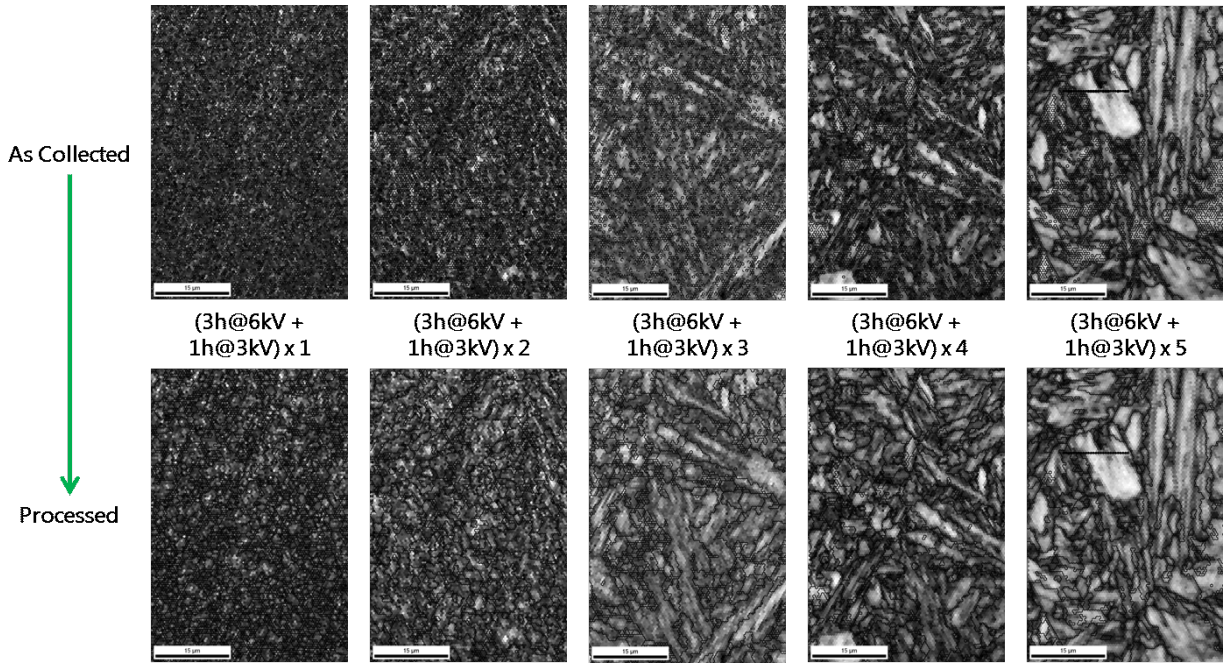

Figure 20: Image Quality Map for Trial #4 as a function of ion milling cycle. The first two cycles show no retrievable data.

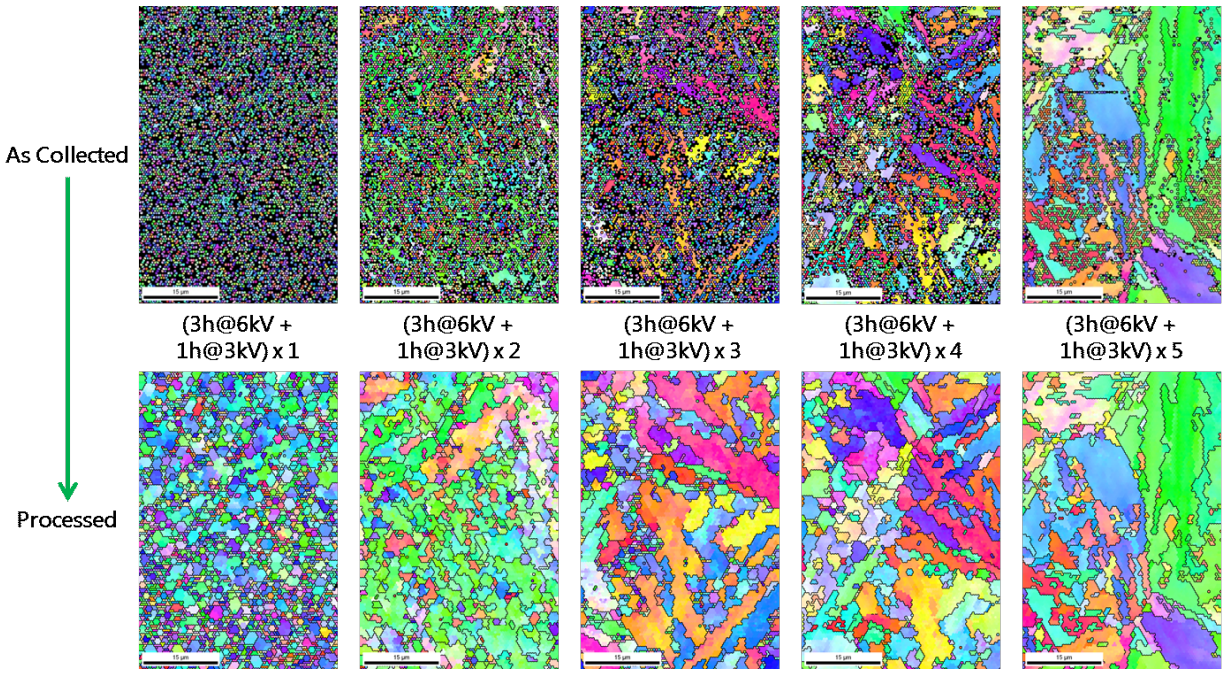

Figure 21: Inverse Pole Figures for Trial #4 as a function of ion milling cycle. Despite the processing routine's results for the first two milling sessions, it is apparent from the raw data that no reliable data was extracted until at least the 3rd milling cycle.

2.3.1.6 Remaining Work

Prior to completing Trial #2, Vickers microhardness indentations were impressed into the surface of the HT-9 stock being analyzed. These indentations were then tracked and imaged with each milling session using both the Zygo optical profilometer and the Leo 1530 FESEM. The

knowledge of how quickly and how symmetrically these well-defined initial shapes deform with increasing milling times is a very important parameter to consider and plan for when designing an analysis program for obtaining 3-D slices of a given region.

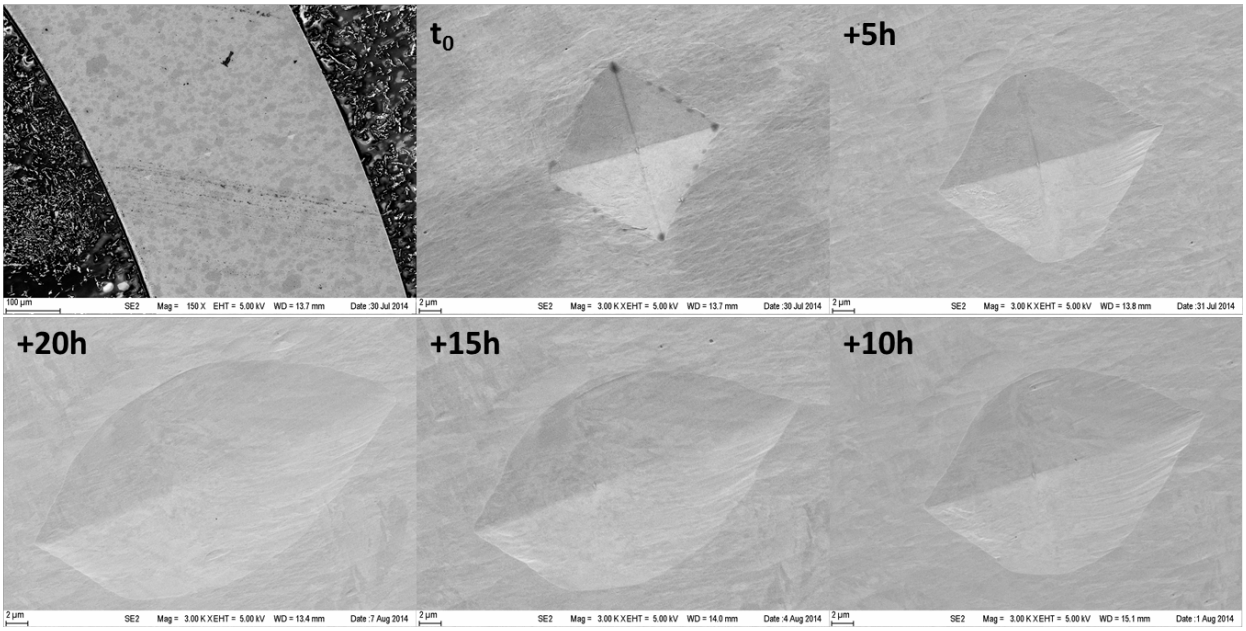

Figure 22: Clockwise from top left: Evolution of a Vickers microhardness indentation. As milling time increases, the indentation is smeared along the radial direction, the direction that is parallel to the incoming ion beam. In between each image, the sample was milled for 5 hours at 3kV.

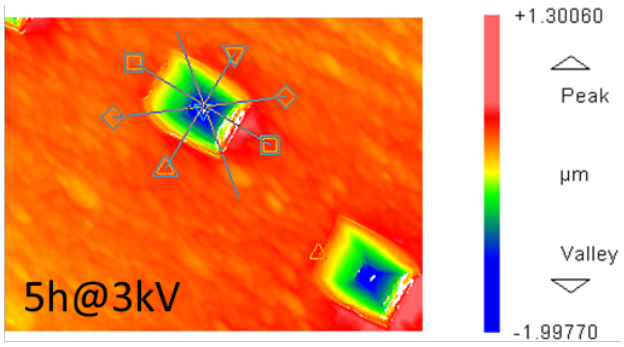

Figure 23: Optical profilometer scan of two Vickers indentations used to track the progress and completeness of ion milling.

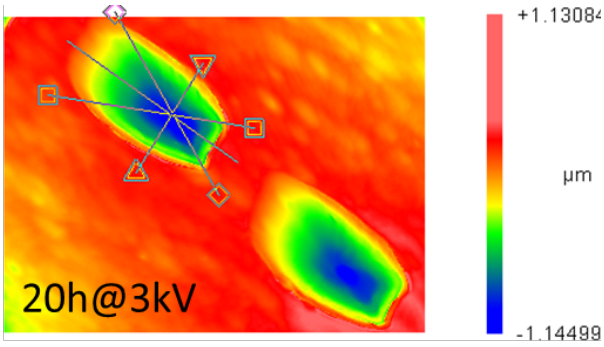

Figure 24: After 20 hours of exposure to 3kV Argon ion, the indentations have still not faded in any appreciable manner. Rounding of the edges is observed, with the smoothing occurring in the local radial direction.

It remains to be seen if further reduction of the sample surface height within the Model 1050 chamber will result in more favorable beam contact and thus more even material removal, instead of the anisotropic nature currently observed.

2.3.2 SiC/SiC Composite

The received SiC/SiC composite is a rectangular sheet measuring 4 cm x 6.8 cm x 3 mm. that is commercially known as Hi-Nicalon Type-S fiber. The material appears to have a brownish / bronzed tint to it. The as-received material was characterized in the SEM with energy-dispersive x-ray spectrometry (EDS), and with x-ray diffractometry (XRD).

2.3.2.1 Initial Characterization

The SiC/SiC composite is visibly multi-layered. Shipping materials received from INL indicate the sample is known as Hi-Nicalon Type-S fiber and contains 4 layers. The long dimension of the received SiC/SiC stock material is hereby referred to as its longitudinal direction. Seven samples were prepared from a horizontal strip of the SiC/SiC bulk, maintaining the relative orientation between longitudinal and transverse orientations.

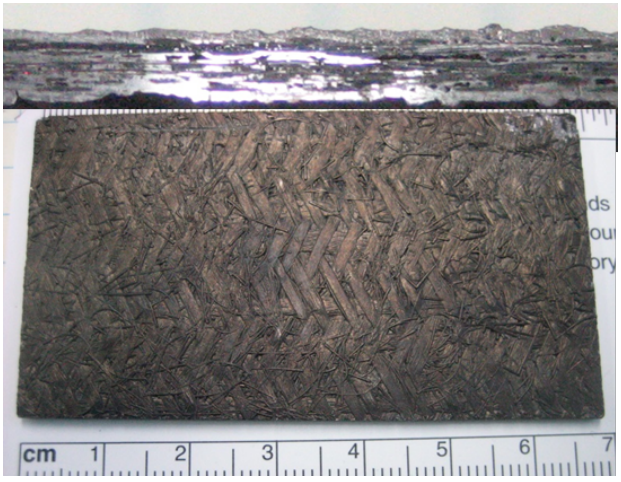

Figure 25: As-Received Hi-Nicalon Type-S Fiber SiC/SiC fiber composite. The layer structure is visible in the top inset.

Figure 26: Transverse (top) and longitudinal (bottom) SiC/SiC cross-sections mounted in conductive epoxy.

2.3.2.2 EDS Results

Analysis of the received material via EDS was performed as a sanity check, as the sensitivity of EDS to materials such as carbon, silicon, and nitrogen is extremely low. No additional elements were detected beyond silicon and carbon.

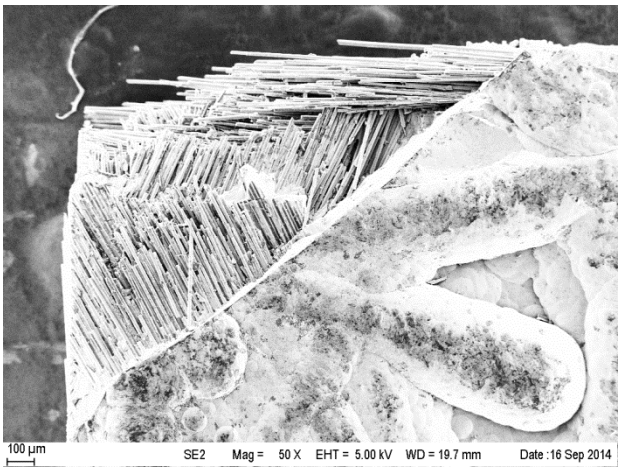

Figure 27: Plan view SEM image of the exposed fibrous strengthener underneath the SiC matrix phase.

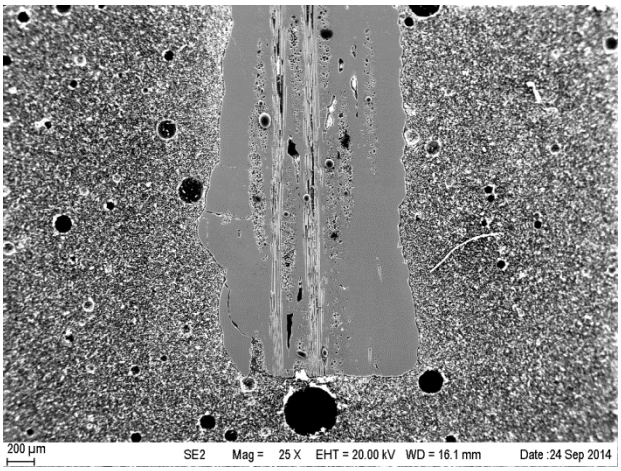

Figure 28: Longitudinal cross-section of the SiC/SiC fiber composite. Bundles of fibers can be seen running lengthways and also lying normal to the plan view.

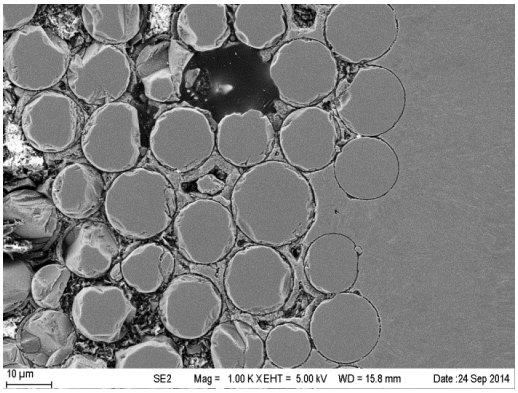

Figure 29: SiC fibers in a SiC matrix

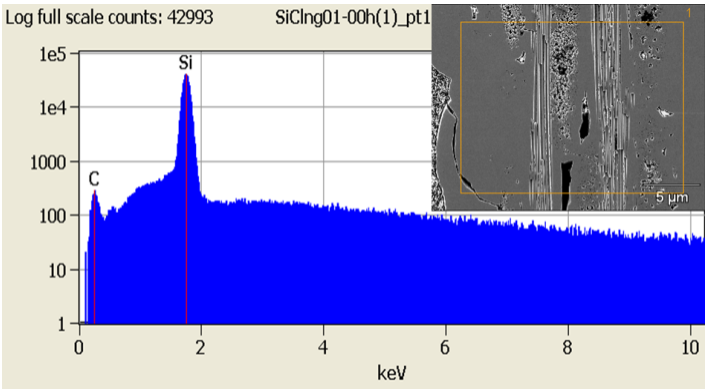

Figure 30: EDS point-and-shoot spectra for the rectangular region outlined in the inset. Only Si and C were identified in the spectra.

2.3.2.3 XRD Characterization

Plan-view x-ray diffraction was performed using a Bruker D8 Discovery diffractometer. Due to the lack of iron in the sample, no fluorescence behavior is observed.

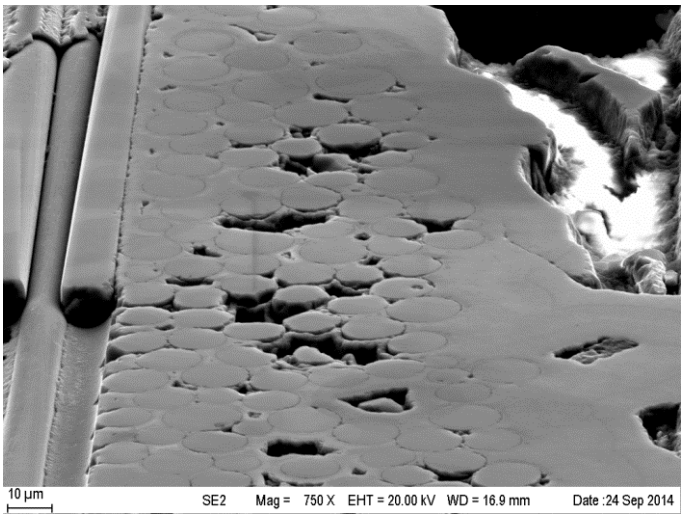

Figure 31: SiC/SiC composite at a 70° tilt angle. Fibers running normal to the surface are plainly visible, as are a few fibers running along the surface.

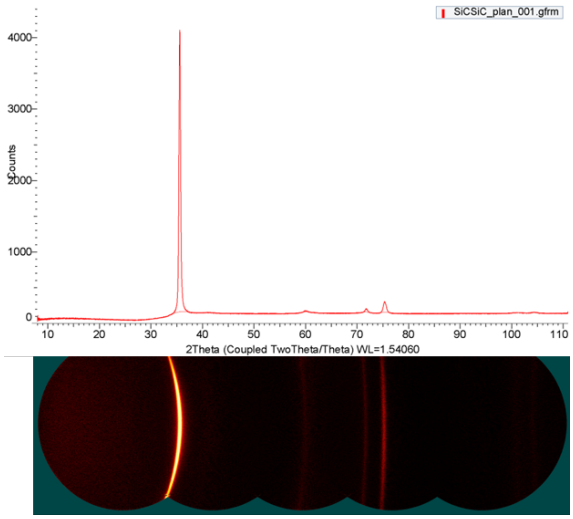

Figure 32: Integrated and raw XRD spectra for the plan view of the Hi-Nicalon Type-S SiC/SiC composite

2.3.2.4 Remaining Work

It remains to be seen how this particular SiC/SiC fiber composite will behave under ion milling. Furthermore, determination of which microstructural components to focus on between ion millings needs to be settled. Given the relative hardness of SiC as compared to HT-9 steel, it is likely ion milling will take longer to achieve the same results as compared to HT-9.

2.3.3 Zircaloy-4

During FY14 we began collaborating with Gatan, Inc. to explore additional broad ion beam sample preparation techniques. A sample of cold-worked stress-relieved Zircaloy-4 tubing was sent to their laboratory for preparation with an Ilion cross-sectioning system. This system differs from the PECS in that it uses a titanium mask to shield the side of the sample from ion erosion and focuses the beam nearly parallel to the sample face. As compared to manual sample preparation methods, this new technique increased the number of points that were successfully indexed with EBSD by 60% and doubled the average confidence index of the dataset. This work will continue during FY15 with a goal of achieving HR-EBSD quality results.

Two samples from Zircaloy-4 cladding tube were sent to UW for characterization and ion milling. Due to the high propensity of Zircaloy-4 for oxidation, no exploratory work is planned for the two samples. After successful demonstration with HT-9 steel and the SiC/SiC composite, including adequate vacuum preparation, ion etching and EBSD experiments with Zircaloy-4 will begin.

A Zircaloy-4 sample was analyzed with a Bruker D8 Discovery diffractometer to assess its current state. Scans were taken of the cross section, and along the axial and transverse directions. Scan differences, likely due to the method of fabrication, are detected between the cross-section scan and the scans that impinge on the cladding's external surface.

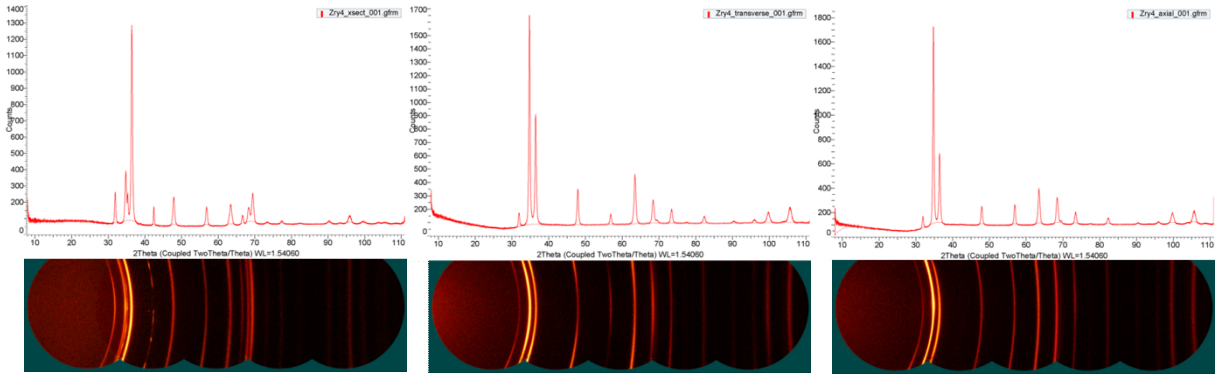

Figure 33: XRD spectra for the Hi-Nicalon Type S SiC/SiC fiber composite: (l) Cross-section scan, (c) longitudinal scan, (r) axial scan. The axial and longitudinal scan are quite similar, but have different peak intensity ratios than the cross-section scan, in addition to two much more prominent peaks at ~100° and ~106°.

2.4 High Resolution Electron Backscatter Diffraction

Milestone 2 requires the implementation of the high-resolution electron backscatter diffraction technique to estimate dislocation density in 2D datasets. Accordingly, a high quality 10 µm x 10 µm HR-EBSD dataset of HT9 cladding was recovered during FY14. With a spatial resolution of 50 nm, the 10 µm x 10 µm dataset resulted in 40,000 individual points. Inverse pole figure (IPF) and image quality (IQ) maps of the HT-9 material are plotted in Figure **34**(a) and 1(b).

In order to estimate residual strain and dislocation density within the HT-9 material, CrossCourt software from BLGVantage was purchased. This software package automates the cross-correlation technique needed to measure small variations between each electron backscatter pattern and a chosen reference pattern within each grain. Figure **34** (c) contains an example reference pattern from the HT9 dataset with 20 overlaid regions of interest utilized during the cross correlation process. As part of the software purchase, BLGVantage provided two days of onsite training at INL.

Figure **34** (d) through (h) contain CrossCourt results for the HT-9 dataset. The angular resolution of the high-resolution kernel average misorientation map contained in Figure **34**(d) is 100 times better than the standard EBSD version. Figure **34**(e) - (g) contain plots of ε_{22} strain, σ_{22} stress, and Von Mises stress, respectively. Lastly, a plot of the geometric necessary dislocation is presented in Figure **34**(h). This represents a lower bound estimate within the HT-9 material. The software is also able to disassociate the dislocations into both edge and screw components (not shown due to space limitations).

Note that the results in Figure **34** assume the material is a single phase of ferrite with elastic coefficients based on the default software settings for BCC iron. Future work is needed to differentiate the martensite and ferrite phases. We have discussed this problem with the CrossCourt developers and they are open to working with us on a solution to enable this functionality.

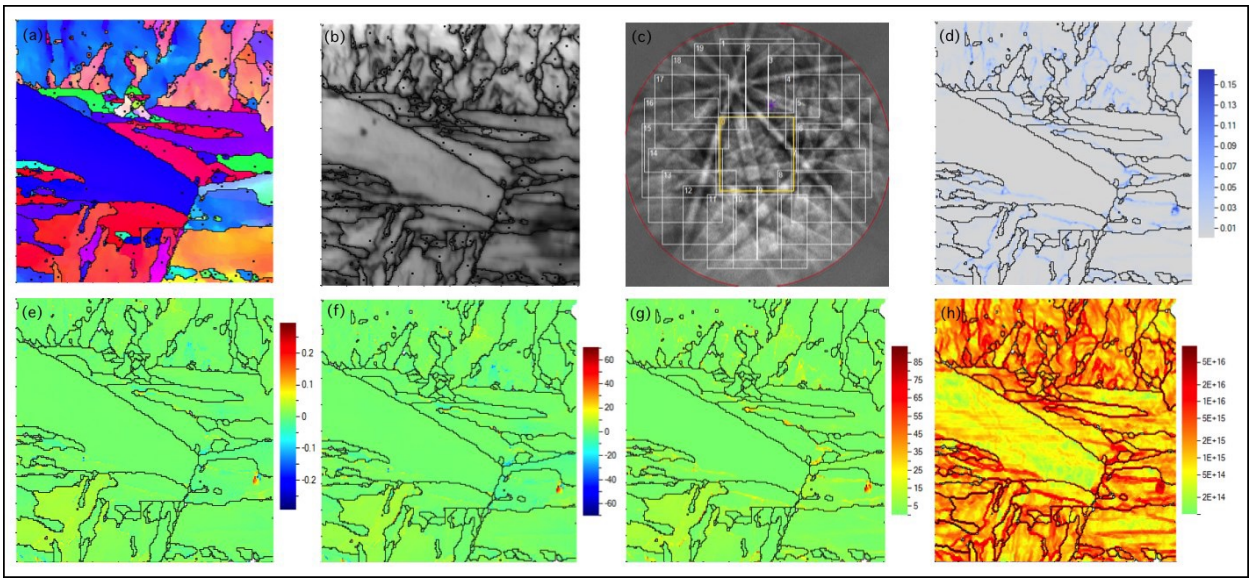

Figure 34: Results from CrossCourt analysis of HT-9 cladding: (a) inverse pole figure map, (b) image quality map, (c) reference EBSP with 20 regions of interest overlaid onto pattern, (d) high resolution kernel average misorientation map, (e) ε_{22} strain map, (f) σ_{22} stress map, (g) Von Mises stress plot, (h) geometric necessary dislocation map

2.5 Equipment Development

As part of the work package this year, we contributed to upgrading the EBSD system on the radiological FIB at the electron microscopy laboratory. The HR-EBSD software requirements were not compatible with any of the EBSD systems at INL, which could look at high-dose radiological samples. The upgraded EBSD system will provide the highest possible quality EBSD data from the ion milled samples, and allow for the best evaluation of our preparation technique. With the previous systems there was some question as to sample preparation issues versus detector system issues. The new system will eliminate these detector issues allowing for quantitative analysis of sample preparations.

Additionally we have an active collaboration with Gatan, testing and developing new ion etching systems, which could expand our capabilities in the future. New systems currently in development are showing promise to greatly reduce milling times while also improving EBSD pattern quality.

3. FY15 Results

3.1 Parameter Development at UW

Building off the success with HT-9 cladding, UW began ion-milling studies of the SiC/SiC fiber composite and the Zircaloy-4 cladding using the same milling parameters. However, these parameters were quickly determined to be insufficient in producing quality surfaces for EBSD from both ground and polished surfaces.

3.1.1 SiC/SiC Composite

The composite nature of the microstructure provides a significant challenge to preparing quality surfaces for EBSD. Traditional grinding and polishing operations often leave the sample surface scarred and pockmarked due to the fiber fractures and pullout. Extensive surface irregularities can prevent the collection of useful background corrections necessary for EBSD analysis.

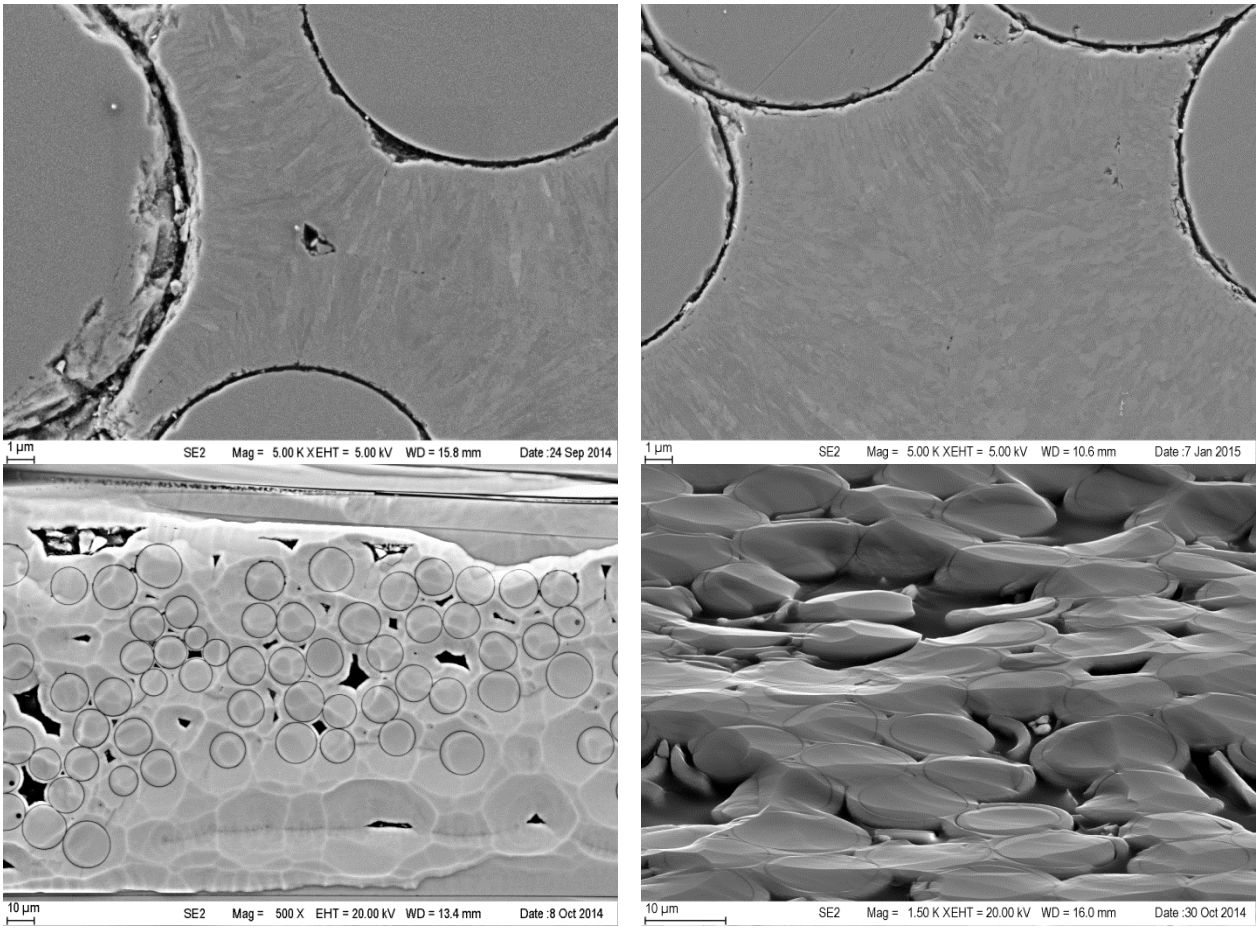

Figure 35: (a) SiC/SiC composite after 1200 grit grinding. The matrix microstructure is visible, showing a columnar structure with grain widths ~500 nm or less. (b) After polishing with colloidal silica, the matrix pattern is less distinguishable (c) Even after extensive ion milling, fractured fibers in the sample center are still present, along with high surface irregularities/damage in regions of interest, such as the fiber-matrix boundary as seen in (d)

At each point in the ion milling examination, EBSD patterns were attempted to be gathered from both the fiber and the matrix. Due to the extremely fine grain size of SiC in the fibers (~5 nm), EBSD patterns are not expected to be possible with SEM. EBSD analysis of matrix properties in Hi-Nicalon Type S may be possible, but ion milling was unable to improve the observed matrix surfaces to enable such analysis.

3.1.2 Zircaloy-4

Initial application of successful HT-9 parameters using 3 kV ions failed to yield EBSD patterns after 46 hours of milling. The sample was then polished with colloidal silica and then a low energy milling rate program was undertaken.

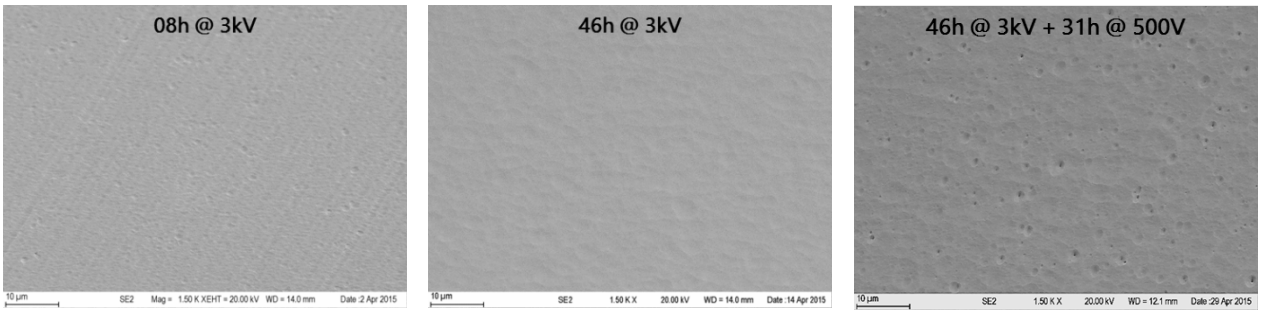

Figure 36: (a) Zircaloy-4-4 surface after 8 hours of ion milling, (b) after 46 hours of ion milling, (c) after another 31 hours at low energy. The surface evolution is consistent with that seen in HT-9 work in FY14, yet each time the sample was unable to produce an EBSD pattern.

In addition to using only ion energies of 500 eV or less, the SEM parameters used for generating the EBSD patterns were adjusted, eventually settling on 10 kV accelerating voltage with a beam aperture of 60 μm. Although individual patterns were now indexable, collecting full resolution scans of Zircaloy-4 is an ongoing challenge.

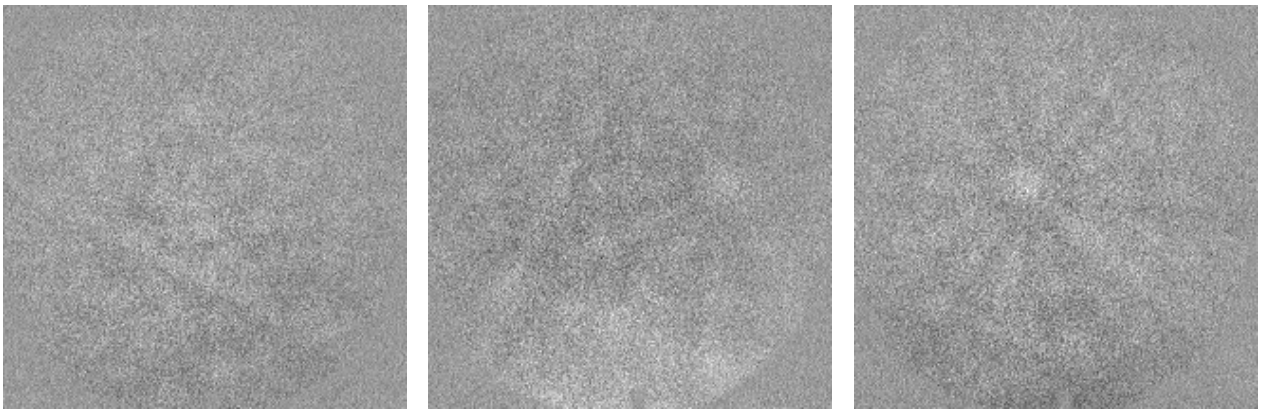

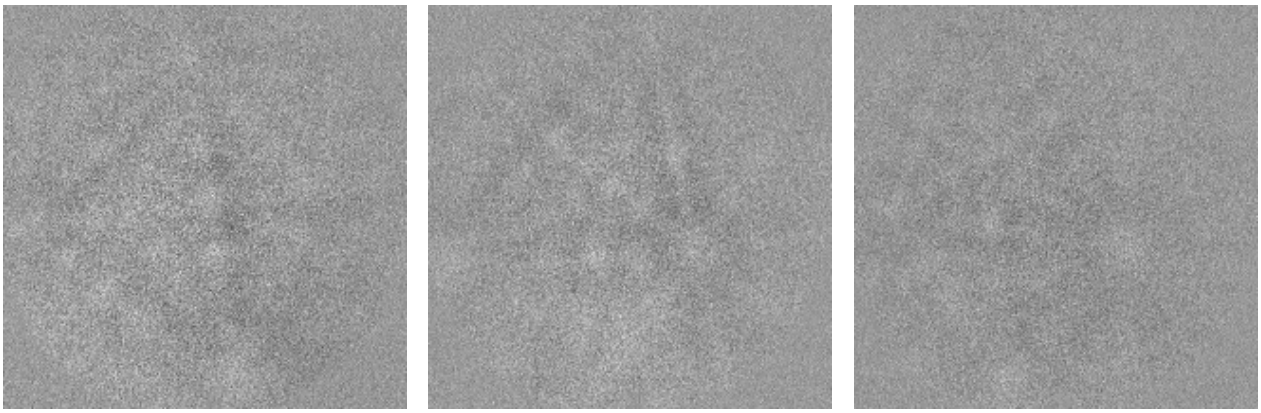

Figure 37: EBSD patterns collected at 10 kV with a 60 µm aperture at increasing durations of low-energy ion milling. (a) colloidal silica, (b) 5 min. 500 eV; (c) 15 min. 500 eV; (d) 30 min. 500 eV; (e) 150 min. 500 eV; (f) 210 min. 500 eV.

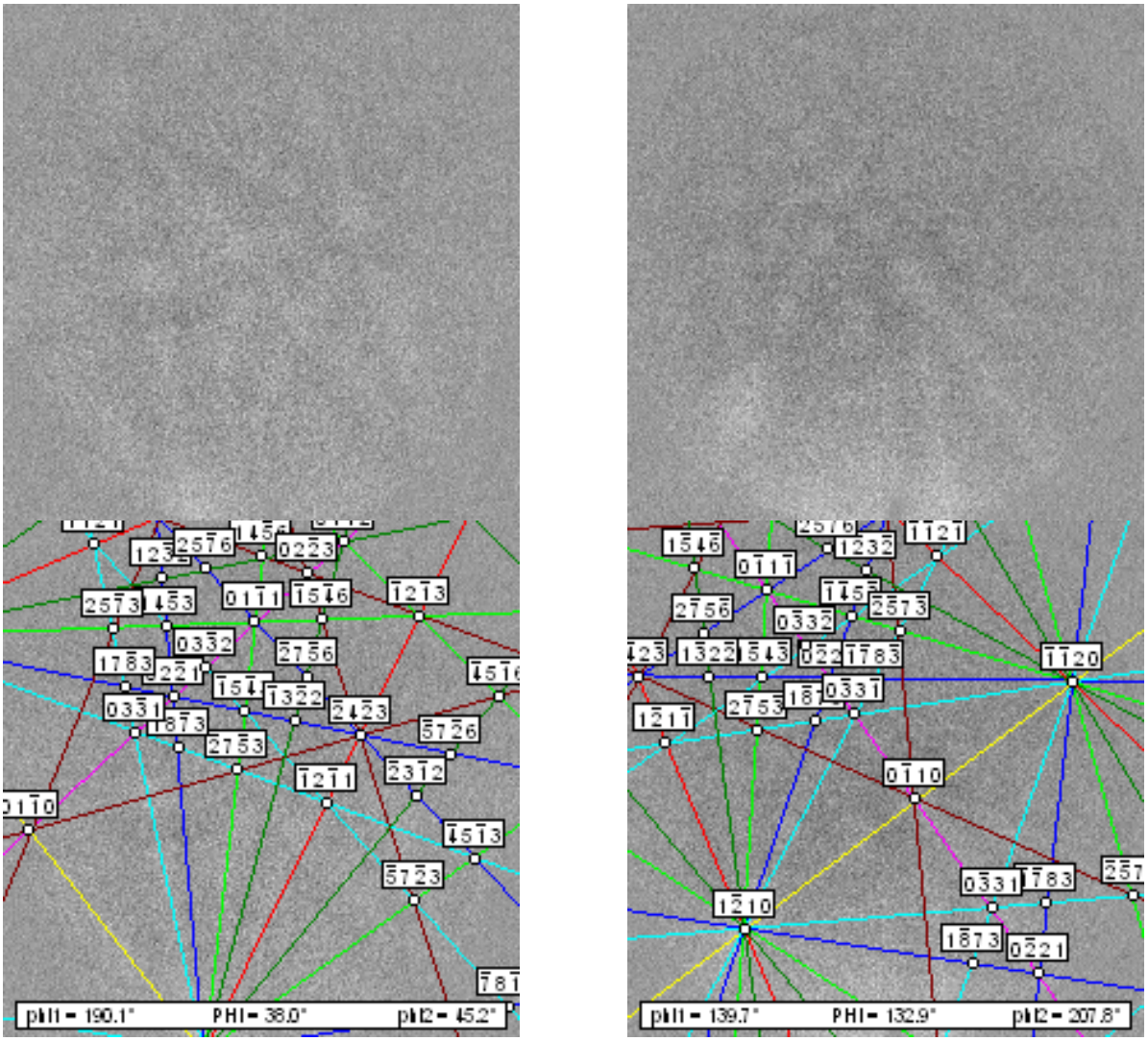

Figure 38: EBSD patterns and indexes after ion milling with 500 eV argon ions for (l) 270 min.

and (r) 450 min.

3.1.3 HT-9

3.1.3.1 Fischione 1050 Milling Rate Analysis

In FY14, initial work was undertaken to investigate the mechanics of ion milling in the Fischione 1050 instrument at the University of Wisconsin-Madison. This work was continued in more detail in order to facilitate serial sectioning in FY15. The locations of 10 Vickers microhardness indentations were measured using an optical microscope and image analysis (Figure **40**). Due to the milling geometry of the Fischione 1050, with two separate ion sources 120° apart, it is expected that the milling rate in the center of the sample will be higher than the milling rate outside of the center, where only one ion gun can act on the surface at a time. According to discussions with Fischione technical staff, each ion gun is configurable to produce a beam between 0.5 and 5 mm in diameter, while the standard configured diameter is 2 mm. Thus, for indentations within 1 mm of the sample center, we expect to find little anisotropy in the material removal rate, and increasingly radial anisotropy as the distance from the rotational center increases.

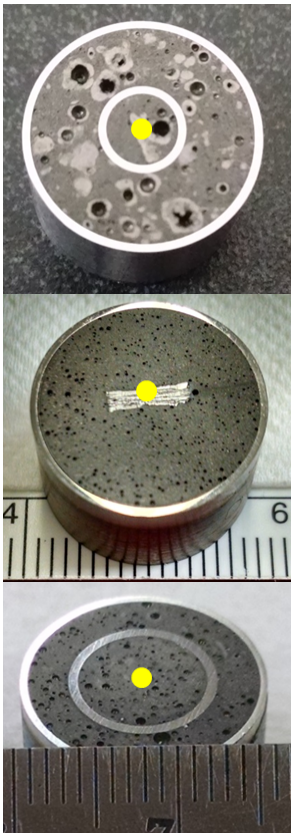

Figure 39: Approximate rotational centers of the previous HT-9 (top), SiC/SiC (mid.), and Zircaloy-4 (bottom) ion-

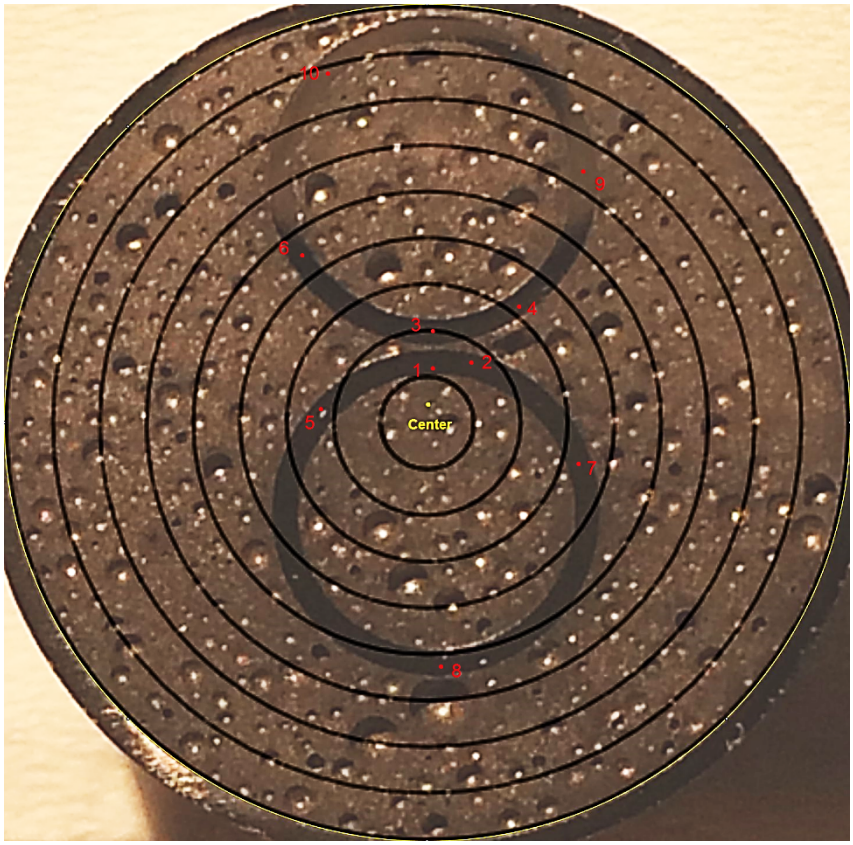

Figure 40: Diagram of indent locations (red) and distance from the rotational center of the sample, in 1 mm increments. Previous HT-9 regions studied were at a similar radius as indent 4, while the regions of the Zircaloy-4 sample were nearest to indents 6 and 8.

milled samples

Micrographs of indents 1, 3, and 4 are shown before and after 3 hours of milling with 6 keV argon ions. As expected, material removal around indent 1 is nearly isotropic, while indent 4 experiences the most anisotropy.

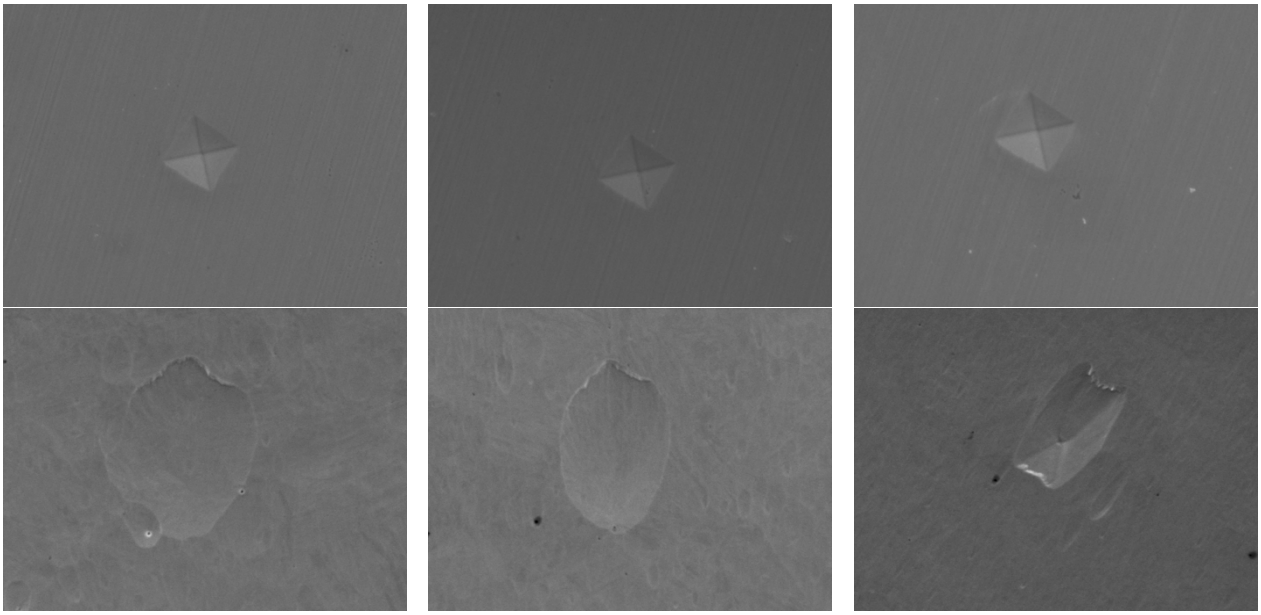

Figure 41: Indents 1, 3, and 4 before and after 3 hours of ion milling with 6 keV argon ions in the Fischione 1050 at the University of Wisconsin-Madison

Due to the large changes in the indents over the 3 hour milling period, the surface was reground to 1200 grit, and indents 1 – 3 were replaced. Each indent was analyzed using white light interferometry and 4 depth profiles were collected per indent after 1, 2, and 3 hours of ion milling at 6 kV energy. The depth profiles (Figure **42**) were used to calculate the depth of the indent after each hour. From the data, it was determined that milling for 21 minutes is sufficient to remove 75 nm of material from the surface near indent #1.

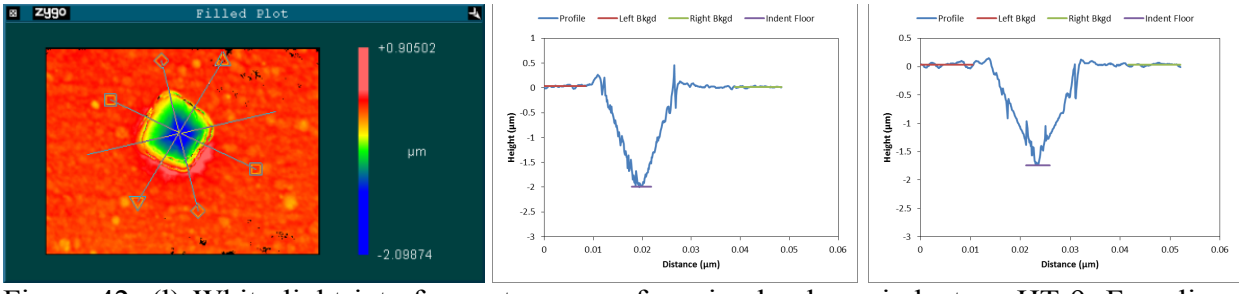

Figure 42: (l) White light interferometry scan of a microhardness indent on HT-9. Four linear scan profiles are collected per indent as indicated (c) A representative depth profile from indent #01 before milling. (r) After 1 hour of milling with 6 keV argon ions. The depth change of the Vickers indentation is 250 nm.

Table 4: Indent depth measurements for ion milling increments of 1 hour (total of 3 hours)

Trace						Statistics		User Confidence			
Time (hr)	Indent #	#1	#2	#3	#4	Average Depth (μm)	Standard Deviation (μm)	C1	C2	C3	C4
0	1	2.03	2.02	2.06	1.96	2.02	0.04 ± 1.9%	true	true	true	true
0	2	2.04	2.08	2.07	2.09	2.07	0.02 ± 0.9%	true	true	true	true
0	3	2.19	2.12	2.04	2.13	2.12	0.06 ± 2.9%	true	true	true	true
1	1	1.77	1.80	1.76	1.75	1.77	0.02 ± 1.1%	true	true	true	true
1	2	1.75	1.84	1.84	1.85	1.82	0.05 ± 2.5%	true	true	true	true
1	3	1.88	1.88	1.92	1.85	1.88	0.03 ± 1.6%	true	true	true	true
2	1	1.69	1.51	1.70	1.31	1.55	0.18 ± 11.9%	maybe	almost	maybe	almost
2	2	1.56	1.85	1.54	1.85	1.70	0.17 ± 10.3%	maybe	maybe	maybe	maybe
2	3	1.65	1.87	1.83	1.67	1.75	0.11 ± 6.3%	maybe	maybe	maybe	true
3	1	1.41	1.44	1.40	1.39	1.41	0.02 ± 1.5%	true	true	true	true
3	2	1.37	1.38	1.47	1.38	1.40	0.05 ± 3.3%	true	true	true	true
3	3	1.52	1.65	1.70	1.64	1.63	0.08 ± 4.6%	true	true	true	true

3.2 Parameter Development at INL

During FY15, research was conducted at INL to determine the correct broad-beam ion parameters needed to perform sample preparation with the Gatan PECS 682 system. Both HT-9 and Zircaloy-4 materials were evaluated.

3.2.1 Sample Holder Redesign

Based on feedback from UW and Gatan, a revised 1.25” diameter met-mount sample holders were machined for use in the PECS 682 system. The existing 0.75” tall holders are too tall for effective milling in the PECS. According to Gatan, a height of 0.276” – 0.315” (7-8 mm) is ideal. Using a tall sample holder results in the removal of material on the OD surface of the holder instead of the top as was previously shown in Figure **10**.

Figure 43: Redesigned sample holder with 0.276" - 0.315" height needed to optimize milling in the PECS

3.2.2 Temperature Analysis

An experiment was conducted to determine the degree of temperature rise the met-mount experiences during milling in the PECS. This is important to prevent unwanted off gassing of the epoxy used to encapsulate the reactor material in the mount. A test of the epoxy found the epoxy stable below 120 °C. A series of tests between 2 kV and 7 kV were performed for 1 hour increments and the temperatures recorded after each test. The temperature ranged between 26.5 °C and 109.1 °C (see Table 5) after 1 hour of etching time in the PECS. We conclude that it is safe to mill in the PECS at any voltage between 2 and 7 kV.

Table 5: Sample holder temperature as a function of voltage

Voltage (kV)	Temperature (°C)
2	26.5
3	35.6
4	52.5
5	66.6
6	88.4
7	109.1

3.2.3 HT-9

An EBSD analysis was conducted at CAES to compare standard sample preparation techniques to broad-beam ion methods. Two identical HT-9 samples (unirradiated) were epoxy encapsulated with a 50% nickel fill ratio in the new sample holder design. Both were hand polished to a 1 µm diamond finish. Next, one sample was polished in the PECS at 4.5 kV for 1 hour, 3 kV for 1 hour, and 2 kV for 2 hours. This was repeated 3 times for a total of 12 hours of etching. The second sample was polished in a VibroMet 2 vibratory polisher for 12 hours using a 0.04 µm colloidal silica suspension. Figure **44** contains the EBSD results of the two samples. EBSD was performed with a JEOL JSM-6610LV SEM and EDAX Hikari EBSD camera and OIM Data

collection software [7]. The average confidence index (CI) of the broad-beam ion prepared sample was 0.62. This is higher than the vibratory polished sample of 0.39.

The results indicate that PECS based sample preparation is a viable option for EBSD sample preparation of reactor materials. Please note that these results were not optimized to improve CI for publication. Equivalent results can be obtained from either method with additional polishing. The advantage of the broad-beam ion etching method is the reduction of radioactive dose to the technician during sample preparation. A second advantage is the absence of colloidal silica on the polished sample. This is a common problem with vibratory polishing samples, which causes a reduction of CI when performing EBSD scans. Third, surface oxidation is reduced since the sample can be removed from the PECS and loaded directly into the SEM for analysis. Vibratory polished samples must be cleaned before loading in the SEM to remove the colloidal silica suspension. This increases the samples exposure to oxidation mediums such as water and oxygen.

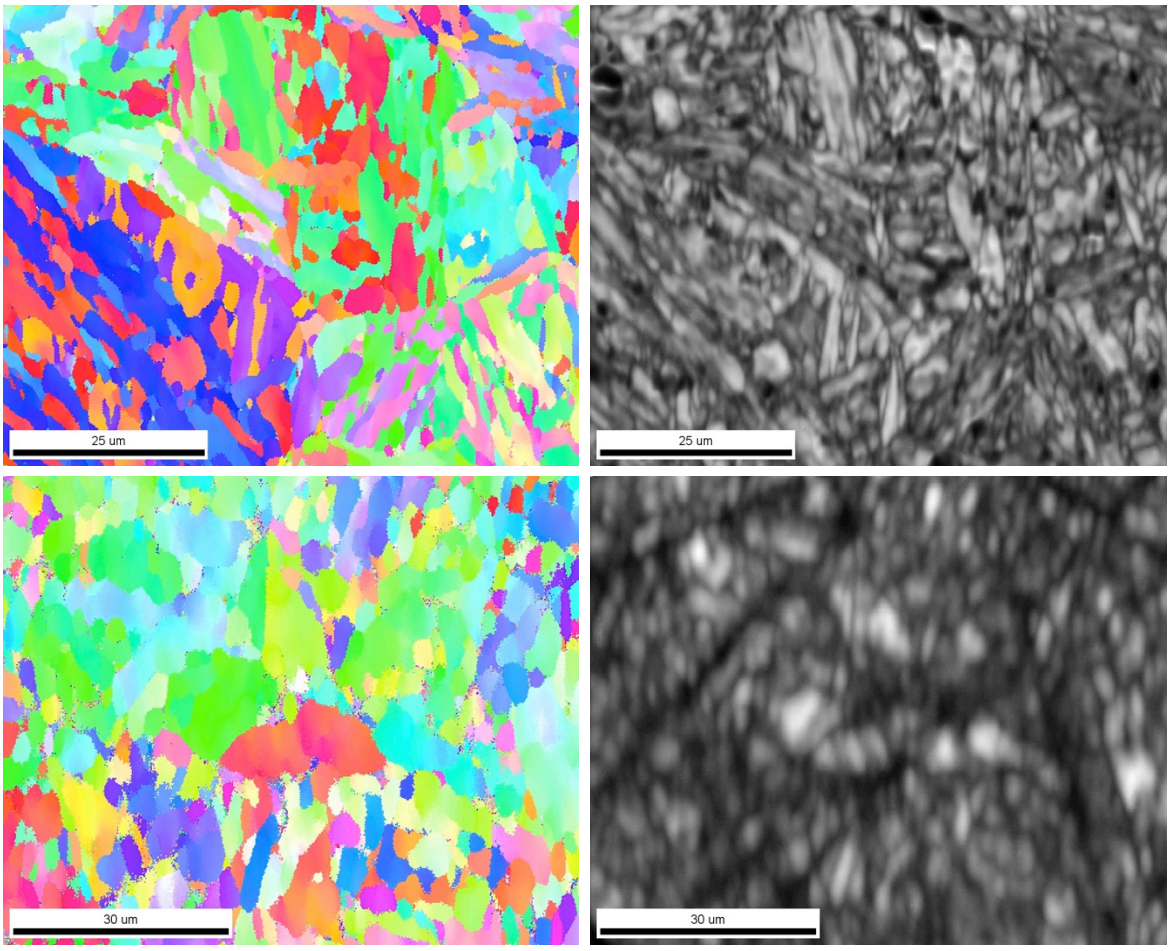

Figure 44: Comparison of HT-9 material prepared by broad-beam ion etching (top) and traditional polishing method (bottom). Inverse pole figure maps are on the left and image quality maps on the right. Results show that PECS based sample preparation is a viable option for sample preparation.

In order to establish a milling rate for the HT-9 material, a Hysitron TI-950 TriboIndenter was utilized to create a set of 7 indentations on the surface of the sample. The depth of the indentations ranged from 200 nm to 1.4 μm as shown in Figure **45**. The removal rate was tracked visually by recording SEM images at regular intervals. The milling rate at 4.5 kV was determined to be approximately 100 nm per hour for the HT-9 material.

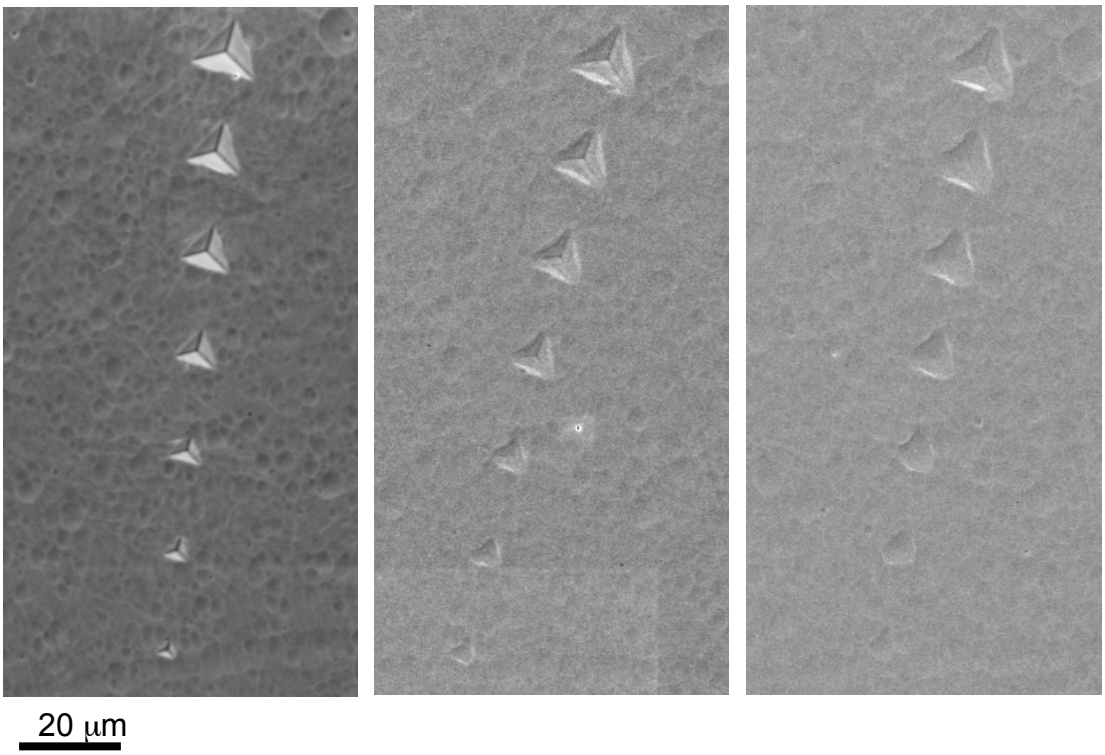

Figure 45: Milling rate analysis of HT-9 sample prepared with the PECS. The image on the left shows the 7 nanoindentation marks prior to etching. The middle image was recorded after 1.5 hours of milling at 4.5 kV. The right image represents 3 hours of milling. The milling rate was estimated to be ~100 nm per hour at 4.5 kV.

3.2.4 Zircaloy-4

Research to determine milling parameters of the Zircaloy-4 material was not as successful as the HT-9 work. Similar to the HT-9 experiments described in Section 3.2.3, an unirradiated sample was prepared and polished to a 1 μm diamond finish. Milling with a variety of ion voltages between 1.6 kV and 8 kV did not produce satisfactory results. Because the PECS has the capability to coat the sample, a thin carbon coating was deposited after etching but prior to removal from the system to determine if oxidation was causing the poor EBSD results. However, this did not improve the EBSD results.

A second irradiated Zircaloy-4 sample sourced from the BR-3 reactor was analyzed in an FEI Quanta 3D FEG FIB/SEM at CAES. A variety of low-energy milling passes were applied to the sample to determine if ion induced damage was occurring. EBSD results were similar to the PECS prepared sample. Nonetheless, after transitioning to a high-energy milling beam, good

quality EBSD results were obtained. Figure **46** contains EBSD results for the irradiated Zircaloy-4 sample after milling with a 30 kV - 15 nA ion beam. The average CI for the scan was 0.38. Using a high-energy ion beam is counter intuitive as Zircaloy-4 is known to be sensitive to ion damage. Additional research is planned for FY16 to replicate the FIB obtained results in the PECS. An 8-10 kV beam will be used without secondary low-kV mills.

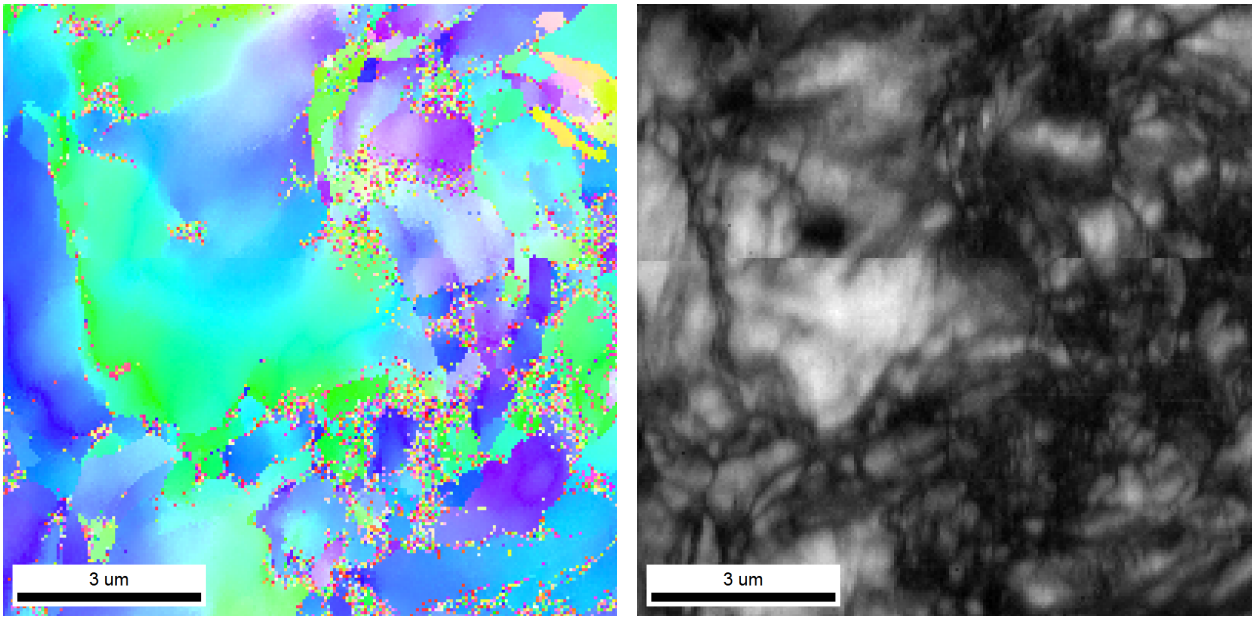

Figure 46: Irradiated Zircaloy-4 EBSD results from focused ion beam

3.3 HT-9 Serial Sectioning

In order to facilitate serial sectioning of the unirradiated HT-9 sample, three additional Vickers indents were placed on the HT-9 sample (see Figure **47**). These marks enable the user to quickly find the same sample region each time it is placed in the microscope. Because stage drift is problematic for large EBSD scans, a wait time of 1 hour was implemented after the sample positioning. When possible, beam shifting was used to return the scan to the desired position. If the stage was moved mechanically, an additional hour was added to the wait time. After the 1 hour pause, background subtraction of the EBSD camera was performed at a magnification of 750X.

A total of 6 EBSD slices were recovered during the serial sectioning process. Each scan was performed at 1500X magnification and covered an area of 32 µm X 32 µm. A square grid was used with a resolution of 75 nm in the x and y-directions. Figure **48** shows the EBSD results for the first slice of HT-9. As in FY14, the data cleaning procedure consists of a single iteration of grain dilation, followed by a grain confidence index standardization routine, and then a neighbor confidence Index correlation with a minimum confidence index of 0.1.

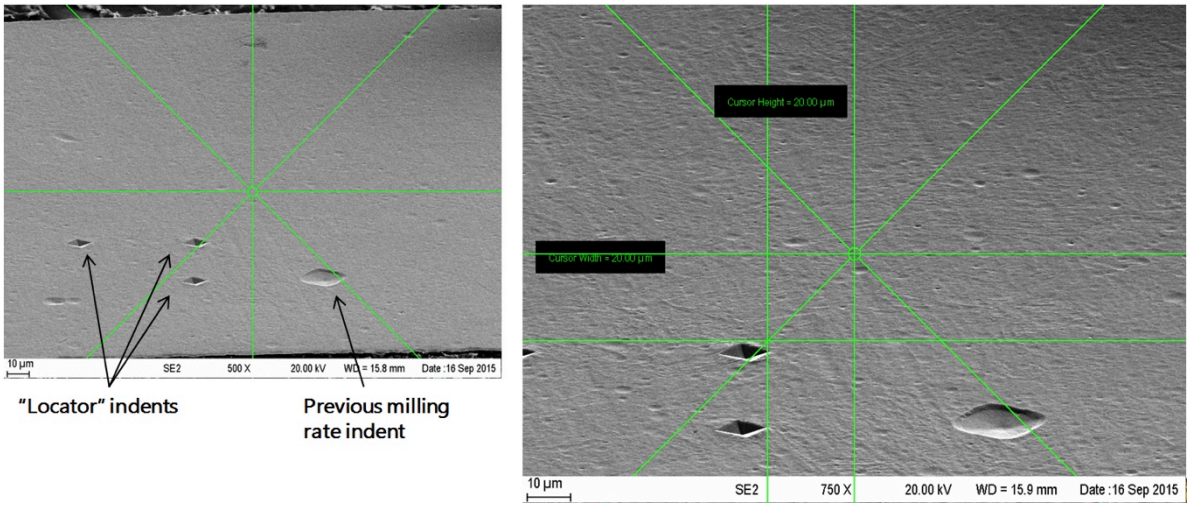

Figure 47: System of three Vickers indents used to return to the same sample area after each successive ion milling layer

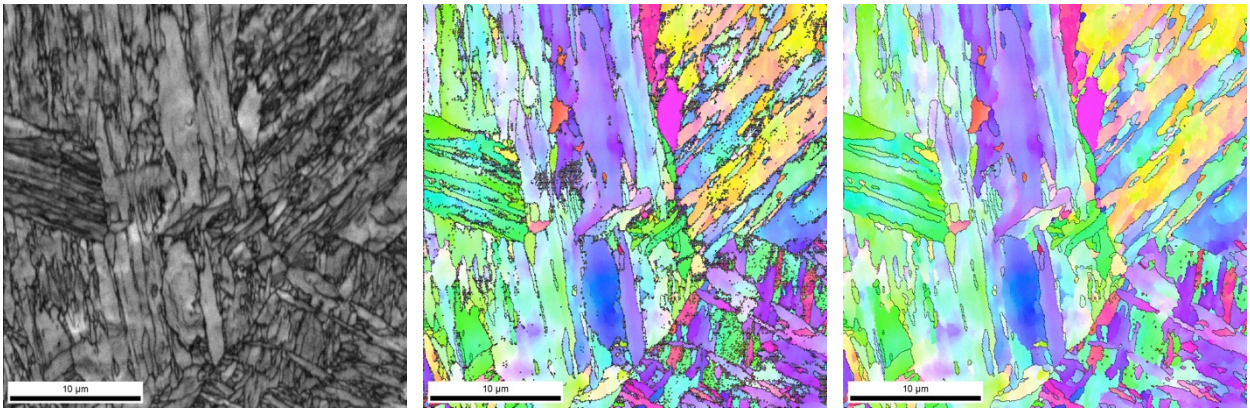

Figure 48: EBSD results for Slice 1; (a) Image Quality map; (b) Inverse Pole Figure before cleanup, (c) Inverse pole figure after cleanup.

Even with the additional 1 hour hold time after stage positioning, stage drift remained an issue throughout each of the 3 hour long EBSD scans. This is evident in Figure **49** for Scans 1, 3, and 6. The black regions represent hydrocarbon deposits caused by the electron beam as it rasters the sample surface. A second set of serial sections were attempted to improve the set of slices, but stage drift remained a problem.

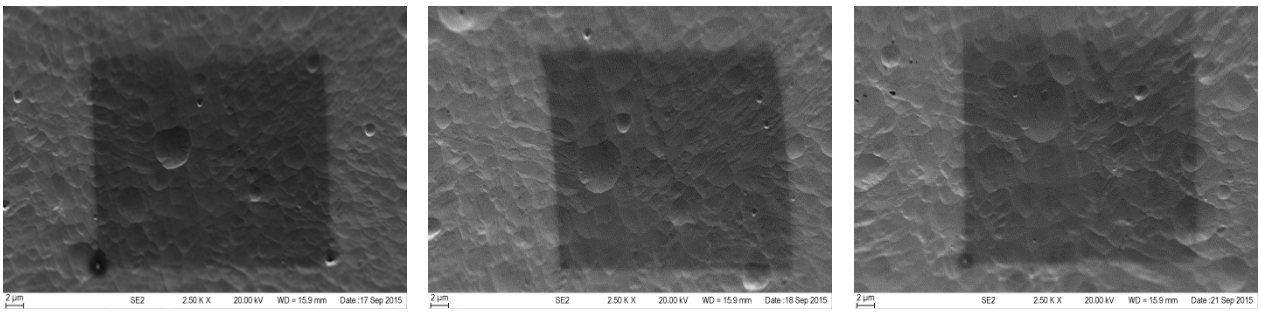

Figure 49: Post-EBSD SEM micrographs reveal the actual EBSD scan area. Due to uncompensated stage drift, the resulting scanned regions may not be identical between scans,

even with the same starting position (from left to Right: Scan #1, #3, and #6).

3.4 Reconstruction

In order to utilize the HT-9 serial sections within MARMOT, the slices must be properly reconstructed. A combination of MATLAB [8] and DREAM.3D [9-10] software were used to perform the digital reconstruction. Because Dream3D requires a square sampling grid, a custom MATLAB script was written to convert the hexagon OIM grid to a square grid. Post-processing (including cleanup, alignment, and cropping of the EBSD data) was performed with Dream3D. An algorithm based on "mutual information" was utilized for image alignment due to the lathe like features of the HT-9 microstructure that do not align properly when using algorithms based on crystallographic misorientation. An image of the reconstructed microstructure can be found in Figure **50** below. Lastly, a MARMOT compatible "txt" file was output using the Dream3D software.

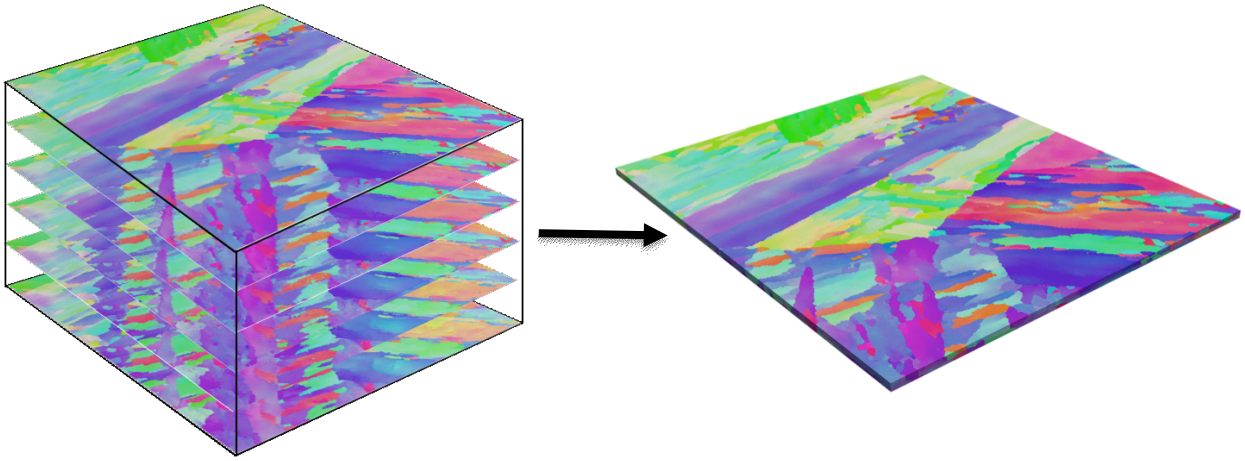

Figure 50: Reconstruction of six HT-9 slices into a digital microstructure for use in MARMOT.

3.5 Irradiated High Resolution Electron Backscatter Diffraction of HT-9

In order to duplicate the un-irradiated HT-9 HR-EBSD results from FY14, the holder for the irradiated HT-9 sample was thinned down to a height of 0.3". Ion milling was performed at EML with a PECS 682 system cleared for radioactive use. The sample was bulk milled for 12 hours at 4.5 kV followed by a 1.5 kV final mill for 2 hours. The HR-EBSD scan was collected with a FEI Quanta 650 field emission SEM utilizing an EDAX Hikari EBSD camera and EDAX OIM software for data collection [7]. With a resolution of 50 nm, the 10 µm x 10 µm HR-EBSD dataset contains 40,000 individual points. An inverse pole figure (IPF) map, image quality (IQ) map, and IPF map with un-indexed points (CI = 0) are plotted in Figure **51**.

The black regions in Figure **51** are points in the scan with poor or no diffraction patterns. This is unique to the irradiated HT-9 sample, as the HR-EBSD in FY14 does not contain these regions. EDS data (see Figure **52**) obtained simultaneously with the EBSD scan show that these regions are depleted of iron and contain higher concentrations of molybdenum, tungsten, manganese, and silicon. Because of overlap in the x-ray peaks of W/Si and Mo/S, it is difficult to determine the exact ratios of elements. Additionally, both chromium and carbon have segregated along the

grain boundaries or are contained within small precipitates much smaller than the average grain size.

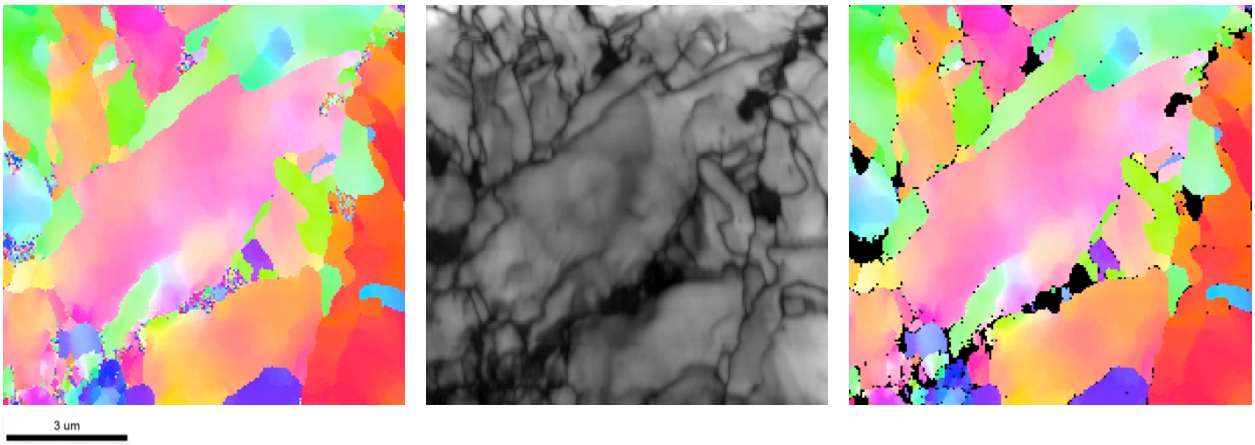

Figure 51: Irradiated HT-9 EBSD Results. Un-processed IPF map on left, IQ map in middle image, and IPF map on right with un-indexed points colored in black.

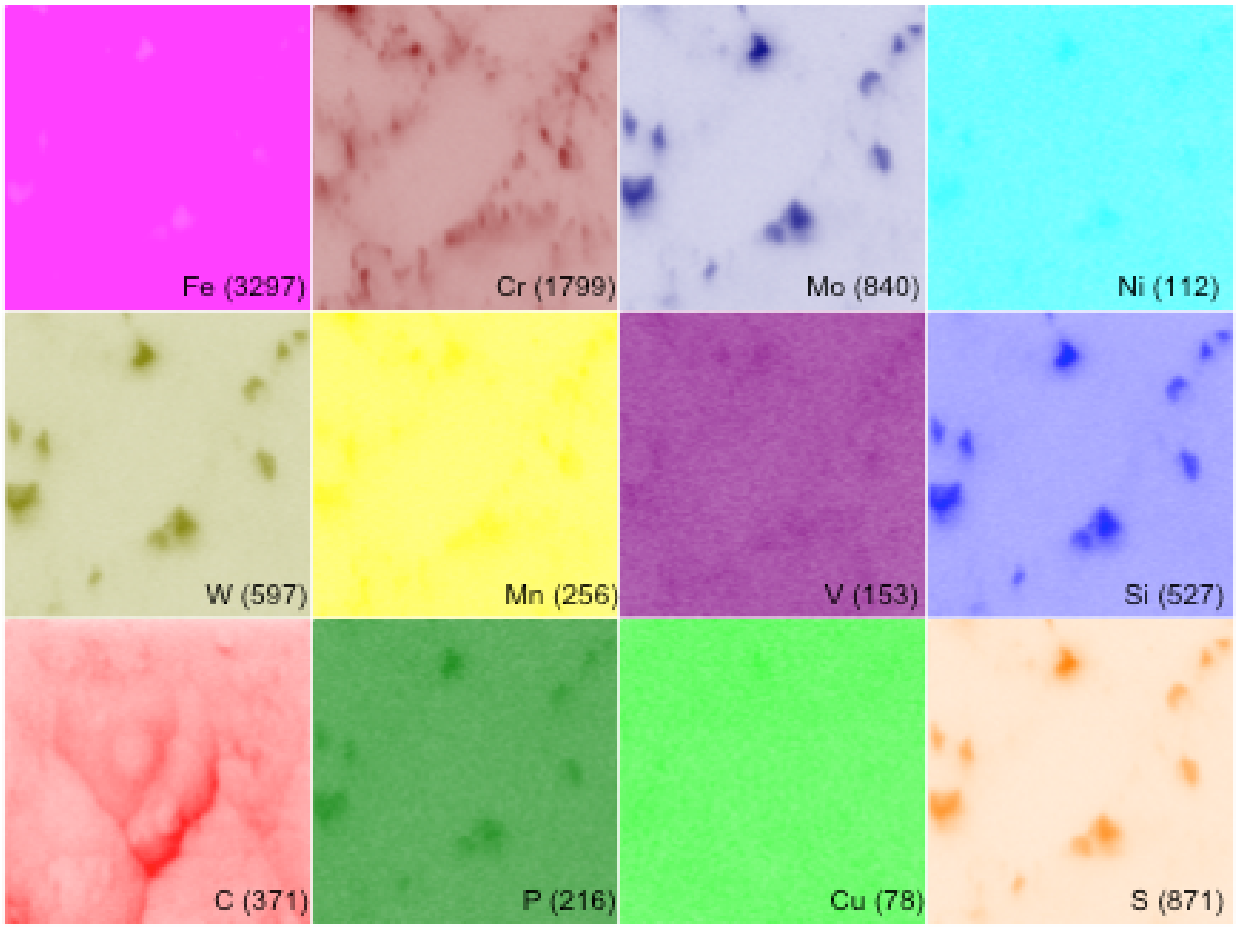

Figure 52: EDS results of irradiated HT-9.

Research is underway to better understand these un-indexable regions. The most likely explanation is that these regions are a secondary phase that does not diffract at the same conditions as the matrix grains. They may also be an irradiation induced amorphous phase. TEM samples have been prepared and results of the analysis will be reported in next years report.

CrossCourt 4 software was used to estimate residual stress, strain and dislocation density within the HT-9 material. Figure **53** contains results from the cross correlation. Note that the values for stress and strain are off by an order of magnitude. This is a result of bad data points within the HR-EBSD dataset. These low CI points must be removed to get good stress/strain agreement with experiments. The CrossCourt software automatically removes points with CI values of 0. However, to get accurate results, data points with CI values between 0 and 0.03 must also be removed. The CrossCourt developers are currently working to implement the ability to remove these points individually or by selecting a threshold value.

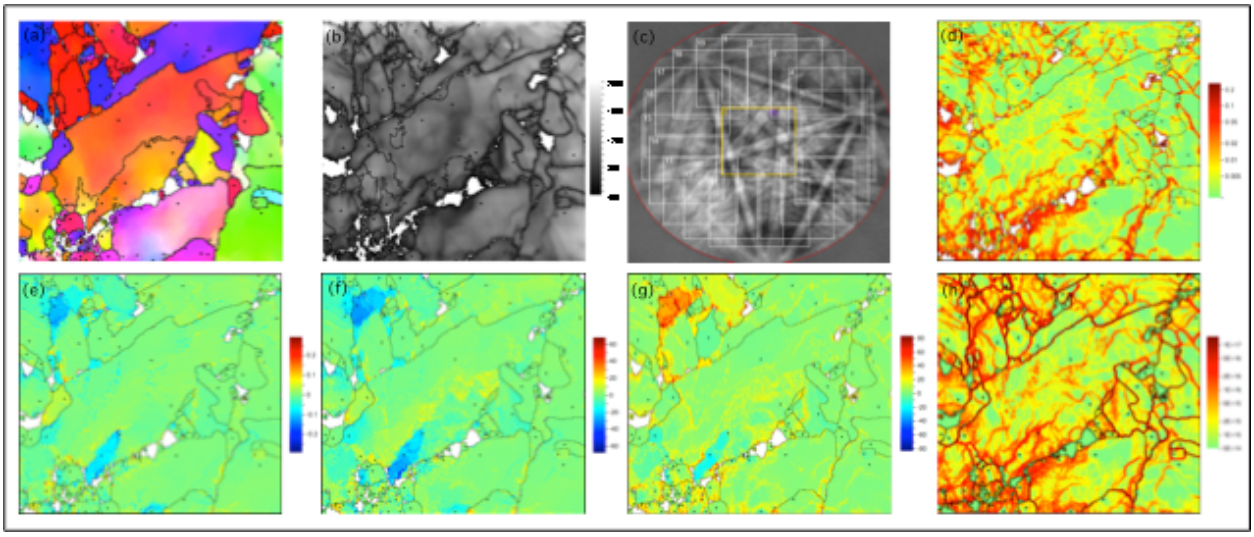

Figure 53: Results from HR-EBSD analysis of irradiated HT9 cladding: (a) inverse pole figure map, (b) image quality map, (c) reference electron backscatter pattern with 20 regions of interest overlaid onto pattern, (d) high resolution kernel average misorientation map, (e) ε_{22} strain map, (f) σ_{22} stress map, (g) Von Mises stress plot, (h) geometric necessary dislocation map.

4. FY 16 Results

As it was requested at the end of FY15, SiC/SiC composite material was replaced with 304H stainless steel material (material replacement was discussed in Section 3.1.1). The work on unirradiated Zircaloy-4 was carried out by University of Wisconsin-Madison in FY16. During FY 16 University of Wisconsin worked on the following: determining ion milling parameters for 304H SS and Zircaloy-4, resolving SEM stage drift issues, and conducting serial sectioning of the 304H SS material.

Idaho National Laboratory concentrated efforts on conducting HR-EBSD of a second irradiated material – 304H SS (in addition to the previously demonstrated HR-EBSD of irradiated HT-9), performing serial sectioning of an irradiated nuclear material (304H SS was selected for this task), reconstructing and integrating 3D datasets into MARMOT; and reconstructing 2D HR-EBSD datasets into MARMOT. Since most of the effort on irradiated materials was conducted on 304H SS, the MARMOT reconstruction used 304H SS dataset input. However, established procedures are representative and can be applied to all reactor materials under investigation. The procedures were validated using data acquired from irradiated HT-9.

The results on irradiated Zircaloy-4 are not shown in the report due to the issues associated with specimen transfers and rapid oxidation. It is important to note that one must attempt to conduct EBSD data acquisition from irradiated sample immediately upon ion etching of the specimen or store the sample in an inert atmosphere if the sample analysis cannot be conducted immediately upon milling. Unfortunately, Gatan PECS ion etching equipment and FEI FIB instruments were not collocated in the same facility, which required highly radioactive specimen transfer from one facility to another. Due to the high activity of the specimens, specimens had to be placed in a lead container that was not sufficiently large to accommodate for sample savers, which could be back-filled with inert gases. This resulted in the inability to acquire usable data from irradiated Zircaloy-4. This was not a pressing concern for irradiated HT-9 and 304H SS, so one must account for specimen limitations during sample characterization.

4.1 University Wisconsin-Madison

EBSD work conducted at UW in FY15 was often compromised by stage drift during the scan. Scan drift has three major sources: the sample, the stage, and the beam. Sample drift results from the mounting method, and variations in the sample's thermal and electrical conductivity during the scan. Stage drift results from environmental vibrations or aging/worn stage motors. Beam drift results from filament instability and poorly calibrated beam optics. Of the three drift sources, sample drift is the most likely. In FY16, UW set out to mitigate the impact of this drift on long duration, high magnification scans.

4.1.1 EBSD Investigation of Super 304 Stainless Steel

Three small pieces of Super 304 stainless steel were cut from an annular cross section of piping for sample preparation. EDM recast was removed from the sample surfaces by hand polishing with 320, 600, 800, and 1200 grit SiO_2 abrasive papers.

4.1.2 Ion Milling

The first sample mount used for S304 preparation was a traditional SEM stub. A small tube that fits inside the collet (Figure 54) can be used to elevate the stub such that the sample's surface is 0.24" above the collet head. Newer ion mill models, especially those geared towards SEM sample preparation, feature dynamic sample height adjustment, and remove the need for specialized sample holder geometries.

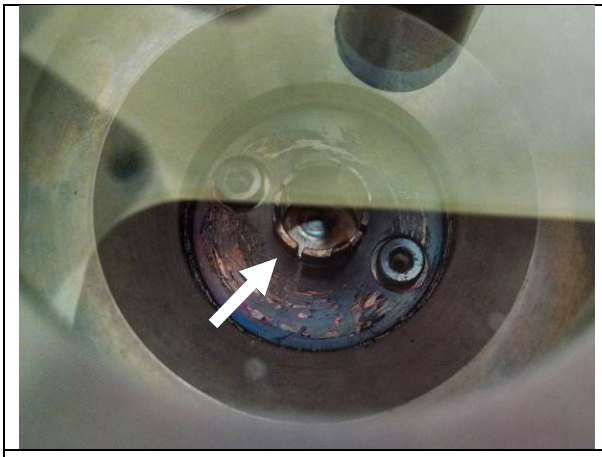

Figure 54: Sample stage of the Fischione Model 1050 TEM Mill. The collet (arrow) used to house OEM sample mounts is used as a point of reference for custom sample mounts

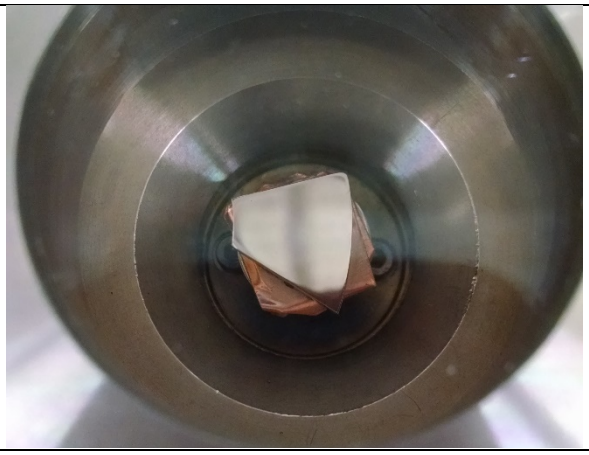

Figure 55: S304 sample #1 prior to milling. The large arc corresponds with the original tube OD, and the smaller arc is the original tube ID.

After 30 minutes of ion milling at 3 kV, the sample was imaged. EBSD pattern collection was not possible. After an additional 1 hour of 3 kV milling, the rotational center of the sample is identifiable with the naked eye due to a gradient in the surface condition. This gradient results from the radial dependence of the material removal rate in this model of ion mill, as discussed in the FY15 report. Within this central region, EBSD patterns were observable, but not in great number.

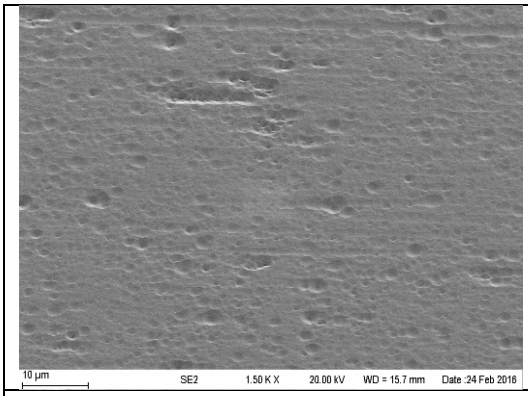

Figure 56: SEM micrograph of the S304s01 surface in the rotational center of the sample mount after 90 minutes of ion milling. Surface dimpling is readily

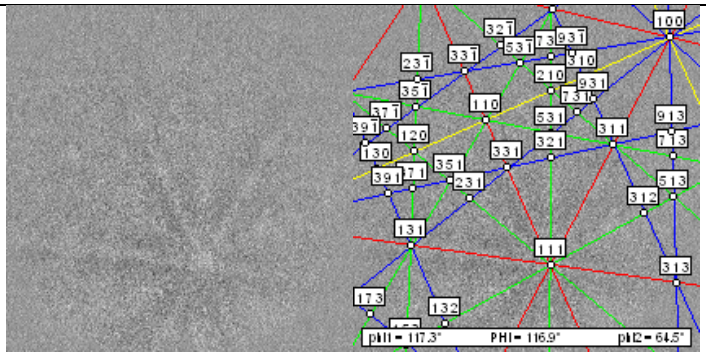

Figure 57: (L) EBSD pattern from the central region after 90 minutes of ion milling using 3 kV energy; (R) Indexed γ-Fe orientation

apparent, and isotropic.	

To ensure reproducibility of sample location in the ion mill after subsequent EBSD scans, the sample was transferred from the SEM stub to a custom aluminum mount that could both hold the sample in place in the ion mill and serve as a stage support for microscopy. Additional ion milling on this flat sample was performed at 3 kV and then at lower energies, including a 45-minute cleaning mill at 0.1 kV. Neither approach yielded satisfactory results. The sample was then hand-polished with colloidal silica to produce a surface known to yield EBSD patterns (Figure 59(l)). Subsequent ion milling and re-polishing were undertaken to characterize the effect on the EBSD patterns. Table 6 contains all ion milling parameters used in the study.

Table 6: Ion milling recipes used to treat Super 304 stainless steel, and a qualitative indicator of the EBSD result. All treatments use an inclination of 4° from horizontal for the ion beam (incidence angle of 86°).

Milling Step	Clean-Up Step	Sample Designation	EBSD Patterns	EBSD Mapping
0.5 h @ 3.0 kV [~80 µA]		S304s01.30m3kV	None	
1 h @ 3.0 kV [~80 µA]		S304s01.90m3kV	Rarely Indexed	
1 h @ 3.0 kV [~82 µA]		S304f01	Rarely Indexed	
2 h @ 1.0 kV [~70 µA]	0.75 h @ 0.1 kV [~60 µA]	S304f01	Rarely Indexed	
Colloidal silica finish	s304sm01 t00	Well Indexed	Successful	
0.5 h @ 2.0 kV [~75 µA]		s304sm01 t030m2kV	Well Indexed	Successful
3.0 h @ 2.0 kV [~75 µA]		S304sm01 t210m2kV	Indexed	Successful
Colloidal silica finish	S304sm01p02 t00	Well Indexed	Successful	
	2 h @ 0.1 kV	S304sm01p02 t00	Well Indexed	Successful
	2 h @ 0.1 kV	S304sm01p02	Well Indexed	Successful

4.1.3 EBSD Results

Successful EBSD pattern collection was performed using a LEO 1530 field-emission filament SEM equipped with a DVC-1312M camera and TSL OIM software, operated with 4x4 binning and a pattern exposure time of 53 milliseconds. The typical scan step size is 250-500 nm, considerably larger than the 75 nm used when mapping HT9. This step size increase should result in a marked decrease in scan distortion due to drift caused by beam heating and surface modification from chamber atmosphere impurities.

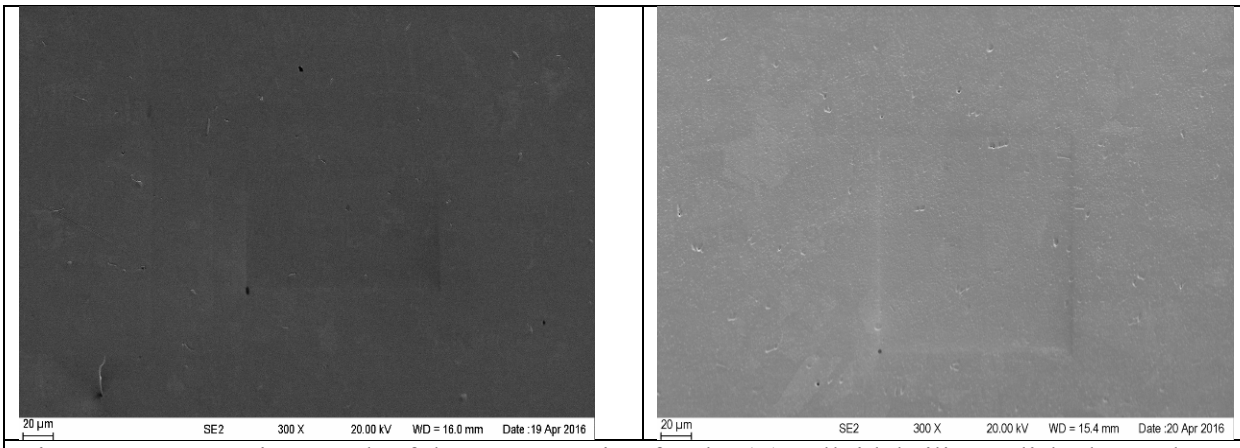

Figure 58: SEM micrograph of the EBSD region for the (L) colloidal silica polished sample and (R) after subsequent 3.5 hours of 2 kV ion milling

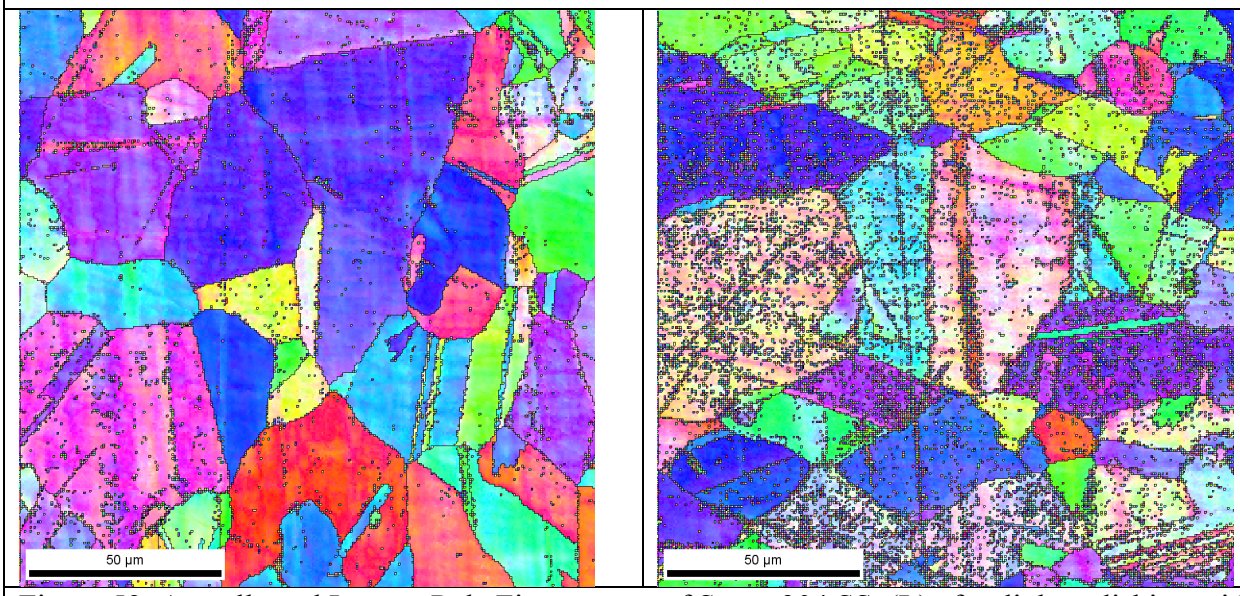

Figure 59: As-collected Inverse Pole Figure maps of Super 304 SS. (L) after light polishing with colloidal SiO_2; and (R) after 3.5 h of ion milling at 2 kV ion energy.

It is not clear why the EBSD patterns degrade following continued ion milling at the 2.0 kV ion beam energy. The surface was finely polished with colloidal silica, and low energy ion beams of 0.1 kV energy were used to treat the surface. After 4 hours of low energy milling, the EBSD patterns had not degraded, but they had also not improved.

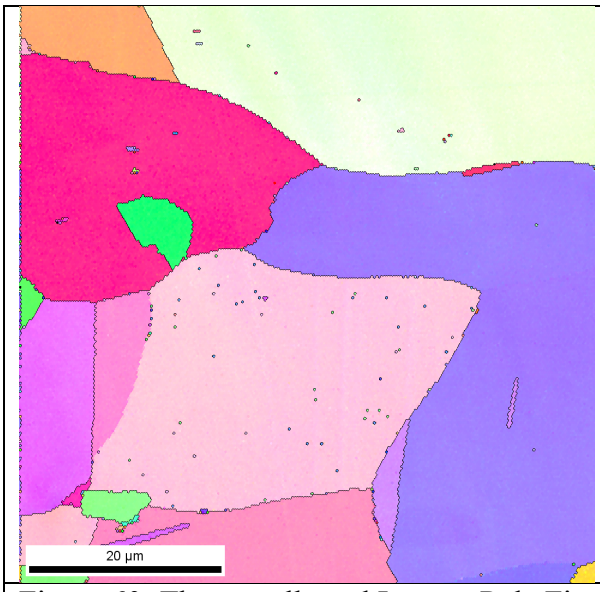

Figure 60: The as-collected Inverse Pole Figure map following the 2nd polishing with colloidal silica (60 x 60, 0.25 step)

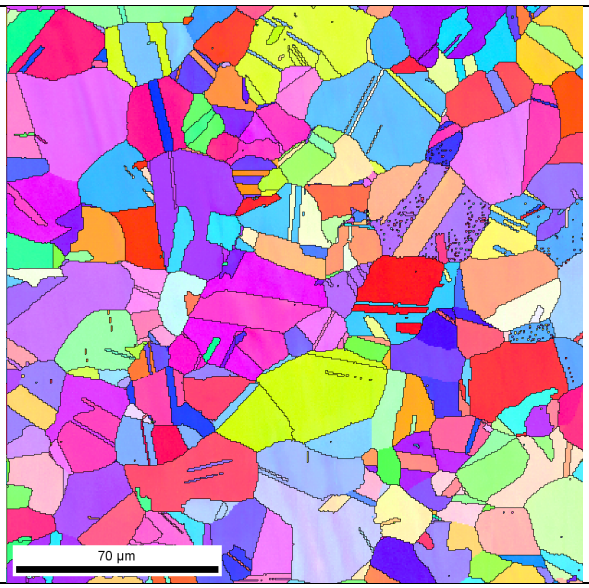

Figure 61: The as-collected Inverse Pole Figure map following 4 hours of 0.1 kV ion milling (200 x 200, 0.5 step). No improvement or degradation of the surface is evident compared to the prior as-polished scan.

As little improvement in the sample surface was obtained with early milling at 3.0 kV, it is not likely that other low energy milling steps would offer an improvement beyond cleaning off particulate matter. Higher energy milling, at 4-6 kV, may be required to improve scan quality from roughly ground or lightly finished surfaces.

4.2 EBSD Investigation of Un-irradiated HT-9

4.2.1 EBSD Collection at CAES

A nickel-filled epoxy mount containing an un-irradiated HT9 clad segment was prepared in accordance with past work. A LECO LM247AT microhardness tester was used to imprint an asymmetric indentation grid spanning 40 x 40 µm² (Figure 62). An EBSD scan overlapping most or all the features would provide an estimate of any vertical or horizontal drift that may have occurred, as in Figure 63. The EBSD scans at CAES were performed using a JEOL JSM-6610LV tungsten filament SEM, equipped with a EDAX Hikari EBSD camera. An accelerating voltage of 30 kV and a spot size of 72 were used for all but one scan, which was collected at 25 kV to limit the rate of surface fouling. Broad-beam ion milling at CAES is performed using a Gatan Model 682 PECS, with a beam energy of 4.5 kV and exposures of 30 minutes. The observed pre- and post- exposure beam currents ranged between 140 and 180 µA. Due to the design of its current-measuring system, *in situ* current readings are unavailable. The 30-minute exposure was chosen due to the past work that indicated its milling rate was ~100 nm per 60 minutes.

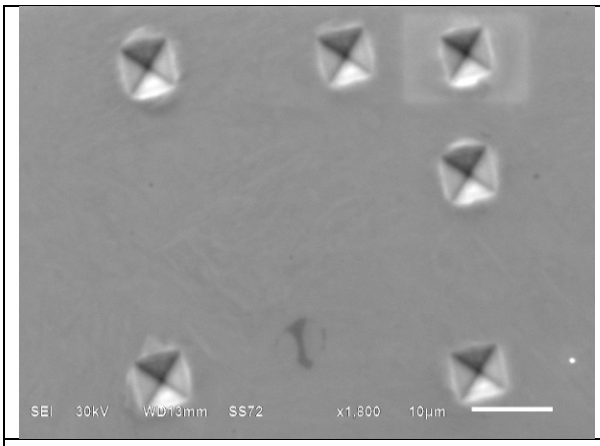

Figure 62: Indentation grid used to align successive EBSD scans and track drift that occurs during a scan

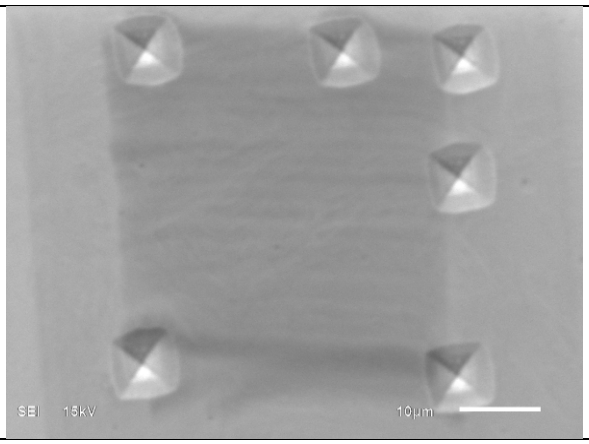

Figure 63: Sample surface after 9 iterations of ion milling and EBSD mapping, a nominal depth of 450 nm.

Ten complete slices were collected at CAES before the end of the available instrument time. Due to small variations in the rotation of the sample in the SEM stage and additional small variations in the positioning of the SEM stage between each session, the scans are not of the exact same size. However, each scan was positioned such that it would contain multiple fiducial markers. As successive scans were conducted, the average as-collected confidence index remained steady, fluctuating from 0.11 to 0.18. After applying the clean-up procedure introduced in FY14, the average confidence index rises to 0.69-0.76.

Table 7: EBSD Scan Summary for HT9 datasets collected at CAES

Scan #	X [µm]	Y [µm]	Step [µm]	# Points	Avg. CI [Raw]	% GD Changed	% NCCI Changed	Avg. CI [Cleaned]	Avg. IQ	Avg. Fit
0	45	45	0.075	360,600	0.14	21.8%	28.2%	0.71	2036.03	1.77
1	46.35	43.65	0.075	360,877	0.14	21.7%	27.5%	0.72	2026.10	1.76
2	45.97	46.5	0.075	381,294	0.13	15.5%	18.0%	0.71	753.02	1.93
3	45.38	46.13	0.075	373,296	0.15	14.4%	14.3%	0.76	1144.62	1.87
4	47.17	46.13	0.075	388,080	0.11	17.2%	19.2%	0.69	1759.25	1.98
5	43.95	44.7	0.075	350,439	0.14	14.5%	15.6%	0.75	1784.33	1.89
6	45	44.48	0.075	356,994	0.15	14.1%	15.6%	0.75	1844.89	1.87
7	43.35	37.8	0.075	292,395	0.16	14.5%	10.2%	0.77	1911.21	1.82
8	40.2	36.15	0.075	259,371	0.14	14.9%	11.0%	0.75	1928.78	1.89
9	44.33	34.13	0.075	269,952	0.18	12.5%	20.0%	0.79	925.84	1.79
10	48.3	39.68	0.075	341,850	0.14	19.6%	36.6%	0.73	755.34	1.74

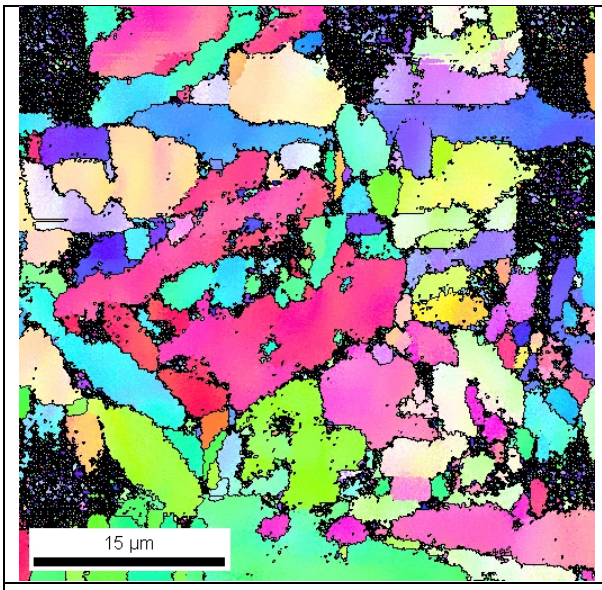

Figure 64: Inverse Pole Figure of the cleaned initial scan. The six marker indents present as large black regions.

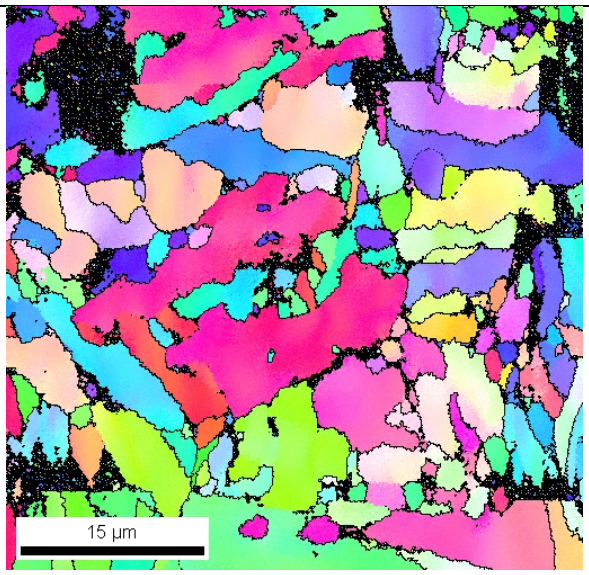

Figure 65: Inverse Pole Figure of the 5th scan. Ion milling has improved the surface within the marker indents to the point that the cleanup routine can partially fill them.

As can be seen on the individual scans, the indent regions manifest as large clusters of randomly oriented and/or low confidence index patterns. Considerable regions along the grain boundaries also indexed poorly, but as milling continued, indexing along grain boundaries and within the fiducial markers improved (Figure 65). Three scans were repeatedly interrupted by problems with the acquisition sequence, either in the software, hardware, or due to a sample surface phenomenon. These manifest as frequent horizontal, striped regions in the IPF, such as shown in Figure 66. Adjusting the scanned region to include as little of the fiducial markers as possible did not alleviate the issues.

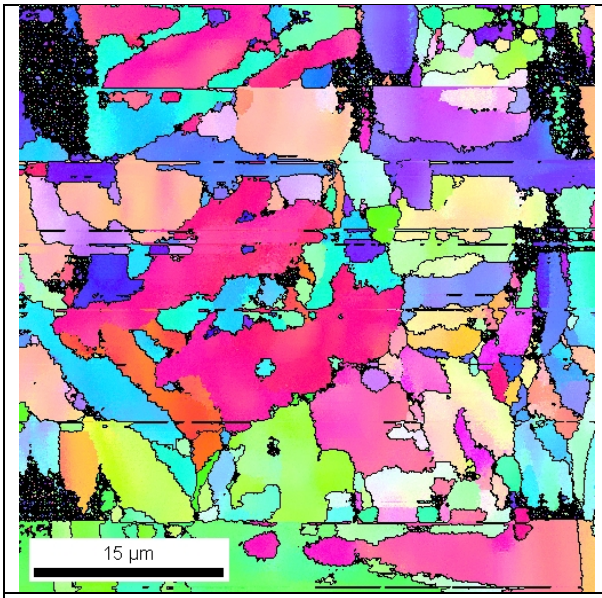

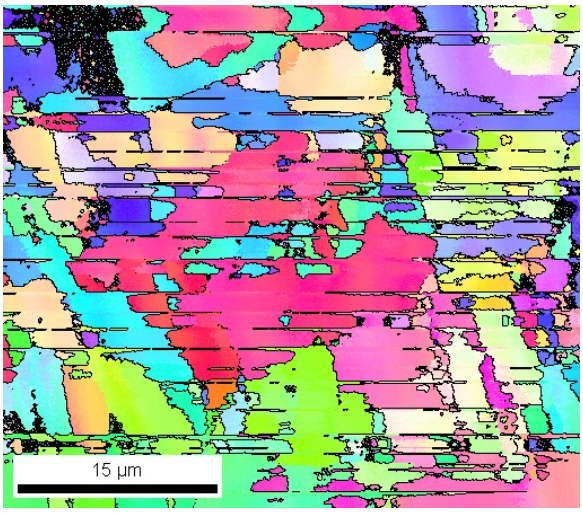

Figure 66: Scan artifacts manifested in a handful of scans, such as the 4th (l) and 8th (r) scans

Despite the issues in the collected data, an attempt to piece together the 11 scans into a 3-D volume was made. OIM Data Analysis v5.31 software was used to perform an automated alignment and then export the scans to the plaintext.ANG file format. Version 6.3.29 of the software package DREAM3D was used to further align the scans based on the only the fiducial markers, crop to the central region, and generate the input file for the image rendering software ParaView. The reconstructed volume is shown in Figure 67.

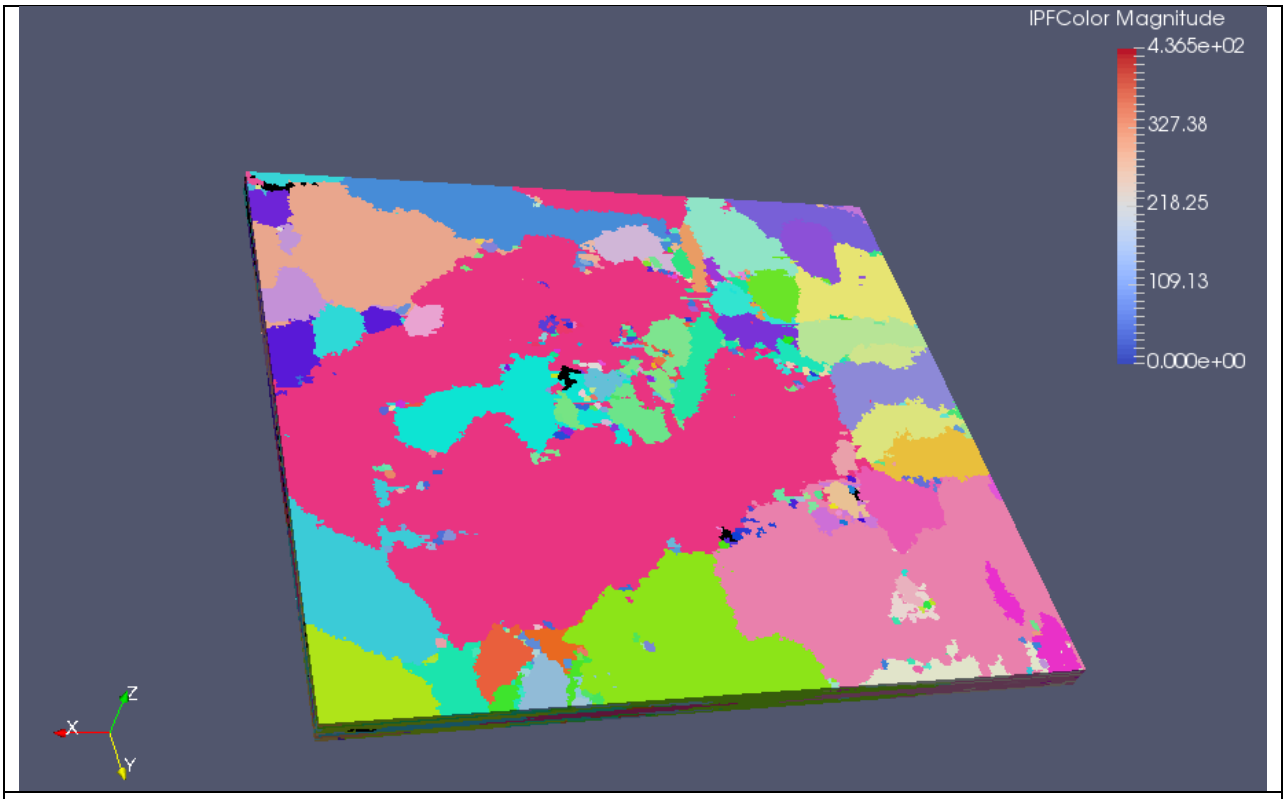

Figure 67: Reconstructed HT9 volume measuring approximately 29.7 µm x 26.9 µm x 0.5 µm.

4.2.2 Conclusion

Accurate 3-D reconstruction is a very challenging task and is not currently well-suited to automated methods, especially in similar cases where the data to be assembled contains artifacts and other noisy data. Further improvements to the 3-D reconstruction are possible by manual calculations of the projective transformations to shift, rotate, and skew each individual scan until its visible fiducial markers align with those in the other scans. As future collected EBSD datasets improve in quality and positional reproducibility, automated tools will be better suited to rapid reconstruction of analyzed microstructures.

4.3 EBSD Investigation of Zircaloy-4 TEM Discs

TEM disc punches of un-irradiated Zircaloy-4 flats were prepared at INL and shipped to UW for ion milling and EBSD analysis. Prior examinations of cross-sectioned Zircaloy-4 cladding in FY14 and FY15 at UW had failed to produce reliable or usable results, while successes in examining irradiated Zircaloy-4 clad had been made at INL.

4.3.1 Initial Examination

The TEM discs were mounted in plan view on SEM stubs and the initial state of the surfaces was assessed via SEM. The first disc (Disc A) examined was free of physical deformations on the surface, while the second disc (Disc B) examined was marred by visible cracking. To better ascertain if the ion milling program was having the intended effect of removing deformation associated with the manufacturing process, the first disc was selected for experimentation. Selection of Disc B, in the event of an unsuccessful experimental result, would have cast doubt as to whether the failure to generate EBSD data resulted from the ion milling, or the inherent microstructural defects evidenced by the cracking.

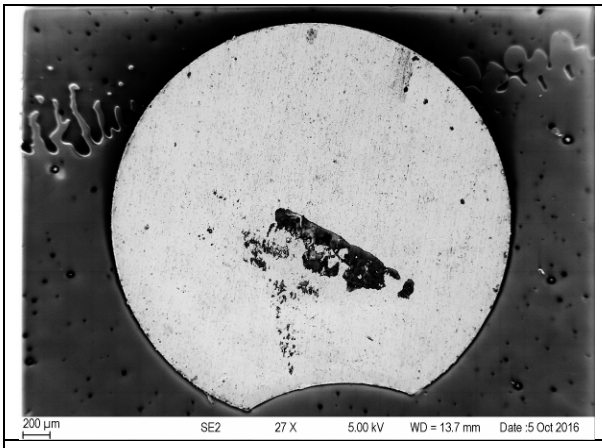

Figure 68: Disc A, 27x. Surface debris is visible, but no obvious microstructural damage from the fabrication process is present.

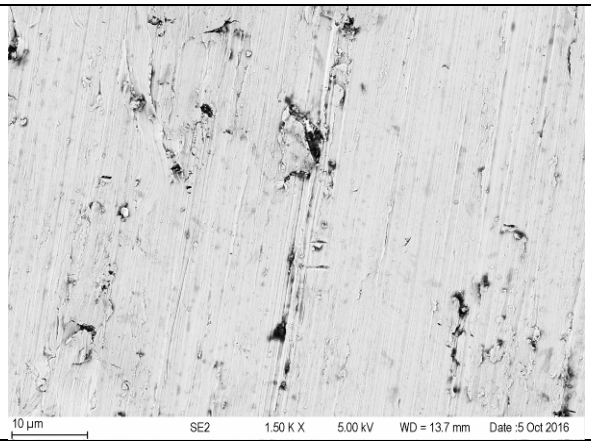

Figure 69: Disc A, 1500x. Surface marring from fabrication is readily visible.

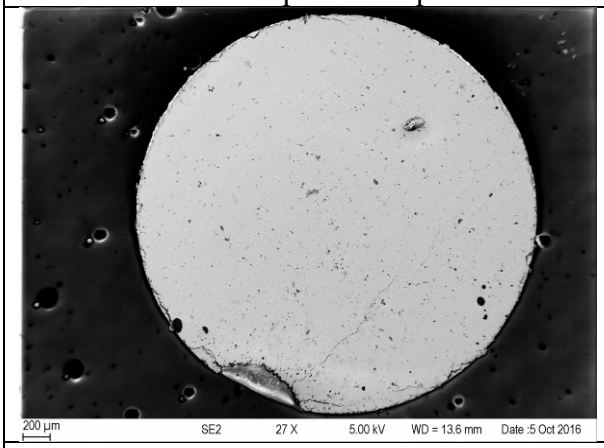

Figure 70: Disc B, 27x. Microstructural damage from the TEM disc punch process is apparent in the bottom region of the sample.

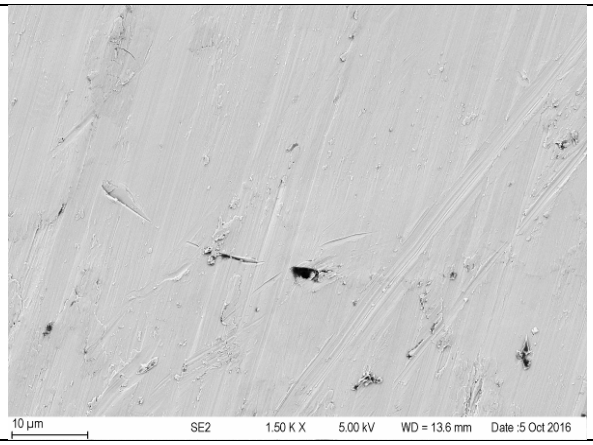

Figure 71: Disc B, 1500x. Surface marring from fabrication is readily visible.

4.3.2 Ion Milling Steps

Disc A was mounted on a custom aluminum sample holder using conductive Cu foil. This custom sample holder enables proper positioning of the sample in the ion mill, and rapid transfer to the SEM chamber without the need to reposition the sample on a SEM stub. This enables transfer times of less than 2 minutes between the ion mill vacuum and the SEM chamber vacuum. Ion milling is performed using a Fischione Model 1050 TEM Ion Mill, with a nominal inclination angle of 4° from the sample's surface normal. The available maximum ion energy of 6.0 kV was used for removal of the damage layer resulting from fabrication processes, while sample clean-up was initially performed using a beam energy of 0.1 to 1.0 kV. All ion milling steps utilized in the analysis of the Zircaloy-4 TEM discs are identified in Table 8 with the corresponding measured ion currents, and a qualitative assessment of the EBSD result. The gas flow rate in each of the two ion guns is 0.2 sccm at all ion energies.

After an initial short-term milling of 2 hours with 6 kV and 30 minutes of clean-up with 1.0 kV, the sample was re-examined. The surface had readily improved (Figure 72), but was not sufficiently clean for EBSD purposes. After an additional 2 hours of 6.0 kV milling and 30 minutes of 1.0 kV clean-up, the sample was re-examined. After the cumulative 4 hours of milling, the surface exhibited grain structure, shown in Figure 75. The surface also exhibits what appear to be orientation dependent precipitates, which are also visible in Figure 75. Despite the apparent sample cleanliness, EBSD pattern collection was not fruitful. The cumulative ion milling exposure was then doubled, with 4 hours of 6.0 kV ion milling and 30 minutes of 1.0 kV clean-up, to total 8 hours of milling at 6.0 kV. The grain structure remained visible, and the size and number of the apparent precipitates grew (Figure 77). EBSD patterns were faint, and not present in sufficient quantity to merit mapping of the substrate.

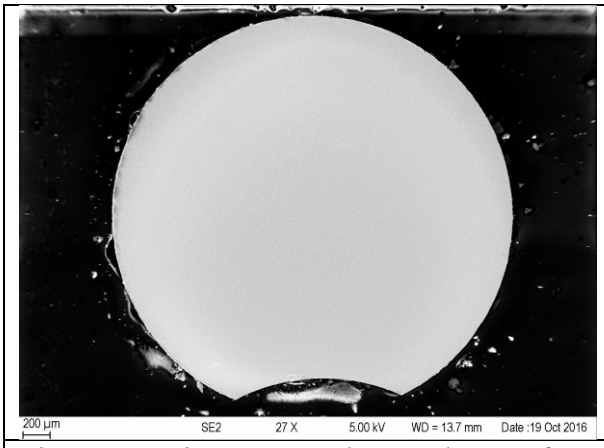

Figure 72: Disc A, 27x, 2h. Two hours of milling at 6kV have markedly improved the surface finish

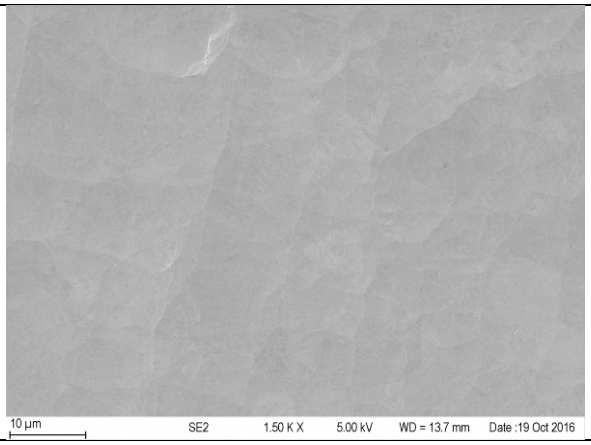

Figure 73: Disc A, 1500x, 2h. Surface dimpling exhibited by previous materials is visible.

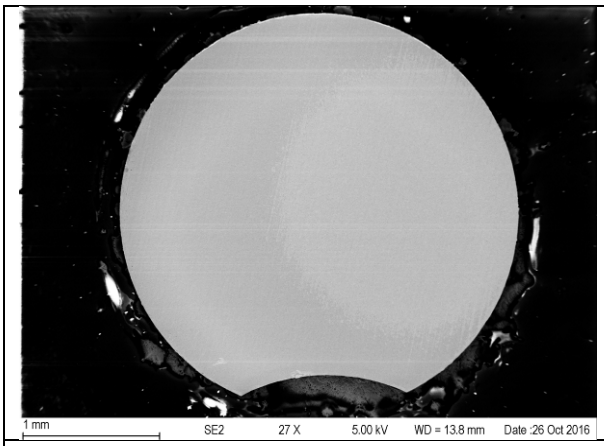

Figure 74: Disc A, 27x, 4h. Four hours of ion milling at 6 kV has resulted in the formation of two distinct regions. The outermost region is more roughly finished than the lighter gray, circular region in the middle-right of the sample.

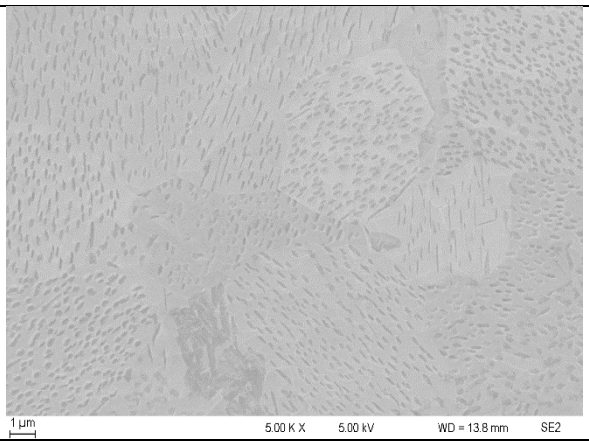

Figure 75: Disc A, 5000x, 4h. Grain structure is evident. Also evident are structures that exhibit an orientation dependence with the underlying grain.

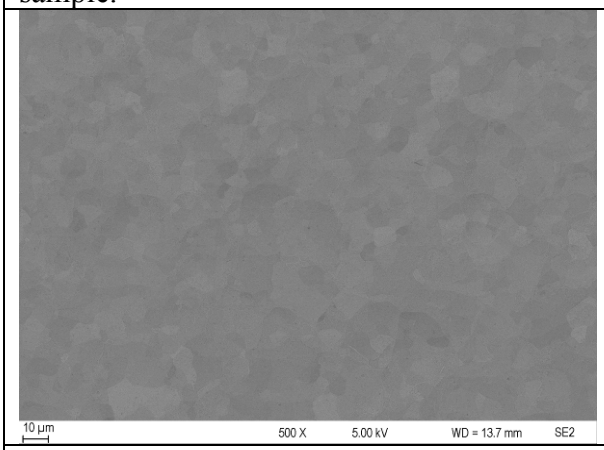

Figure 76: Disc A, 500x, 8h. Eight hours of milling have enhanced the contrast between grains.

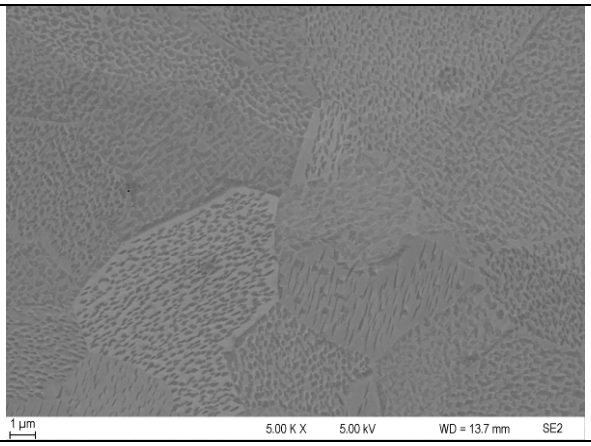

Figure 77: Disc A, 5000x, 8h. The size and number density of the precipitate-like features has increased.

Another 2-hour milling at 6.0 kV and clean-up of 30 min at 1.0 kV was performed. Due to the continued increase in size and number of the "precipitates" readily visible on the sample, their composition was briefly investigated using EDS. Spectral mapping and "point and shoot" analyses were unable to distinguish them from the sample matrix.

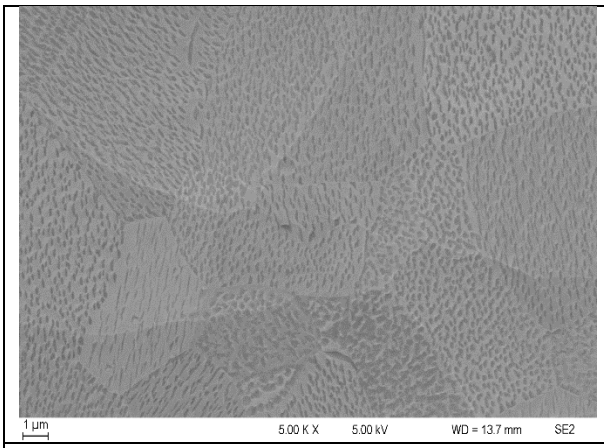

Figure 78: Disc A, 5000x, 10h. The features observed on the Zircaloy-4 sample continue to grow in size and number.

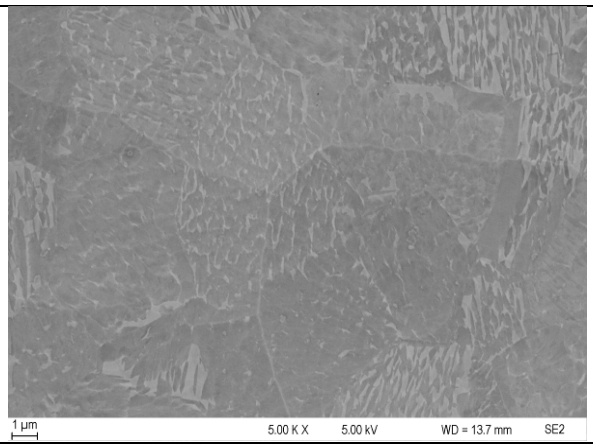

Figure 79: Disc A, 5000x, 16h. The features have greatly increased, and now blanket the grains almost entirely.

Additional low-energy clean-up sessions and high-energy milling sessions were used to determine if 1.0 kV is too aggressive to serve as the clean-up energy. Despite long times and low energies, improvements were not observed. The behavior of the artifacts with additional milling (Figure 79) offers further evidence that they are not precipitates, resulting in the conclusion they are not precipitates, but rather the result of deposition of previously milled material. Finally, a mid-level ion energy of 3.0 kV was used to clean the surface. Following the 2.75-hour exposure, EBSD patterns were readily present and indexable, allowing for the successful collection of an EBSD map measuring 50 µm x 50 µm with a step size of 250 nm.

The successful milling program was then applied to the remaining as-received Zircaloy-4 TEM disc. A 4 hour, 6.0 kV milling step was used to remove the initial deformation layer from the fabrication process, and then a 2.75 hour, 3.0 kV clean-up step was used to finish the sample for EBSD collection. The ion milling treatment adequately removed the initial surface deformation (Figure 80), and only a minor amount of redeposited material is observed (Figure 81)

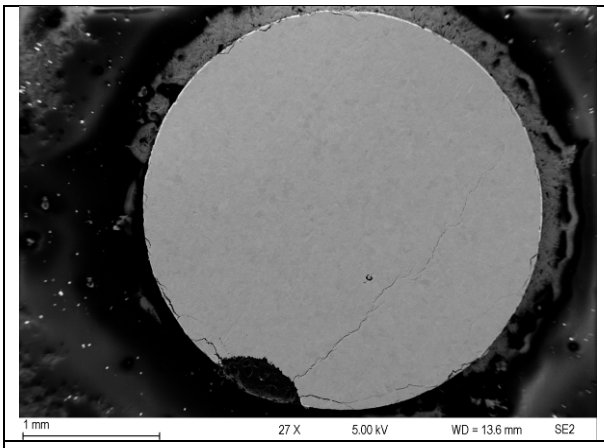

Figure 80: Disc B, 27x, 4h. After 4 hours of 6.0 kV ion milling, and 2.75 hours of 3.0 kV milling, the sample surface is considerably cleaner.

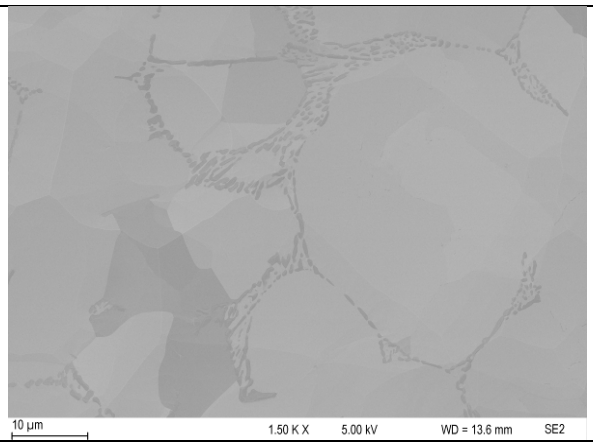

Figure 81: Disc B, 1500x, 4h. The redeposited material is already accruing on the sample surface, and may be mistaken for grain boundaries

Table 8: Ion milling parameters used to prepare EBSD quality surfaces from Zircaloy-4 TEM discs. Blank entries indicate the relevant item was not performed or attempted.

Milling Step	Clean-Up Step	Sample Designation	EBSD Patterns	EBSD Mapping
		A_AR		
2 h @ 6.0 kV [~153 µA]	30 min @ 1.0 kV [~65 µA]	A_60k02h	None	
2 h @ 6.0 kV [~155 µA]	30 min @ 1.0 kV [~67 µA]	A_60k04h	Not Indexable	
4 h @ 6.0 kV [~160 µA]	30 min @ 1.0 kV [~70 µA]	A_60k08h	Rarely Indexable	
2 h @ 6.0 kV [~146 µA]	30 min @ 1.0 kV [~63 µA]	A_60k10h		
	30 min @ 0.1 kV [~60 µA]	A_60k10h	Rarely Indexable	Large non-indexed regions
	4 h @ 0.1 kV [~60 µA]	A_60k10h	Somewhat Indexable	Large non-indexed regions
6 h @ 6.0 kV [~110 µA]	5 min @ 0.1 kV [~60 µA]	A_60k16h_1	Somewhat Indexable	Large non-indexed regions
	2 h @ 0.1 kV [~65 µA]	A_60k16h_2	Somewhat Indexable	Large non-indexed regions
	2 h @ 1.0 kV [~75 µA]	A_60k16h_3	Somewhat Indexable	Large non-indexed regions
	2 h @ 0.1 kV [~67 µA]	A_60k16h_4	Somewhat Indexable	Large non-indexed regions
	2.75 h @ 3.0 kV [~94 µA]	A_60k16h_5	Indexable	Good
		B_AR		
4 h @ 6.0 kV [~120 µA]	2.75 h @ 3.0 kV [~90 µA]	B_60k04h	Indexable	Good

4.3.3 EBSD Results

Successful EBSD pattern collection was performed using a LEO 1530 field-emission filament SEM with an accelerating voltage of 20.0 kV, an aperture of 120 µm, and a working distance of 17 mm with a nominal sample tilt of 70° immediately following ion milling at 3.0 kV with the Fischione 1050 TEM Ion Mill. Unsuccessful SEM parameters attempted included smaller apertures and lower energies. These smaller apertures and energies were not used after a cumulative time of 10 hours of 6.0 kV milling, and may yet prove effective or useful with the properly finished sample surface. Both scans presented here were collected at an SEM magnification of 750 X.

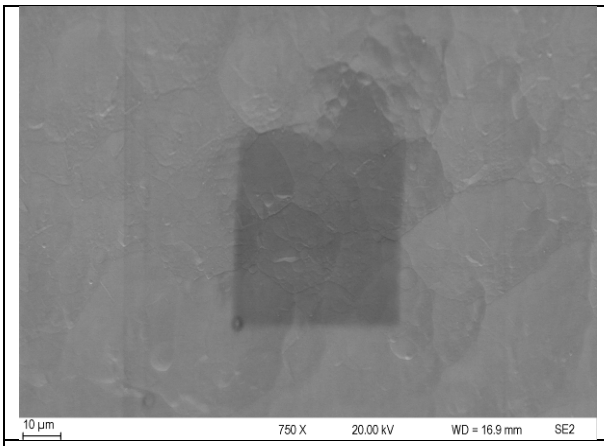

Figure 82: Tilt-corrected SEM micrograph of the EBSD mapped region from Disc A following the 2.75 hour, 3 kV ion milling procedure.

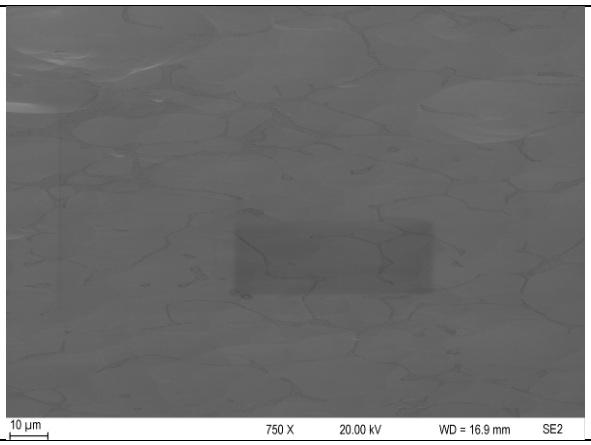

Figure 83: Tilted (70°) SEM micrograph of the EBSD mapped region from Disc B following the 2.75 hour, 3kV ion milling procedure.

The image quality (IQ) maps of the heavily-milled sample (Disc A) and the single-set milled sample (Disc B) are presented in Figures Figure 84 and Figure 85, respectively, both with and without identified grain boundaries of varied orientation rotations: blue (>15°), green (5-15°), and red (2-5°). The brighter regions of an IQ map correspond to EBSD patterns that have a high degree of contrast, indicating the relative strength of the observed pattern. Low contrast indicates a faint or non-existent pattern. The surface dimpling commonly observed on samples milled in the Fischione 1050 results in regions with imprecise orientation determination.

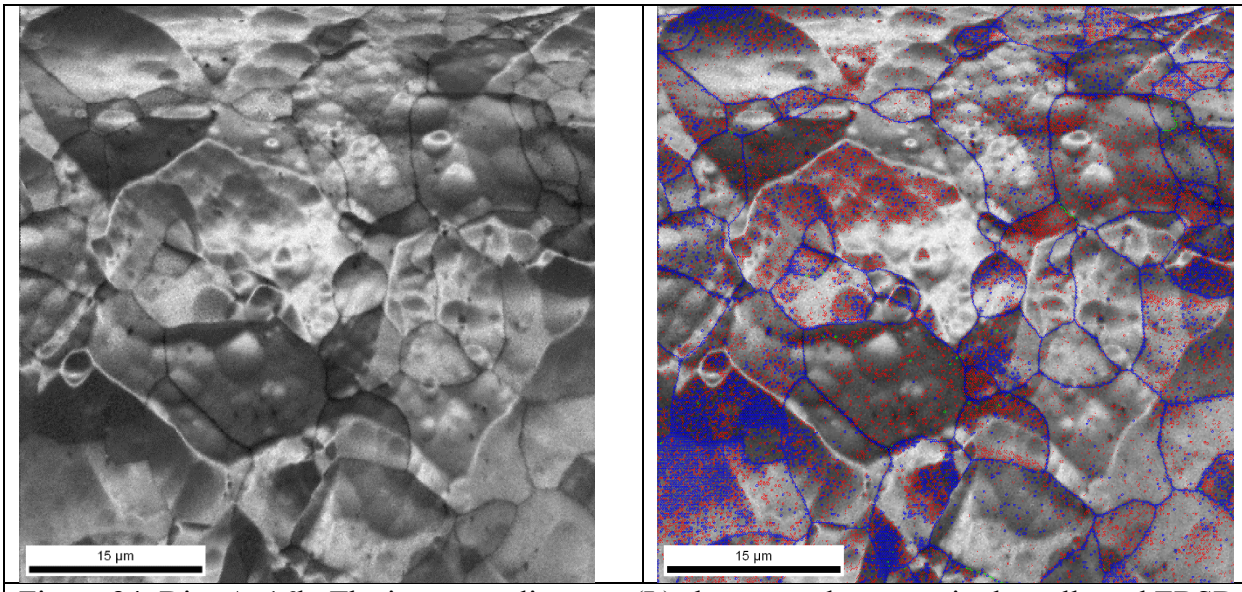

Figure 84: Disc A, 16h. The image quality map (L) shows good contrast in the collected EBSD patterns at most points. Superimposing the rotation angle boundaries (R) onto the IQ map identifies the grain boundaries. High angle (>15°) grain boundaries are marked in blue, while green and red signify lower rotation angles between neighboring points in the map.

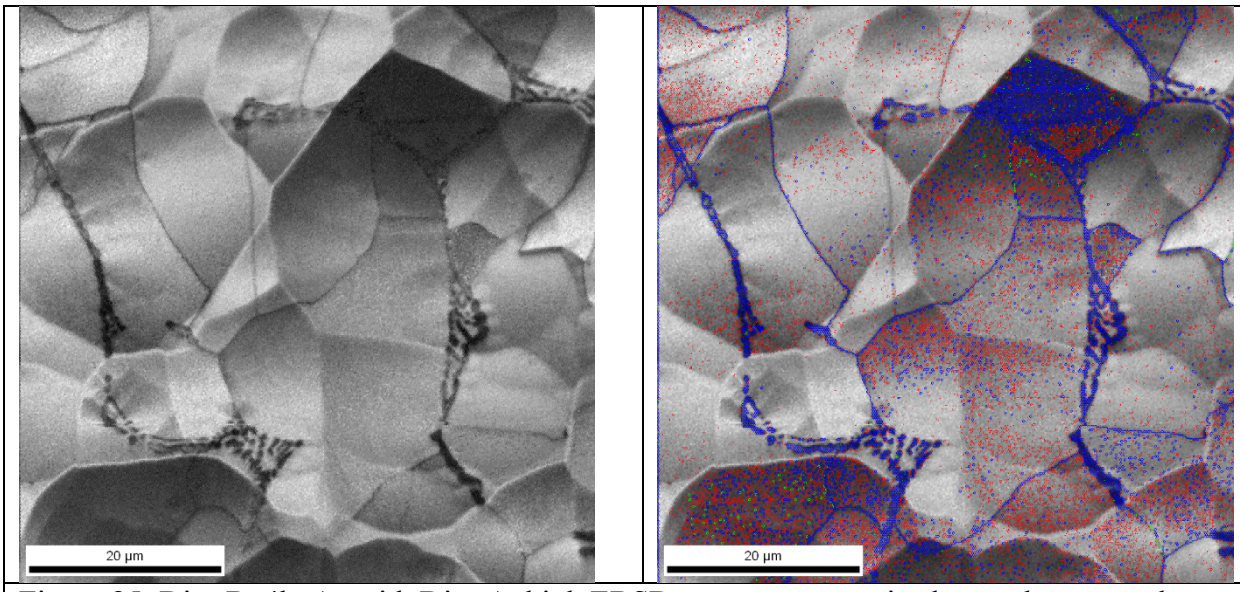

Figure 85: Disc B, 4h. As with Disc A, high EBSD pattern contrast is observed on most the scanned area. Inclusion of rotation angle information (R) again indicates the dimpling of the surface plays a role in precise orientation determination. The darkest streaks on the sample correspond to the surface artifacts identified during the ion milling of Disc A

The as-collected and "cleaned" inverse pole figure (IPF) maps are presented in Figures 86(L) and 86(R). The cleaning procedure is identical to that used in FY14 and FY15. The Grain Dilation step resulted in changes to 5.5% and 5.9% of the data points, and the Neighbor CI Correlation step resulted in changes to 2.6% and 2.2%, respectively.

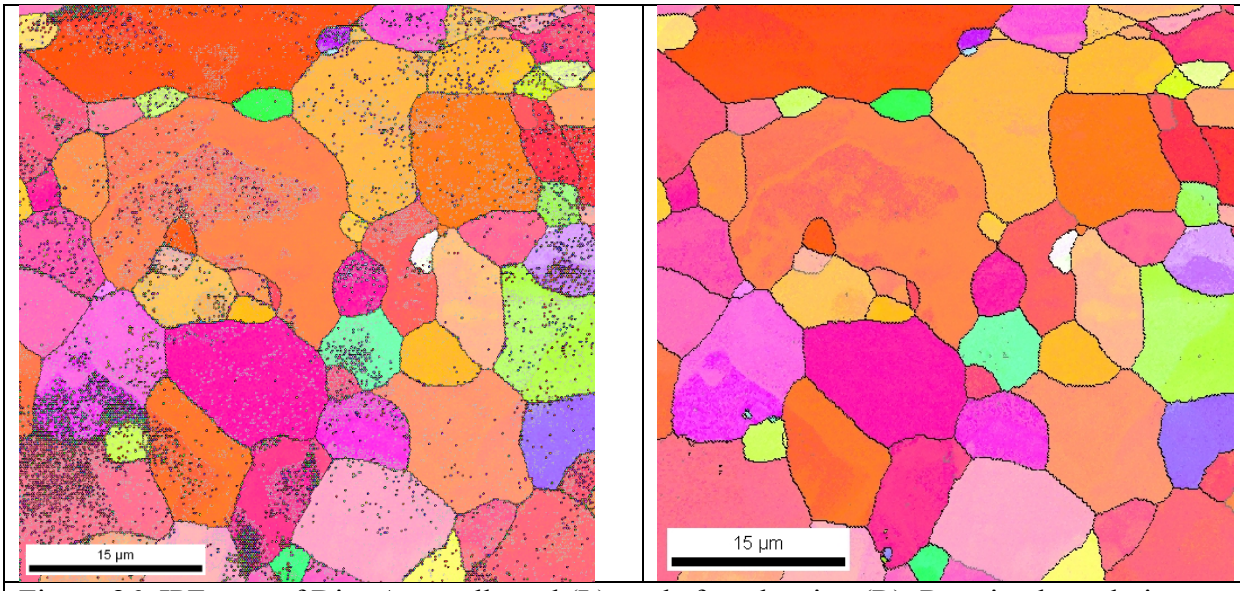

Figure 86: IPF map of Disc A as collected (L), and after cleaning (R). Rotation boundaries greater than 15° are marked black, 5° - 15° in grey, and 2° - 5° in light grey.

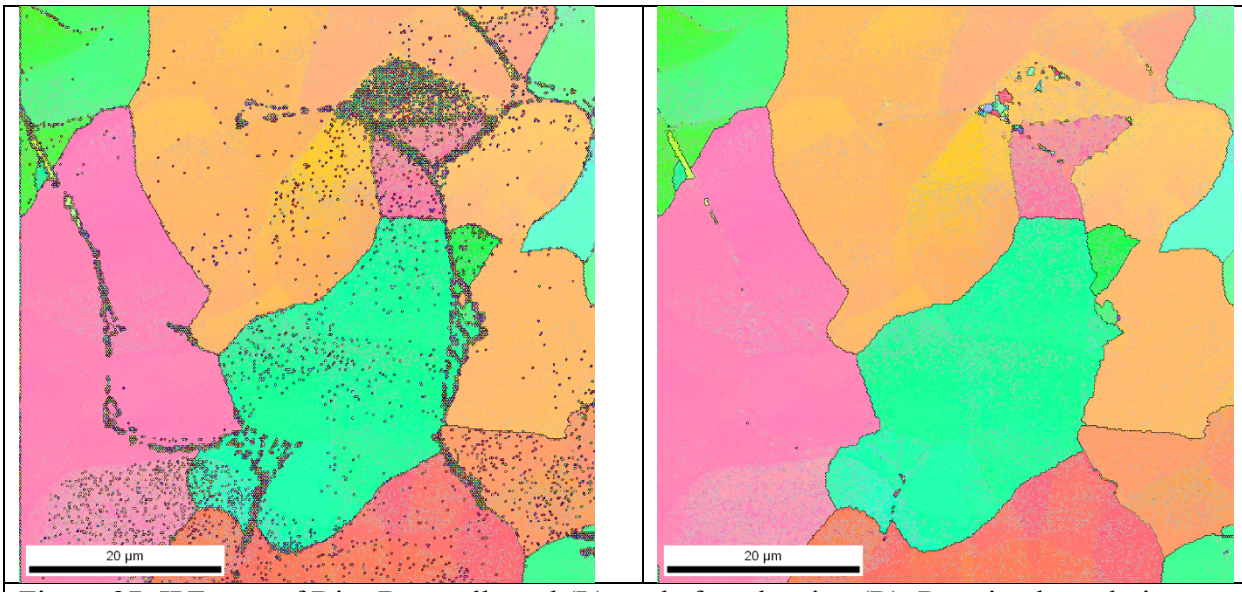

Figure 87: IPF map of Disc B as collected (L), and after cleaning (R). Rotation boundaries greater than 15° are marked black, 5° - 15° in grey, and 2° - 5° in light grey.

4.3.4 Conclusion

Flats of Zircaloy-4 material can be successfully prepared for EBSD analysis using only broad-beam ion milling. When possible, analyzed regions should be as free as possible from surface dimpling if precise characterization of local misorientation is the intended goal.

4.4 Idaho National Laboratory

4.4.1 High Resolution Electron Backscatter Diffraction of 304H SS Material

In order to duplicate the un-irradiated 304H SS HR-EBSD results, the holder for the irradiated 304H SS sample was thinned down to a height of 0.3". Ion milling was performed at EML with a PECS 682 system cleared for radioactive use. The sample was bulk milled for 7 hours at 4.5 kV followed by a 1.5 kV final mill for 1 hour. The HR-EBSD scan was collected with a FEI Quanta 650 field emission SEM utilizing an EDAX Hikari EBSD camera and EDAX OIM software for data collection [7]. With a resolution of 50 nm, the 10 µm x 10 µm HR-EBSD dataset contains 40,000 individual points. An inverse pole figure (IPF) map and image quality (IQ) map are provided in Figure 88.

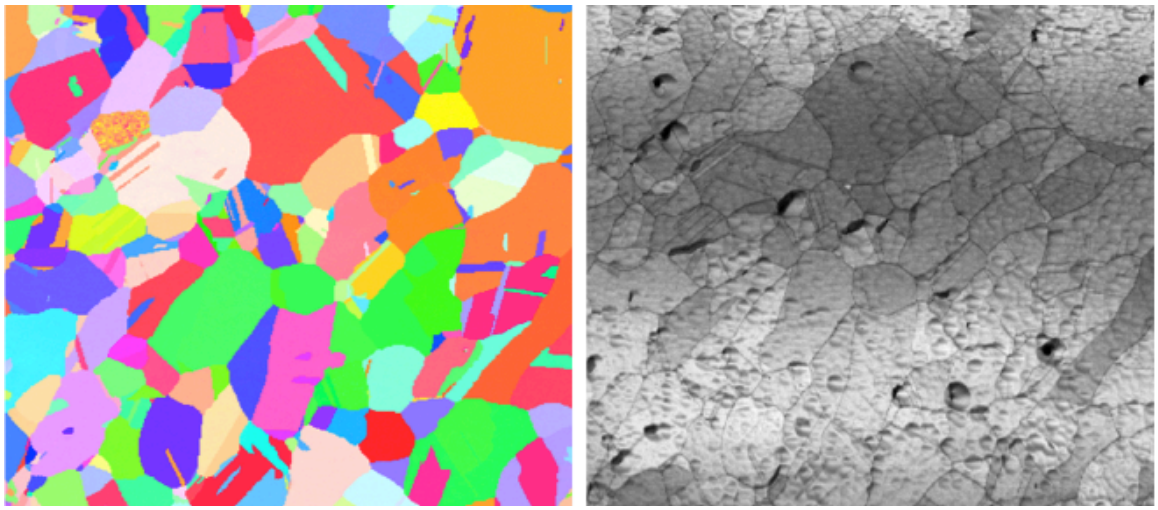
Figure 88: Results from HR-EBSD analysis of irradiated 304H SS cladding: (a) inverse pole figure map and (b) image quality map.

4.4.2 Serial sectioning of irradiated 304H SS material

To ensure proper positioning of the sample, three identifying fiducial marks were milled on the sample in FIB instrument. These marks enable the user to quickly find the same sample region each time it is placed in the microscope. Because stage drift is problematic for large EBSD scans, a wait time of ~1 hour was implemented after the sample positioning. When possible, beam shifting was used to return the scan to the desired position. If the stage was moved mechanically, an additional 15-30 min wait time was added to the wait time.

A total of 8 EBSD slices were recovered during the serial sectioning process. Each scan has a scan size of 200 µm X 200 µm and 0.5 µm step size. The dataset contains 698 grains. Figure 89 shows the 3D reconstruction of irradiated 304H microstructure with inverse pole figure coloring output from MARMOT framework. As in FY15, the data cleaning procedure consists of a single iteration of grain dilation, followed by a grain confidence index standardization routine, and then a neighbor confidence Index correlation with a minimum confidence index of 0.1.

In order to utilize the 304H serial sections within MARMOT, the slices must be properly reconstructed. A combination of MATLAB [8] and DREAM.3D [9-10] software were used to perform the digital reconstruction. Because Dream3D requires a square sampling grid, a custom MATLAB script was written to convert the hexagon OIM grid to a square grid. Post-processing (including cleanup, alignment, and cropping of the EBSD data) was performed with Dream3D. An algorithm based on "mutual information" was utilized for image alignment due to the lathe like features of the 304 SS microstructure that do not align properly when using algorithms based on crystallographic misorientation. Lastly, a MARMOT compatible "txt" file was output using the Dream3D software.

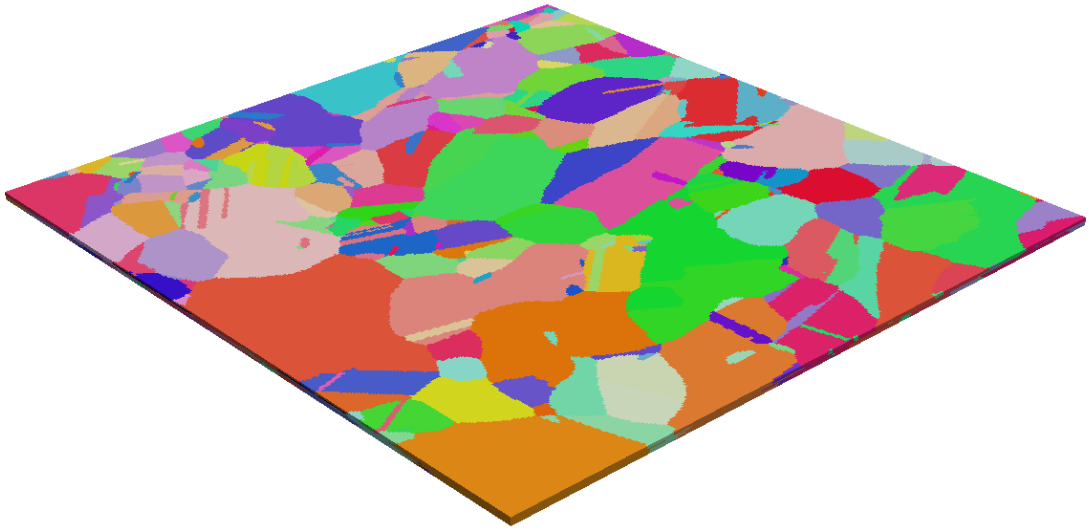

Figure 89. Reconstruction of 8 slices (acquired from irradiated 304H SS sample) into a digital microstructure for use in MARMOT.

4.4.3 Integration of experimental data into MARMOT

4.4.3.1 Reconstruction of 2D HR-EBSD datasets into MARMOT

The experimental data acquired from irradiated S304H SS specimen (discussed in Section 4.4.1) was reconstructed and initialized into MARMOT using "EBSD Reader" algorithm and is provided in Figure 90. In addition to EBSD data acquisition, simultaneously acquired EDS data confirmed the presence of small niobium carbonitride Nb(C,N) precipitates.

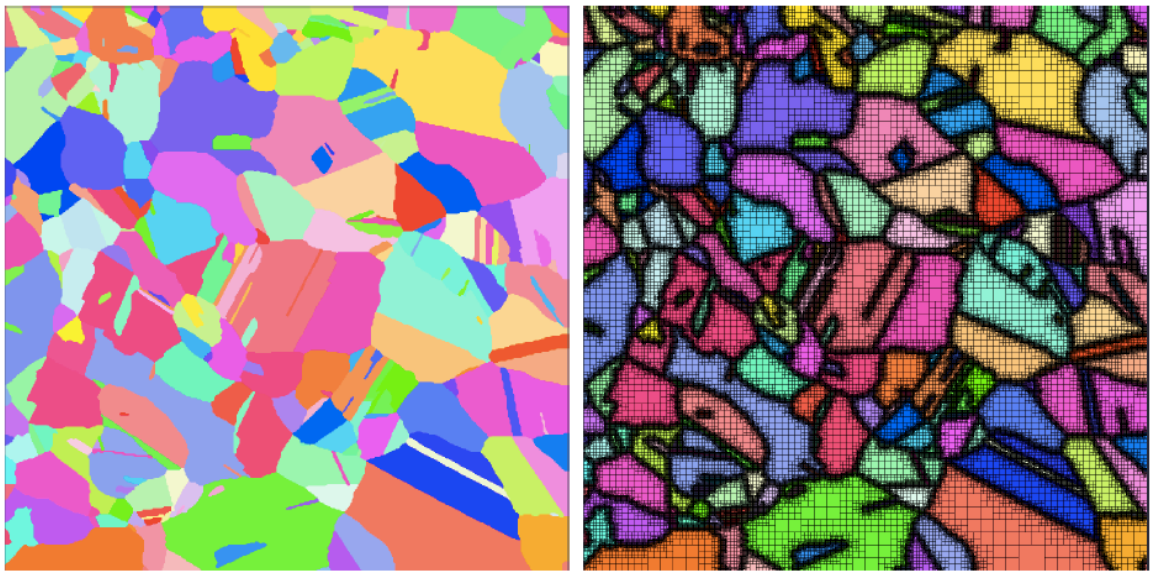

Figure 90. HR-EBSD dataset of irradiated 304H SS and microstructure reconstructed and initialized into MARMOT.

As it was previously mentioned, the collected EBSD dataset was collected within 175 µm X 175 µm area with a step size of 0.5 µm. The grain boundary plot of reconstructed irradiated 304H SS microstructure was smoothed 5 times in MARMOT and is provided in Figure 91. The zoomed region demonstrates the use of adaptive mesh refinement in MOOSE after 4 levels of coarsening, the base level (0.5 µm), and 1 level of mesh refinement, all of which resulted in 6 total levels of adaptive mesh refinement.

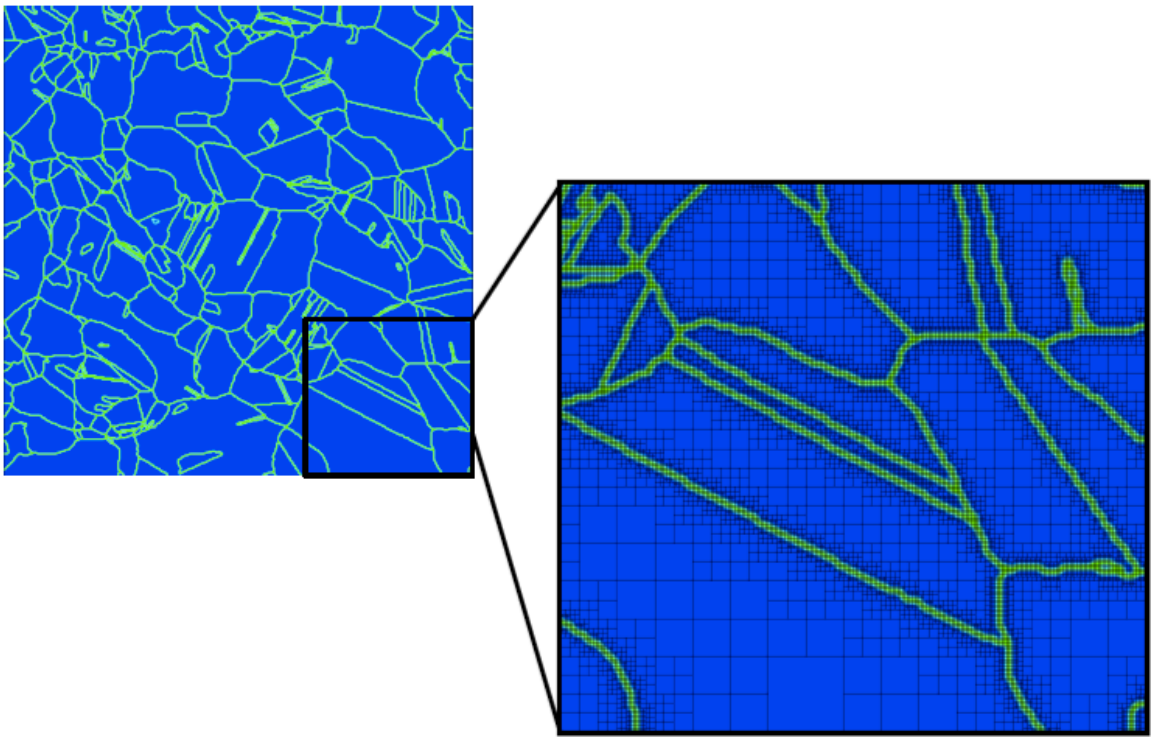

Figure 91. Grain boundary plot of reconstructed 304H microstructure and demonstration of the adaptive mesh refinement in MOOSE.

FEM based phase field models require substantial memory to perform simulations. Therefore, the "Grain Tracker" algorithm was utilized to minimize memory usage by grouping individual order parameters into a reduced set of variables that can be remapped during the simulation to prevent coalescence of the grains (order parameters #8 out of 10 are shown in the Figure 92 (R)). Only 10 variables are needed to represent the 304H grains in the 304H dataset.

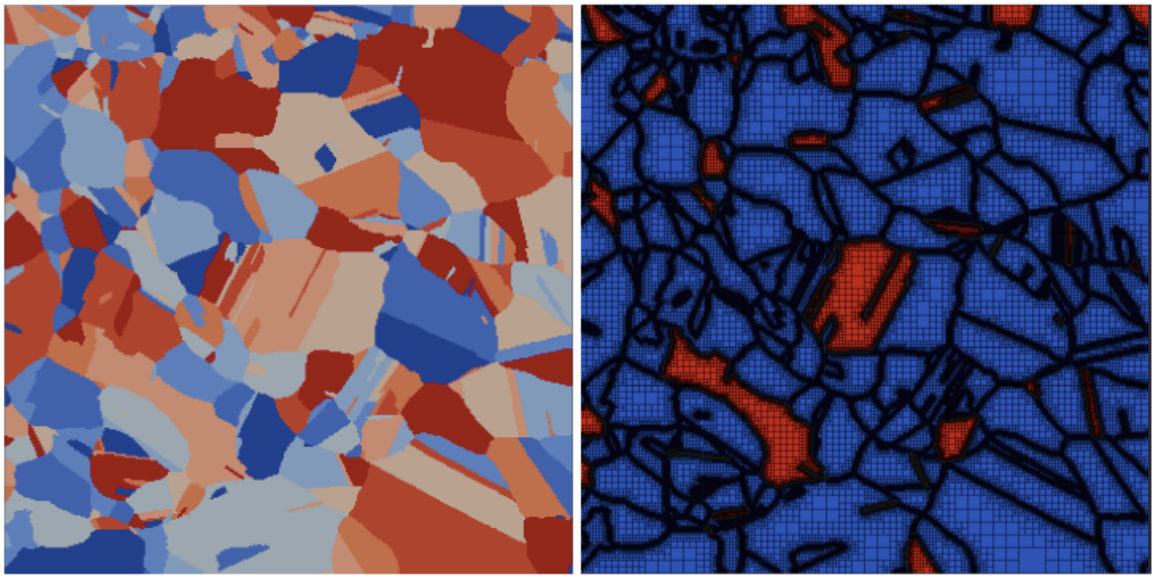

Figure 92. MARMOT reconstruction of irradiated 304H microstructure that demonstrates the "grain tracker" algorithm.

CrossCourt 4 software was utilized to perform cross-correlation analysis of the HR-EBSD dataset (shown in Fig. 88). The "EBSD Reader" interface was updated to allow material properties to be exported from CrossCourt and input into MARMOT as initial conditions for phase field modeling. The geometrically necessary (GND) dislocation map and the Von Mises stress map are provided in Figure 93 and σ_{22} stress and ε_{22} strain maps are provided in Figure 94. These σ_{22} stress and ε_{22} strain maps acquired from irradiated S304H SS material can be used as initial conditions for new phase field models or for validation purposes of existing models.

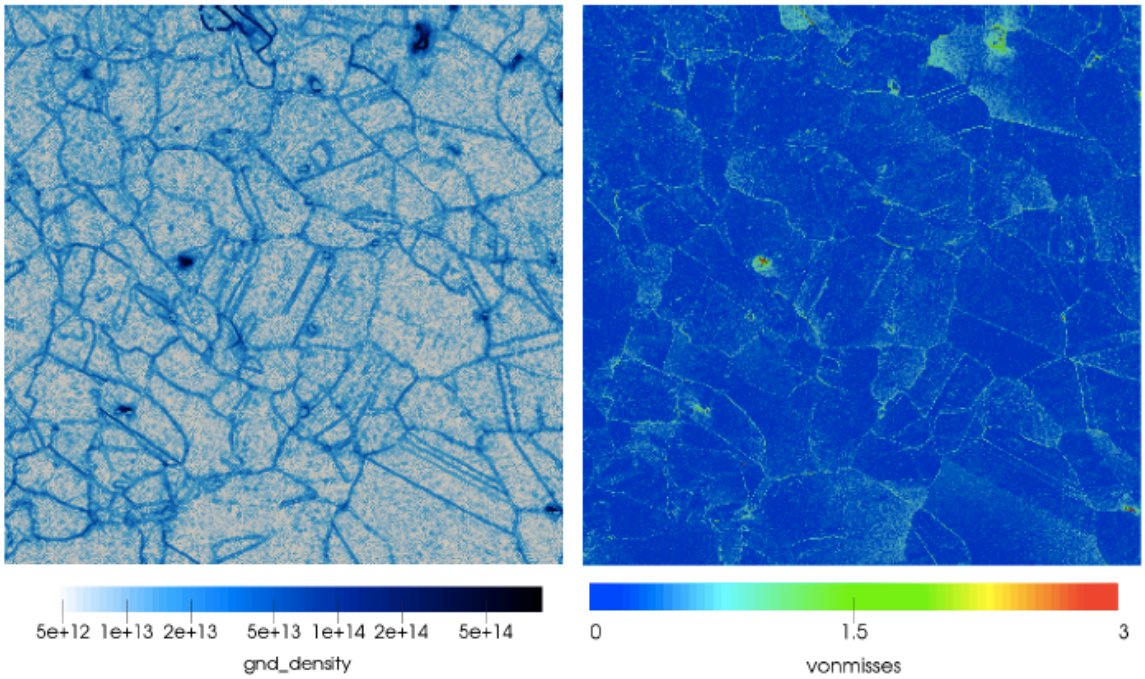

Figure 93. Cross-correlation analysis of the HR-EBSD dataset acquired from irradiated 304H specimen. Geometrically necessary (GND) dislocation map is shown on the left and the Von Mises stress map on the right.

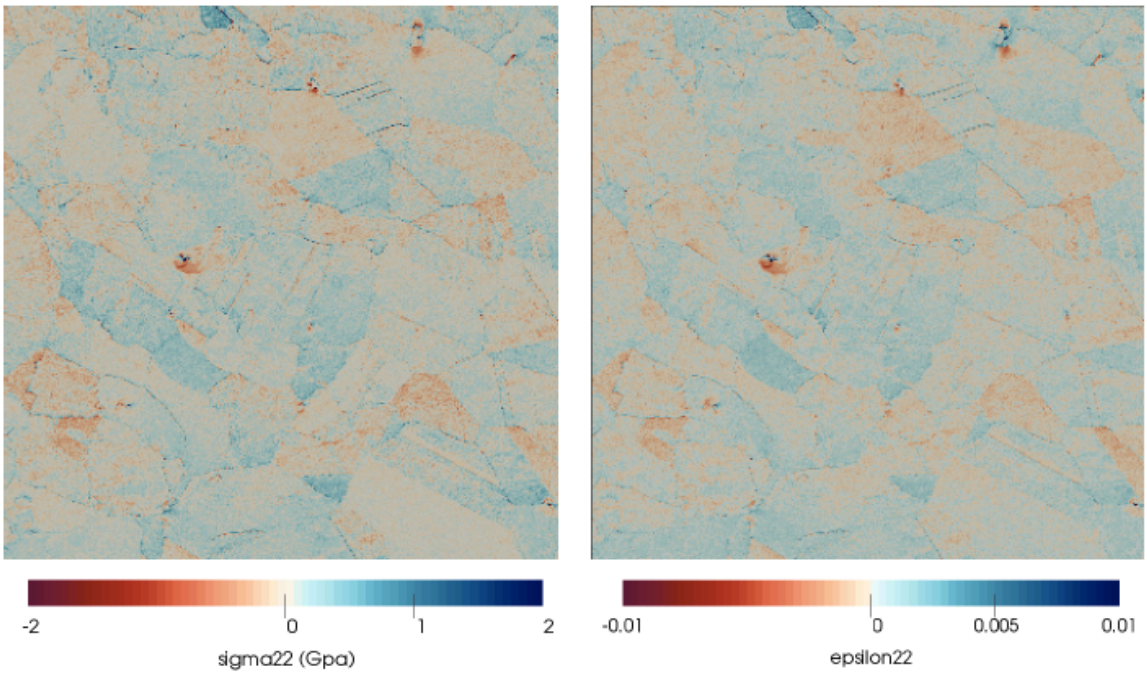

Figure 94. σ_{22} stress and ε_{22} strain map output from CrossCourt and input into MARMOT for the irradiated 304H SS specimen.

In addition to EBSD data, EDS data can also be imported into MARMOT through the "EBSD Reader" interface. Similar to CrossCourt properties, the EDS results can be used as initial conditions or validation of phase field models that employ chemical concentrations of that model nucleation. The example of the EDS data imported into MARMOT is provided in Figure 95.

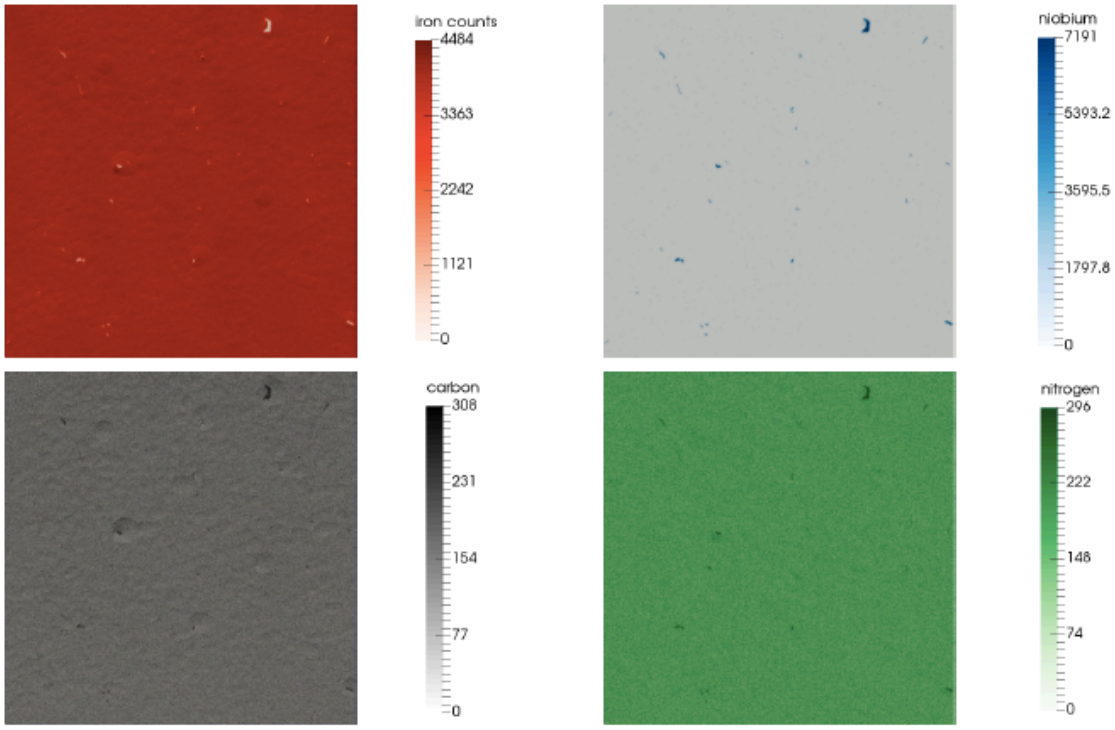

Figure 95. MARMOT 2D EDS maps for irradiated 304H specimen.

4.4.3.2 Reconstruction of 3D datasets into MARMOT

The 3D reconstruction of irradiated 304H SS microstructure with inverse pole figure coloring output from MARMOT framework has been provided in Section 4.4.2. As it was mentioned, 8 slices were serial sectioning with Gatan PECS system. Each slice had a scan size of 200 µm X 200 µm and 0.5 µm step size. The dataset contained 698 grains and is shown in Figure 89. This experimentally acquired and MARMOT processed microstructure was used to construct grain boundary plots for use in MARMOT. Figure 96 shows the grain boundary plot after 3 time steps in MARMOT phase field model. The dataset contains ~3.6 million elements and is too dense to visualize the entire mesh. After 3 levels of coarsening, the base level (0.5 µm) and 1 level of mesh refinement, the model contains 5 total levels of adaptive mesh refinement.

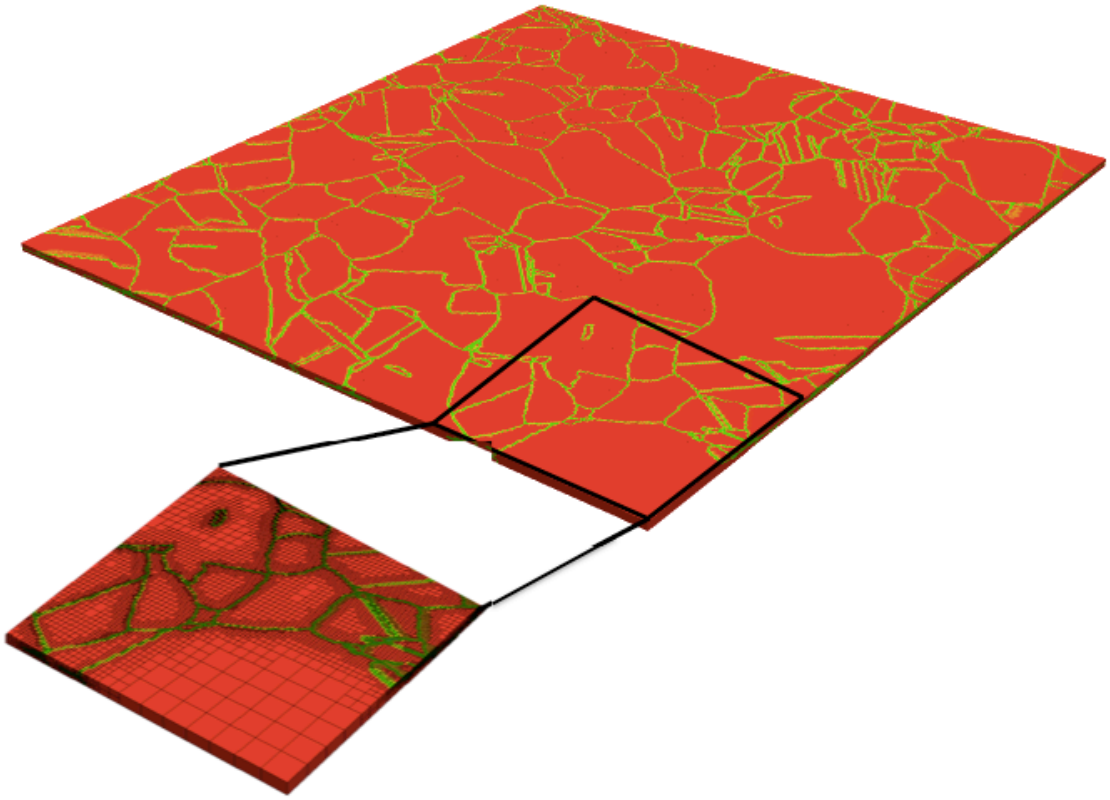

Figure 96. Grain boundary plot of irradiated 304H specimen after 3 time steps in MARMOT phase field model.

"Grain Tracker" algorithm was utilized to minimize memory usage by grouping individual order parameters into a reduced set of variables that can be remapped during the simulation to prevent coalescence of the grains. Figure 97 top image shows the order parameter #0 out of 20 and the bottom image is color plot of the 20 order parameters that were used to represent the 698 grains found in the dataset. Each order parameter is plotted with a different color.

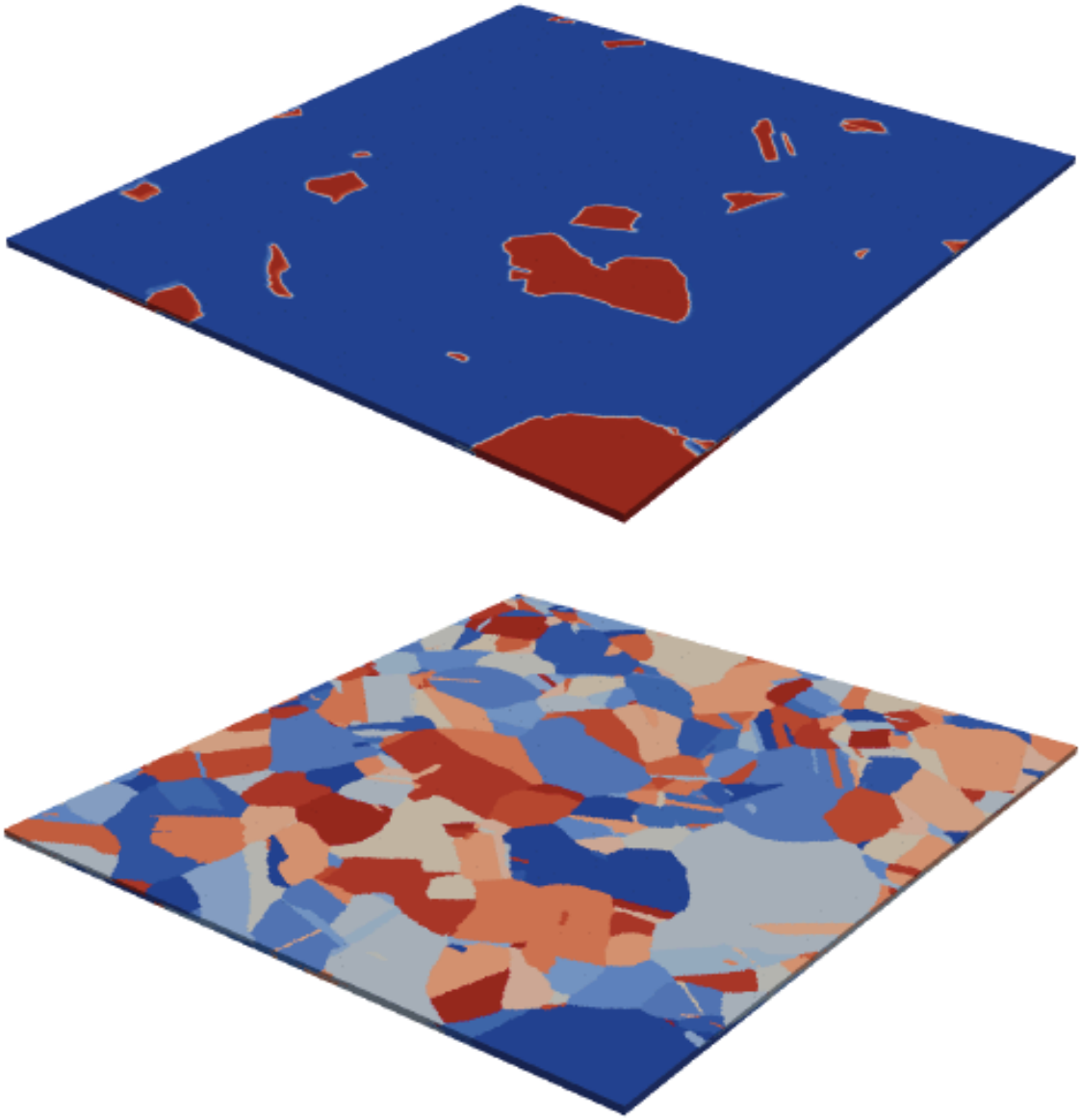

Figure 97. MARMOT reconstruction of the irradiated 304H dataset.

In addition to integrating datasets from irradiated 304H SS material, same procedures were implemented for irradiated HT-9. The developed procedures for integration of experimental data into MARMOT framework can be used for any other material of interest and can be made available to interested users. Multiple algorithms discussed in Section 4.4.3 are well known in modeling community and do not require exhaustive training before usage.

The report demonstrates that all project objectives have been reached during the course of the project (FY 14-16). Broad beam ion etching technique (using two different instruments Gatan PECS and Fischione TEM mill) has been implemented for preparation of highly radioactive irradiated materials and recipes for each material selected for the study have been provided. These broad beam ion-etching methods decrease sample preparation time, substantially improve scan quality, increase scan size, and reduce radiation exposure and waste. The largest demonstrated scan included an area of roughly 200 µm X 200 µm (2 µm in volume) but even

larger volumes can be analyzed in a reasonable amount of time. The selected volume was optimized for the system available for analysis but other users can characterize larger volumes using their tools. Experimental serial sectioning of irradiated materials was performed and the data was reconstructed using a combination of MATLAB and Dream.3D software and input into MARMOT. Advanced characterization technique known as HR-EBSD was implemented for highly radioactive specimens. HR-EBSD enabled estimation of critical material properties such as dislocation density and residual strain from irradiated reactor materials.

The necessary post-processing tools and procedures to utilize HR-EBSD and 3D EBSD/EDS data were developed for microstructure reconstruction in MARMOT. The experimental data was integrated into MARMOT, as shown in Section 4.4.3. One of the examples is that the experimentally acquired and MARMOT processed microstructure can be used to construct grain boundary plots for use in MARMOT. Such microstructures can be used to establish realistic initial conditions for simulations in MARMOT, predict physical properties of the material (ex: thermal conductivity), and for validation of the existing computational models.

Bibliography

[1] MC Teague, B Gorman, B Miller, J King, EBSD and TEM characterization of high burn-up mixed oxide fuel, *Journal of Nuclear Materials*, 444(1-3):475-480, 2014.

[2] MC Teague and B Gorman, Utilization of dual-column focused ion beam and scanning electron microscope for three dimensional characterization of high burn-up mixed oxide fuel, *Progress in Nuclear Energy*, 72:67-71, 2014.

[3] MR Tonks, D Gaston, PC Millett, D Andrs, P Talbot, An object-oriented finite element framework for multiphysics phase field simulations, *Computational Materials Science*, 51(1):20-29, 2012.

[4] MR Tonks, P Millett, P Nerikar, S Du, D Andersson, CR Stanek, D Gaston, D Andrs, R Williamson, Multiscale development of a fission gas thermal conductivity model: Coupling atomic, meso and continuum level simulations, Journal of Nuclear Materials, 440(1-3):193-200, 2013.

[5] MC Teague, BS Fromm, MR Tonks, DP Field, Using Coupled Mesoscale Experiments and Simulations to Investigate High Burn-up Oxide Fuel Thermal Conductivity, *The Journal of The Minerals, Metals & Materials Society*, 66(12):2569-2577, 2014.

[6] MR Tonks, D Schwen, Y Zhang, P Chakraborty, X Bai, B Fromm, J Yu, MC Teague, DA Andersson, Assessment of MARMOT: A Mesoscale Fuel Performance Code, INL/EXT-15-35108, 2015.

[7] EDAX Inc., OIM Data Analysis, Version 7.1 (Mahwah, NJ: EDAX Inc., 2014).

[8] Math-Works Inc., MATLAB, Version 8.6.0.267246 (R2015b) (Natick, MA: The Math-Works Inc., 2014).

[9] MA Groeber and MA Jackson, DREAM.3D: A Digital Representation Environment for the Analysis of Microstrucutre in 3D, Integrating Materials and Manufacturing Innovation, 3(5), 2014.

[10] BlueQuartz Software, DREAM.3D, Version 6.2 (Springboro, OH: BlueQuartz Software, 2015)